

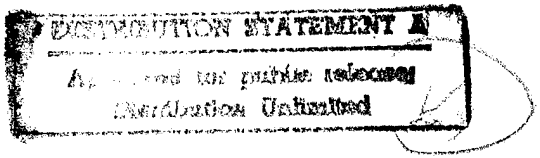
NASA Contractor Report 172359

Note: Order CR 172358, 172360, CP 2321 & 2322, ~~all~~ ^{Index group as cont}
~~Index all papers~~
see P V



ACEE COMPOSITE STRUCTURES TECHNOLOGY

Papers by Douglas Aircraft Company



19960318 016

**McDonnell Douglas Corporation
Douglas Aircraft Company
Long Beach, California 90846**

**Contract NAS1-14869
NAS1-16857
NAS1-17701**

FOR EARLY DOMESTIC DISSEMINATION

Because of its possible early commercial potential, this data, which has been developed under a U.S. Government program, is being disseminated within the United States in advance of general publication. This data may be duplicated and used by the recipient with the express limitation that it not be published. Release of this data to other domestic parties by the recipient shall be made subject to these limitations. Foreign release may be made only with prior NASA approval and appropriate export licenses. This legend shall be marked on any reproduction of this data in whole or in part. Date for general release will be three (3) years from date indicated on the document.

TL
680
.N10

NASA

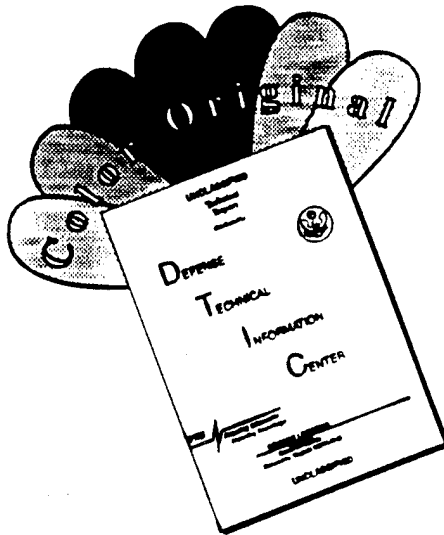
National Aeronautics and Space Administration

Langley Research Center
Hampton, Virginia 23665

DEPARTMENT OF DEFENSE
PLASTICS TECHNICAL EVALUATION CENTER
ARRADCOM, DOVER, N. J. 07801

THE QUALITY INSPECTED 1

DISCLAIMER NOTICE



THIS DOCUMENT IS BEST
QUALITY AVAILABLE. THE COPY
FURNISHED TO DTIC CONTAINED
A SIGNIFICANT NUMBER OF
COLOR PAGES WHICH DO NOT
REPRODUCE LEGIBLY ON BLACK
AND WHITE MICROFICHE.

Add 438839 - 438843

1. Report No. NASA CR-172359	2. Government Accession No.	3. Recipient's Catalog No.	
4. Title and Subtitle ACEE COMPOSITE STRUCTURES TECHNOLOGY Papers by Douglas Aircraft Company		5. Report Date August 1984	6. Performing Organization Code
7. Author(s) Compiled by M. Klotzsche		8. Performing Organization Report No.	
9. Performing Organization Name and Address McDonnell Douglas Corporation Douglas Aircraft Company Long Beach, California 90846		10. Work Unit No.	
12. Sponsoring Agency Name and Address National Aeronautics and Space Administration Washington, DC 20546		11. Contract or Grant No. NAS1-17701, NAS1-16857, NAS1-14869	
15. Supplementary Notes Langley technical monitor: A. J. Chapman, III		13. Type of Report and Period Covered Contractor Report	
		14. Sponsoring Agency Code 534-06-13	
16. Abstract The NASA Aircraft Energy Efficiency (ACEE) Composite Primary Aircraft Structures Program has made significant progress in the development of technology for advanced composites in commercial aircraft. Under NASA sponsorship, commercial airframe manufacturers have demonstrated technology readiness and cost effectiveness of advanced composites for secondary and medium primary components and have initiated a concerted program to develop the data base required for efficient application of safety-of-flight wing and fuselage structure. The third special oral review of the ACEE Composites Program was held in Seattle, Washington, on August 13-16, 1984. The conference included comprehensive reviews of all composites technology development programs by ACEE Composites contractors. In addition, special sessions included review of selected NASA-sponsored research and several important Department of Defense programs in composite materials and structures. The papers were compiled in five documents. Papers prepared by personnel from Boeing Commercial Airplane Company, Douglas Aircraft Company, and Lockheed-California Company are contained in NASA CR-172358, <u>CR-172359</u> , and CR-172360, respectively. Papers on selected NASA-sponsored research are contained in NASA CP-2321. Papers on selected Department of Defense programs in composites are contained in NASA CP-2322.			
17. Key Words (Suggested by Author(s)) Composite materials Composite structures Composite aircraft structures	18. Distribution Statement FEDD Distribution		
Subject Category 24			
19. Security Classif. (of this report) Unclassified	20. Security Classif. (of this page) Unclassified	21. No. of Pages	22. Price*

Available: NASA's Industrial Applications Center

FOREWORD

The NASA Aircraft Energy Efficiency (ACEE) Composite Primary Aircraft Structures Program has made significant progress in the development of technology for advanced composites in commercial aircraft. Under NASA sponsorship, commercial airframe manufacturers have now demonstrated technology readiness and cost effectiveness of advanced composites for secondary and medium primary components and have initiated a concerted program to develop the data base required for efficient application to safety-of-flight wing and fuselage structure. Timely dissemination of technical information acquired in these programs is achieved through distribution of reports and periodic special oral reviews.

The third special oral review of the ACEE Composites Programs was held in Seattle, Washington, on August 13-16, 1984. The conference included comprehensive reviews of all composites technology development programs by ACEE Composites contractors - Boeing, Douglas, and Lockheed. In addition, special sessions included selected papers on NASA-sponsored research in composite materials and structures and reviews of several important Department of Defense programs in composites.

Individual authors prepared their narrative and figures in a form that could be directly reproduced. The material is essentially the same material that was orally presented at the conference. The papers were compiled in five documents. Papers prepared by personnel from Boeing Commercial Airplane Company, Douglas Aircraft Company, and Lockheed-California Company are contained in NASA CR-172358, CR-172359, and CR-172360, respectively. Papers on selected NASA-sponsored research are contained in NASA CP-2321. Papers on selected Department of Defense programs in NASA CP-2322.

The assistance of all authors, contractor personnel, and the Research Information and Applications Division of the Langley Research Center in publishing these proceedings is gratefully acknowledged.

The identification of commercial products in this report does not constitute an official endorsement of such products, either expressed or implied, by the National Aeronautics and Space Administration.

John G. Davis, Jr.
Technical Chairman for
ACEE Composite Structures
Technology Conference
Langley Research Center

CONTENTS

FOREWORD	iii
AGENDA	vii
DAMAGE TOLERANCE AND FAILSAFE TESTING OF THE DC-10 COMPOSITE VERTICAL STABILIZER	47196 . . . 1
John M. Palmer, Jr., Clive O. Stephens, and Jason O. Sutton	
THEORY AND ANALYSIS FOR OPTIMIZATION OF COMPOSITE MULTI-ROW BOLTED JOINTS	47197 . . . 45
L. John Hart-Smith	
DESIGN AND TEST OF LARGE WING JOINT DEMONSTRATION COMPONENTS	47198 . . . 71
Bruce L. Bunin	
DOUGLAS - JOINTS AND CUTOUTS IN FUSELAGE STRUCTURE	47199 . . . 95
D. Joseph Watts	

ACEE COMPOSITE STRUCTURES TECHNOLOGY CONFERENCE

A G E N D A

MONDAY, AUGUST 13, 1984

¹SESSION 1: OUTLOOK FOR COMPOSITES IN FUTURE AIRCRAFT

SESSION CHAIRMAN: Robert L. James, Jr., Manager, ACEE Project Office, NASA Langley Research Center

AIR TRANSPORTATION SYSTEMS AT THE END OF THE MILLENNIUM - Howard T. Wright, Director for Projects, NASA Langley Research Center

FUTURE COMMERCIAL VIABILITY OF COMPOSITES - Kenneth F. Holtby, Corporate Senior Vice President, The Boeing Company

"THE WAY AHEAD" - Russell H. Hopps, Vice President and General Manager, Engineering and Development, Lockheed-California Company

"COMPOSITE AIRCRAFT MATERIALS - THE FUTURE" - John B. DeVault, Vice President, Composite Materials and Structures, Hercules Aerospace

TUESDAY MORNING, AUGUST 14, 1984

SESSION 2: ACEE SECONDARY AND MEDIUM PRIMARY COMPOSITE STRUCTURES - STATUS REPORT

SESSION CHAIRMAN: Andrew J. Chapman, Technical Manager, Composites, ACEE Project Office, NASA Langley Research Center

²737, 757 and 767 COMPONENTS - John T. Quinlivan, Boeing Commercial Airplane Company

³DAMAGE TOLERANCE AND FAILSAFE TESTING OF THE DC-10 COMPOSITE VERTICAL STABILIZER - John M. Palmer, Jr., Clive O. Stephens, and Jason O. Sutton, Douglas Aircraft Company

⁴INITIAL STRENGTH AND HYGROTHERMAL RESPONSE OF L-1011 VERTICAL FIN COMPONENTS - Anthony C. Jackson, Lockheed-California Company

⁵RESIDUAL-STRENGTH TESTS OF L-1011 VERTICAL FIN COMPONENTS AFTER 10 AND 20 YEARS OF SIMULATED FLIGHT SERVICE - Osvaldo F. Lopez, NASA Langley Research Center

⁵WORLDWIDE FLIGHT AND GROUND BASED EXPOSURE OF COMPOSITE MATERIALS - H. Benson Dexter, NASA Langley Research Center, and Donald J. Baker, U. S. Army Structures Laboratory, NASA Langley Research Center

TUESDAY MORNING, AUGUST 14, 1984

⁵COMPARISON OF TOUGHENED COMPOSITE LAMINATES USING NASA STANDARD DAMAGE TOLERANCE TESTS - Jerry G. Williams, NASA Langley Research Center, T. Kevin O'Brien, U.S. Army Structures Laboratory, NASA Langley Research Center, and Andrew J. Chapman, NASA Langley Research Center

TUESDAY AFTERNOON, AUGUST 14, 1984

SESSION 3: REVIEW OF SELECTED NASA RESEARCH IN COMPOSITE MATERIALS AND STRUCTURES

SESSION CHAIRMAN: James H. Starnes, Jr., Head, Structural Mechanics Branch, NASA Langley Research Center

⁵SYNTHESIS AND TOUGHNESS PROPERTIES OF RESINS AND COMPOSITES - Norman J. Johnston, NASA Langley Research Center

⁵TENSILE STRENGTH OF COMPOSITE SHEETS WITH UNIDIRECTIONAL STRINGERS AND CRACK-LIKE DAMAGE - Clarence C. Poe, Jr., NASA Langley Research Center

⁵IMPACT DYNAMICS RESEARCH ON COMPOSITE TRANSPORT STRUCTURES - Huey D. Carden, NASA Langley Research Center

⁵POSTBUCKLING BEHAVIOR OF GRAPHITE/EPOXY PANELS - James H. Starnes, Jr., NASA Langley Research Center; John N. Dixon, Lockheed-Georgia Company; Marshall Rouse, NASA Langley Research Center

¹DAMAGE TOLERANCE RESEARCH ON COMPOSITE COMPRESSION PANELS - Jerry G. Williams, NASA Langley Research Center

⁵STUDIES OF NOISE TRANSMISSION IN ADVANCED COMPOSITE MATERIAL STRUCTURES - Louis A. Roussos, Michael C. McGary, and Clemens A. Powell, NASA Langley Research Center

WEDNESDAY MORNING, AUGUST 15, 1984

SESSION 4: ACEE WING KEY TECHNOLOGIES

SESSION CHAIRMAN: Marvin B. Dow, Technical Manager, Composites, ACEE Project Office, NASA Langley Research Center

²COMPOSITE WING PANEL DURABILITY AND DAMAGE TOLERANCE TECHNOLOGY DEVELOPMENT - Robert D. Wilson, Boeing Commercial Airplane Company

²DESIGN DEVELOPMENT OF HEAVILY LOADED WING PANELS - Peter J. Smith, Boeing Commercial Airplane Company

WEDNESDAY MORNING, AUGUST 15, 1984

³THEORY AND ANALYSIS FOR OPTIMIZATION OF COMPOSITE MULTI-ROW BOLTED JOINTS -
L. John Hart-Smith, Douglas Aircraft Company

³DESIGN AND TEST OF LARGE WING JOINT DEMONSTRATION COMPONENTS - Bruce L. Bunin,
Douglas Aircraft Company

⁴COMPOSITE WING FUEL CONTAINMENT AND DAMAGE TOLERANCE TECHNOLOGY DEVELOPMENT -
Charles F. Griffin, Lockheed-California Company

⁴COMPOSITE WING FUEL CONTAINMENT AND DAMAGE TOLERANCE TECHNOLOGY DEMONSTRATION -
Tom W. Anderson, Lockheed-California Company

WEDNESDAY AFTERNOON, AUGUST 15, 1984

SESSION 5: REVIEW OF SELECTED DOD PROGRAMS

SESSION CHAIRMAN: H. Benson Dexter, NASA Langley Research Center

⁶MANUFACTURING TECHNOLOGY FOR LARGE AIRCRAFT COMPOSITE PRIMARY STRUCTURE (FUSELAGE) -
DESIGN SELECTION - Hank R. Fenbert, Boeing Commercial Airplane Company; Harry S.
Reinert, U.S. Air Force, MLTN, Wright-Patterson AFB, Vere S. Thompson, Boeing
Commercial Airplane Company

⁶MANUFACTURING TECHNOLOGY FOR LARGE AIRCRAFT COMPOSITE WING STRUCTURE - Melvin A.
Price, North American Aircraft Operations, Rockwell International Corporation, and
D. R. Beeler, U.S. Air Force, AFWAL/MLTN, Wright-Patterson AFB

⁶MANUFACTURING TECHNOLOGY FOR LARGE COMPOSITE FUSELAGE STRUCTURE - Richard L.
Circle and R. Dennis O'Brien, Lockheed-Georgia Company

⁶DAMAGE TOLERANCE OF COMPOSITES - John E. McCarty, Boeing Military Airplane Company.

¹ADVANCED COMPOSITE AIRFRAME PROGRAM (ACAP) - Tom Mazza, U.S. Army Applied
Technology Laboratory, Fort Eustis

⁶COMPOSITE STRUCTURES - IMPROVED DESIGNS FOR MILITARY AIRCRAFT - Anthony Manno,
Mark S. Libeskind, Ramon Garcia, and Edward F. Kautz, U.S. Navy, Naval Air
Development Center

¹COMPOSITE STRUCTURES IN THE JVX AIRCRAFT - Keith Stevenson, Bell Helicopter
Corporation

THURSDAY MORNING, AUGUST 16, 1984

SESSION 6: ACEE ADVANCED COMPOSITE STRUCTURES TECHNOLOGY

SESSION CHAIRMAN: Jon S. Pyle, Technical Manager, Composites, ACEE Project Office, NASA Langley Research Center

²BOEING - PRESSURE CONTAINMENT AND DAMAGE TOLERANCE IN FUSELAGE STRUCTURE -
Ronald W. Johnson, Boeing Commercial Airplane Company

³DOUGLAS - JOINTS AND CUTOUTS IN FUSELAGE STRUCTURE - D. Joseph Watts, Douglas Aircraft Company

⁴LOCKHEED - IMPACT DYNAMICS AND ACOUSTIC TRANSMISSION IN FUSELAGE STRUCTURE -
Anthony C. Jackson, Lockheed-California Company

⁴LOCKHEED COMPOSITE TRANSPORT WING TECHNOLOGY DEVELOPMENT

COVER/RIB CONCEPTS - Arthur M. James, Lockheed-California Company

SPAR/ASSEMBLY CONCEPTS - William E. Harvill, Jr., Lockheed-Georgia Company

¹Oral presentations only.

²Papers contained in NASA CR-172358.

³Papers contained in NASA CR-172359.

⁴Papers contained in NASA CR-172360.

⁵Papers contained in NASA CP-2321.

⁶Papers contained in NASA CP-2322.

DAMAGE TOLERANCE AND FAIL-SAFE TESTING
OF THE
DC-10 COMPOSITE VERTICAL STABILIZER
CONTRACT NAS1-14869

J. M. Palmer, Jr.

C. O. Stephens

J. O. Sutton

Douglas Aircraft Company
Long Beach, California

ACEE Composite Structures Technology Conference
Seattle, Washington
August 13-16, 1984

DAMAGE TOLERANCE AND FAIL-SAFE TESTING
OF THE DC-10 COMPOSITE VERTICAL STABILIZER

ABSTRACT

A review of the damage tolerance and fail-safe testing of the DC-10 composite vertical stabilizer is presented. The tests conducted on the two major test articles, a semispan stub box and a full-span ground unit, are described and an assessment presented of test results, including comparison of test data with analysis predictions.

The stub box subcomponent was tested in an environmental chamber under ambient, cold/wet, and hot/wet conditions. The test program included design limit static loading, fatigue spectrum loading to approximately two service lifetimes (with and without damage), design limit damage tolerance tests, and a final residual strength test to structural failure.

The full span ground test unit was tested under ambient conditions, but the tests were otherwise similar to the stub box tests. The test program included design limit static loading, design ultimate static loading, fatigue spectrum loading to two service lifetimes (with and without damage), a fail-safe/damage tolerance test, and a final residual strength test to structural failure (after damage repair).

The broad objective of the DC-10 Composite Vertical Stabilizer (CVS) program is to accelerate the use of primary composite structures in new aircraft by developing technology and process for early progressive introduction of composite structures into production commercial aircraft. Two paramount goals are to achieve a low-cost design and manufacturing process, and to obtain commercial airline service experience of a primary composite structure.

PROGRAM SCOPE

DESIGN AND FABRICATE THREE FULL-SCALE UNITS

QUALIFY THE COMPOSITE STABILIZER STRUCTURE IN ENVIRONMENT WITH AND WITHOUT DAMAGE

CERTIFY THE COMPOSITE STRUCTURE FOR FLIGHT SERVICE THROUGH GROUND AND FLIGHT TESTS

DC-10 COMPOSITE VERTICAL STABILIZER

The composite structure developed under this program consists of the main structural box of the DC-10 vertical stabilizer and includes the trailing edge panels. The box structure is approximately 20 feet tall with a root chord of approximately 8 feet along the base rib (Figure 1).

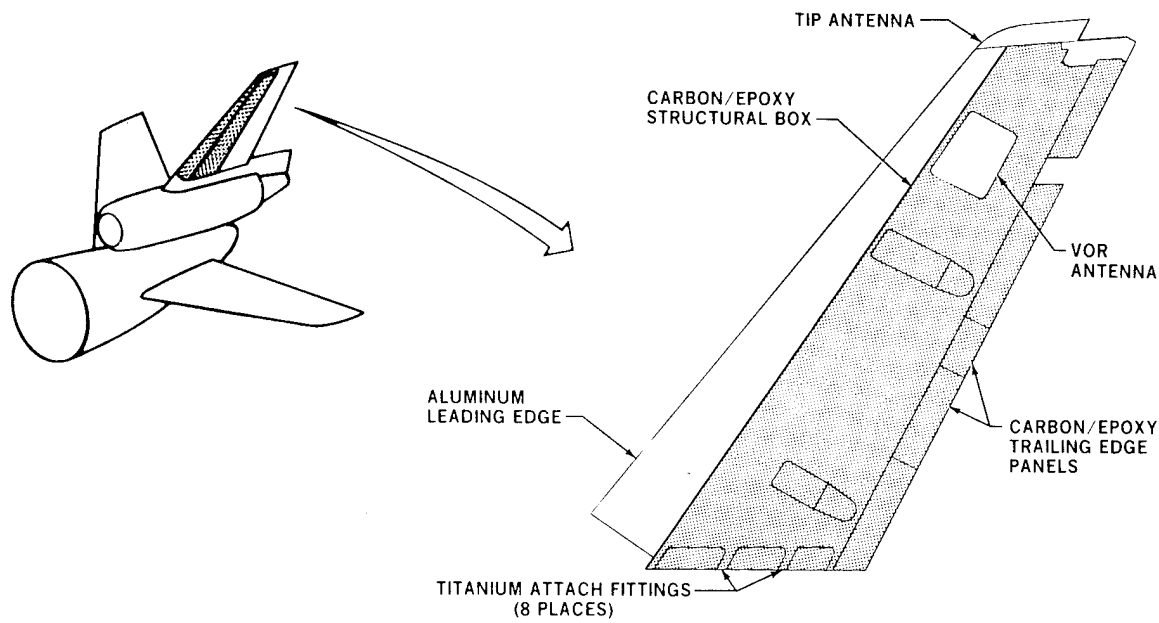


FIGURE 1.

CVS COMPOSITE STRUCTURAL BOX

The DC-10 CVS is a multispar, multirib structure in which the spars resist the major bending loads and sandwich stiffened skin panels resist both torque loads and local airloads. The stabilizer structural box (Figure 2) has four spanwise spars and 14 chordwise ribs. The spar caps and webs are spliced to titanium attach fittings at the root ends through which eight bolts attach the stabilizer to the center engine nacelle at the four forged frames in the lower vertical stabilizer structure.

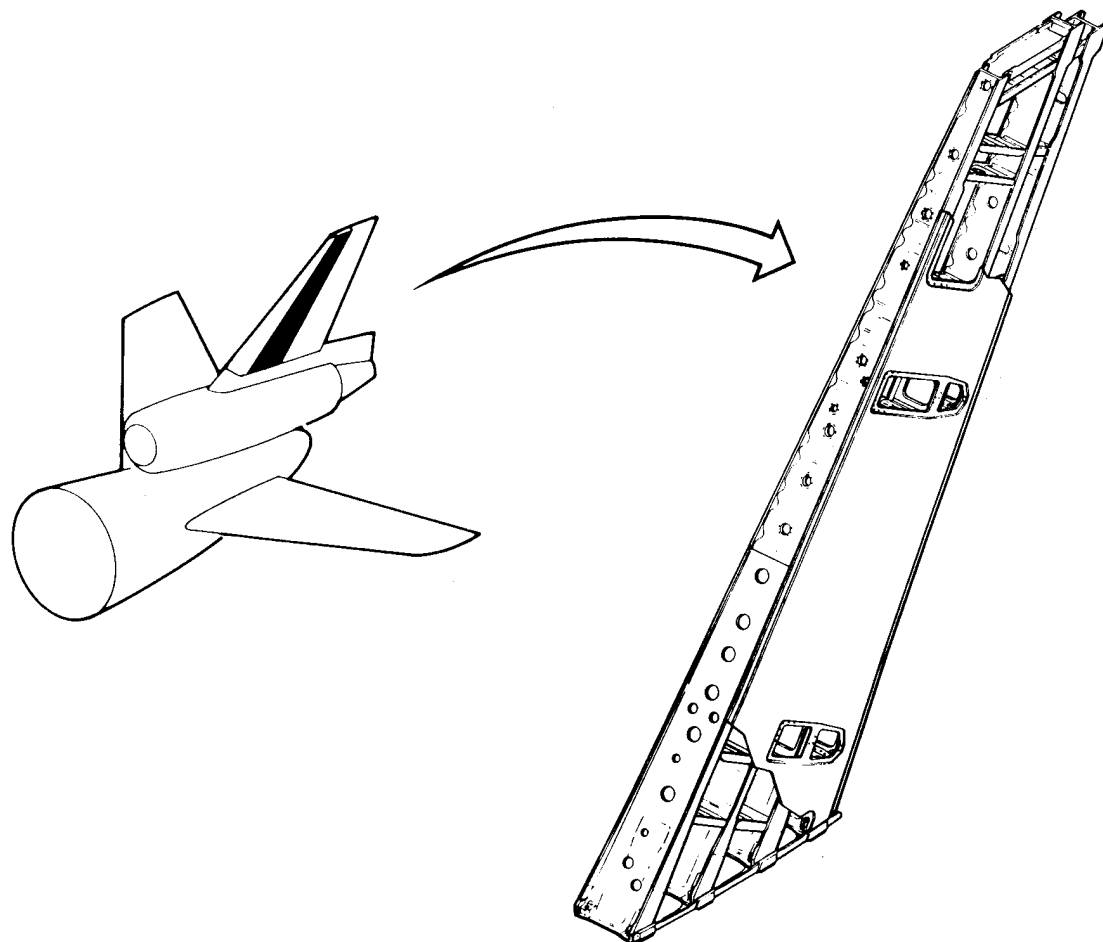


FIGURE 2.

COMPOSITE DETAILS

Figure 3 is an exploded view of the box structure and shows the two one-piece skin panels, the components making up the four spars, the rib components, and the access panels. These details together with the trailing edge panels make up the total of 65 composite components in the CVS.

The skin panels are uniform thickness honeycomb structure assemblies with a core thickness of 0.30 inch. To provide continuity of both spar and rib caps, a quasi-isotropic solid laminate tape layup is employed between the facing layers. The facing layers are woven fabric layed up at ± 45 degrees to the rear spar datum, except in the root region where 0/90 degree layers are added to allow for the rotation of structural axes at the lower vertical interface.

The design of the spar and rib components incorporates convoluted ("sine-wave") web stiffening except where this is precluded by the presence of cutouts or by other design considerations.

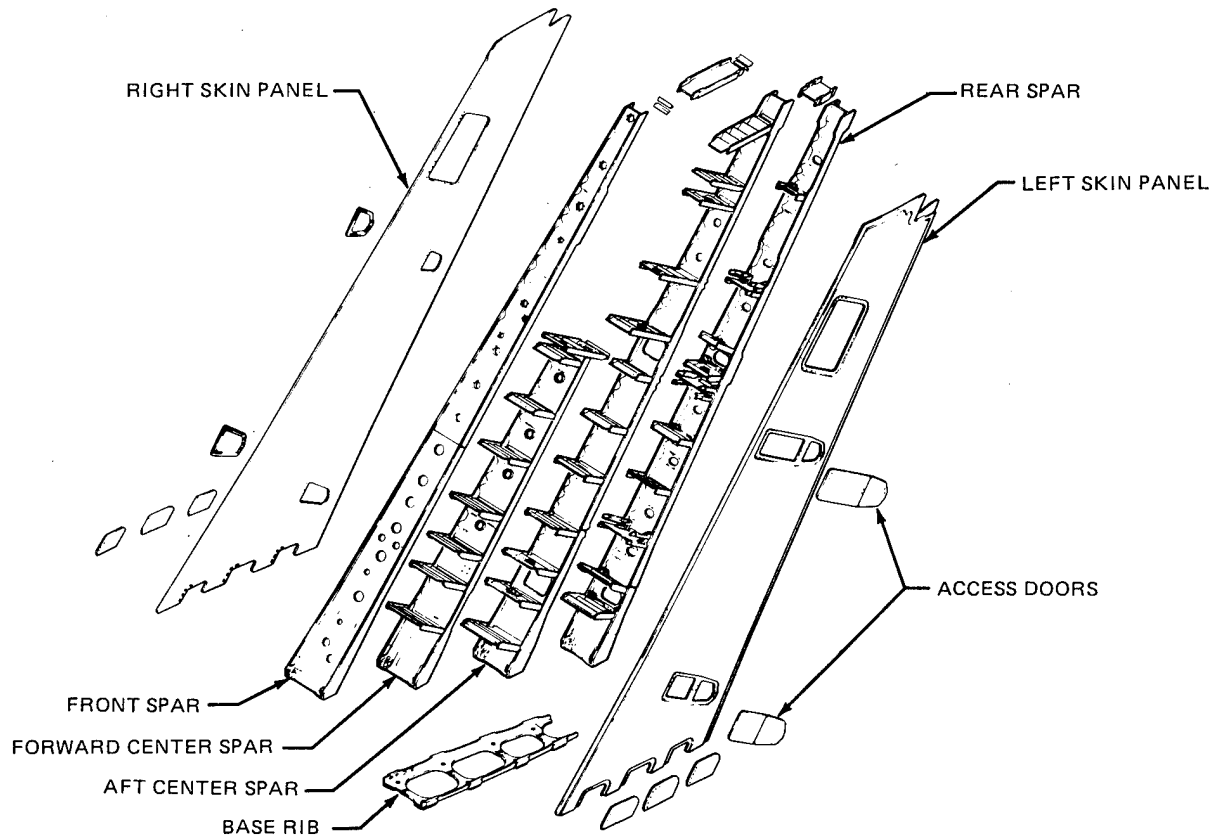


FIGURE 3.

BONDING FIXTURE

During assembly of the composite structural box, the spars and ribs were loaded into a bonding fixture where all rib-web to spar-web joints were bonded. Each joint incorporated B-stage carbon/epoxy prepreg angles which were co-cured and adhesively bonded in one operation. Pressure and heat were applied to each joint to effect the cure. Once all bonds were completed, the substructure was removed from the bonding fixture and all joints ultrasonically inspected. Figure 4 shows the completed substructure assembly being hoisted from the bonding fixture.

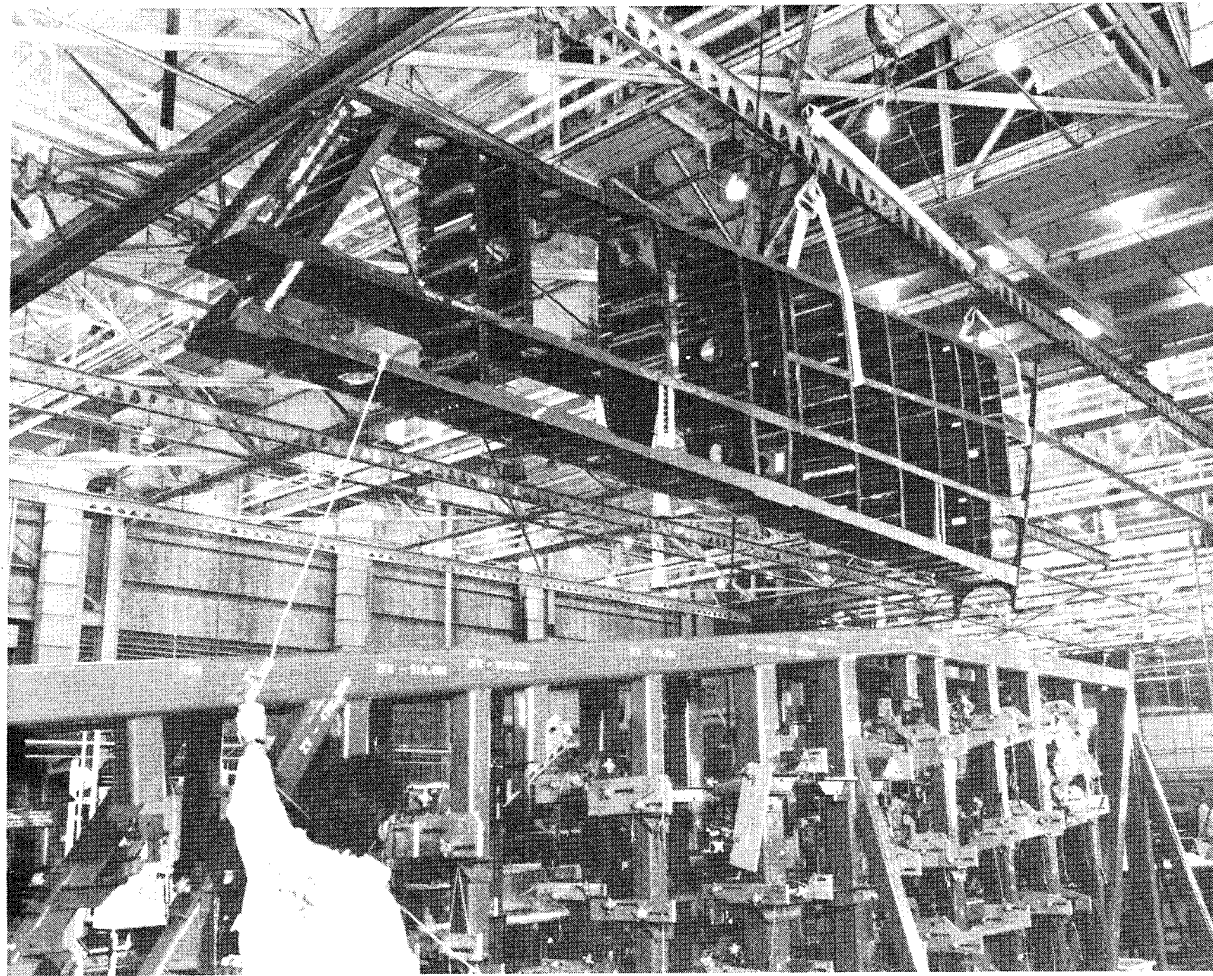


FIGURE 4.

BOX ASSEMBLY

The bonded substructure was next placed in an assembly fixture where the rudder hinge fittings and skin panels were fitted and installed. The skin panels were mechanically attached to the substructure with titanium fasteners. The leading edge and tip antenna assembly were also located and fitted in this operation. Once the skin panel installation was complete, the structural box was removed from the assembly fixture (Figure 5) and the leading edge, tip antenna, and access panels installed.

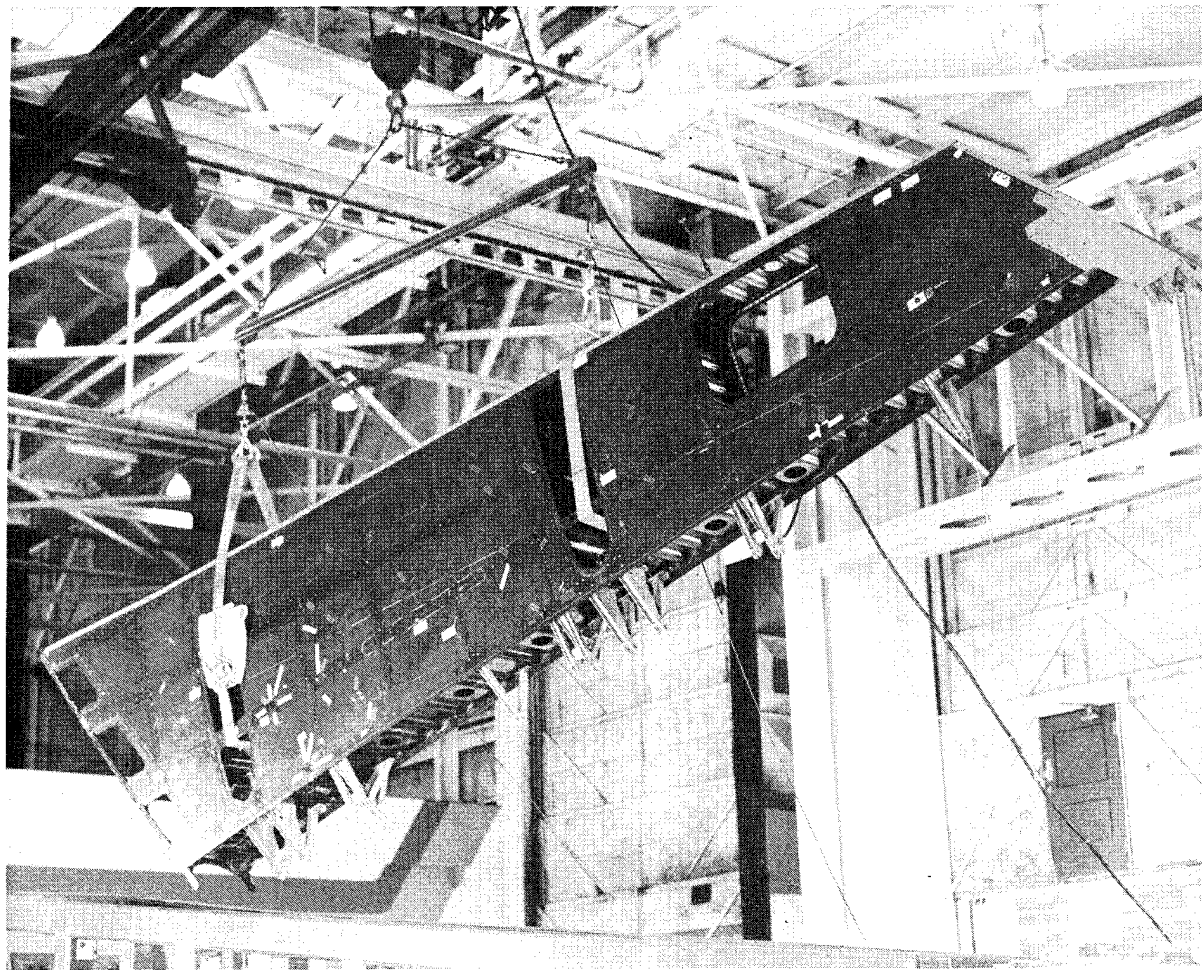


FIGURE 5.

COMPLETED COMPOSITE STABILIZER

Figure 6 shows the completed stabilizer after installation of leading edge, VOR antenna panels, and tip antenna assembly.

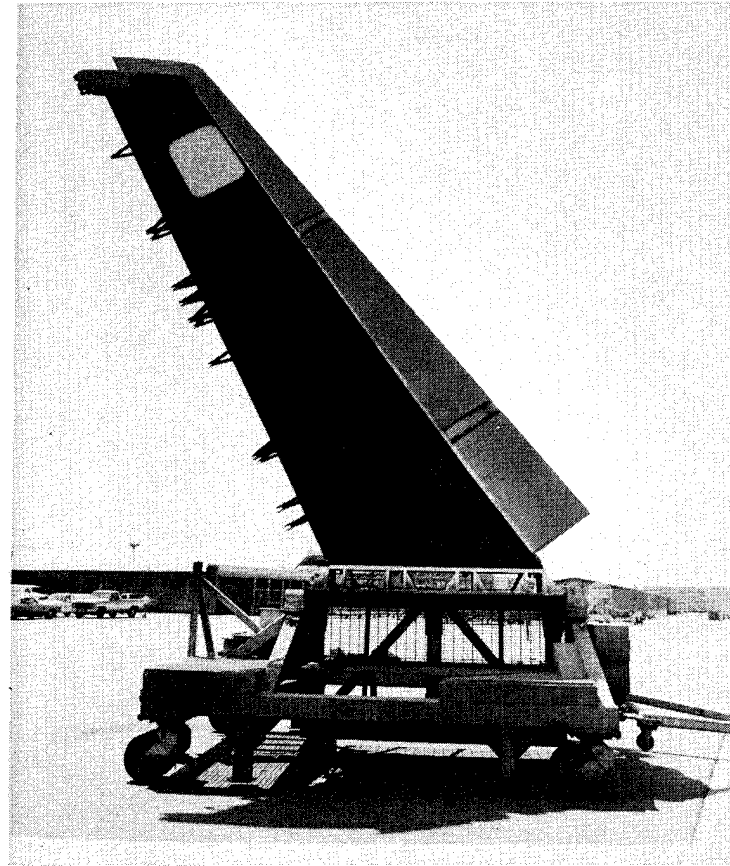


FIGURE 6.

STUB BOX TEST COMPONENT

The test subcomponent, shown in Figure 7, consisted of approximately the lower third of the full-span CVS structure. It included portions of the four spar assemblies, skin cover panels, ribs, root attach fittings, and access panels. Included in the assembly but not part of the test component were the truncated metal leading edge and lower rudder hinge fittings. These were installed primarily to introduce proper test loads into the composite structure. Trailing edge panels and internal hydraulic and electrical subsystems were not installed.

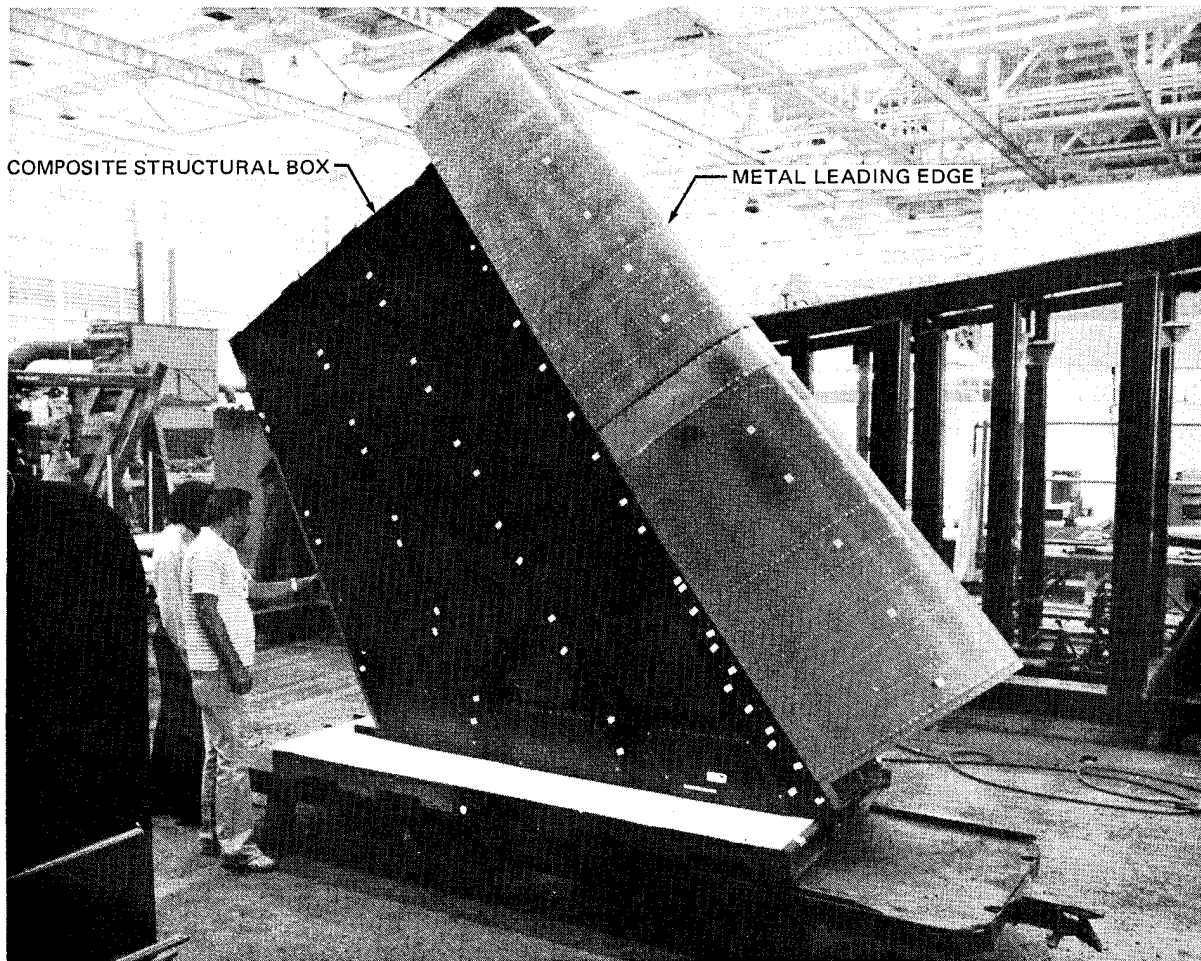


FIGURE 7.

STUB BOX TEST SETUP

The stub box was tested under static and repeated load at temperature to simulate the critical in-service loads and environments. During testing, the stub box was supported in a fixture (Figure 8) which was designed to simulate the structural flexibility of the aircraft fixed-fin structure. The test article together with the test fixture were installed in an environmental chamber.

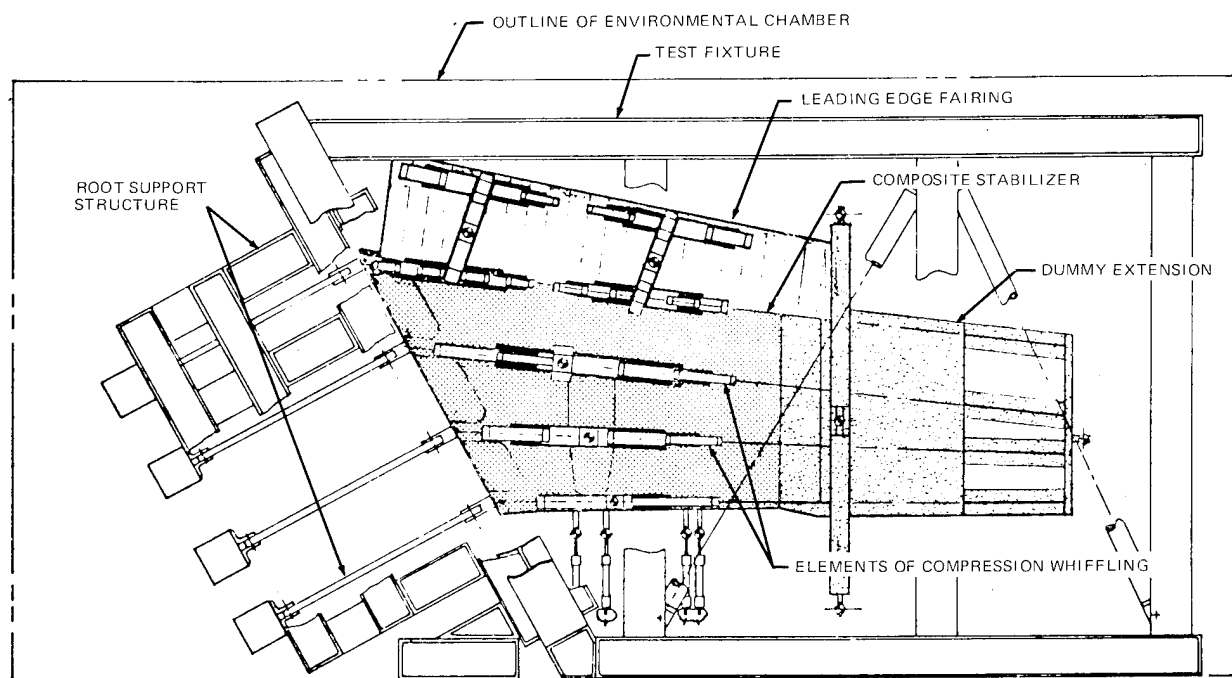


FIGURE 8.

STUB BOX TEST PROGRAM

One of the main objectives of the stub box test program was to evaluate the effects of moisture and temperature on the full-scale structure. The test program is shown in Table 1. The baseline design limit load tests were conducted in a dry condition at two different temperatures. These tests were for the critical shear, torsion, and bending conditions. The structure was then moisture-conditioned for two weeks at 170°F and 98-percent relative humidity to ensure saturation of the graphite structure. Thermal effects were evaluated by taking the structure as rapidly as possible from ambient temperature to 170°F, then reducing the temperature to -65°F, and then returning to ambient. The total time involved in the test was less than 40 hours, with no adverse effects on the structure.

With the structure stabilized at 0°F, a fatigue spectrum test was conducted to an equivalent of 36,000 flights or approximately 86 percent of the service life of the structure. Periodic inspections during and after the test revealed no structural anomalies. Three additional design limit loads were conducted, two at 0°F and one at 130°F, followed by six fail-safe tests at ambient temperature, all without incident.

TABLE 1.

TYPE OF TEST	PURPOSE	TEST ENVIRONMENT	LOADING
1. BASELINE STATIC LOADS	OBTAIN BASELINE TEST DATA	AMBIENT	MAXIMUM SHEAR, TORSION, AND BENDING
		HOT-DRY	MAXIMUM BENDING
2. THERMAL CYCLE	EVALUATE THERMAL EFFECTS	HOT-WET COLD-WET	NONE
3. FIRST FATIGUE SPECTRUM	DEMONSTRATE FATIGUE CAPABILITY	COLD-WET	FATIGUE SPECTRUM TO 36,000 FLIGHTS
4. DESIGN LIMIT LOADS	VERIFY LIMIT LOAD CAPABILITY	COLD-WET	MAXIMUM SHEAR AND TORSION
		HOT-WET	MAXIMUM BENDING
5. FAIL-SAFE	DEMONSTRATE FAIL-SAFE CAPABILITY	AMBIENT	MAXIMUM BENDING AND TORSION
6. SECOND FATIGUE SPECTRUM (WITH DAMAGE)	MONITOR DAMAGE GROWTH	COLD-WET	FATIGUE SPECTRUM TO 42,000 FLIGHTS
7. DAMAGE TOLERANCE	DEMONSTRATE TOLERANCE TO INDUCED DAMAGE	COLD-WET	MAXIMUM SHEAR, TORSION, AND BENDING
8. STRUCTURAL FAILURE	DETERMINE RESIDUAL STRENGTH	COLD-WET	MAXIMUM BENDING TO FAILURE

INDUCED DAMAGE

Following the completion of the fail-safe testing and prior to the second fatigue spectrum test, damage was inflicted on the structure as shown in Figure 9. Impact damage was inflicted on the thick spar cap laminate in two locations and in the center of a skin panel bay in one location. A one-inch-diameter debond and a one-inch-long sawcut were made in two other skin panel bays. A 1/4-inch-long sawcut in the corner of the rear spar actuator cutout completed the inflicted damage. Each damage site was inspected ultrasonically to determine the extent of damage not apparent by visual examination. Testing was then resumed and continued through the end of the second life-cycle fatigue spectrum test. None of the damaged areas exhibited any damage growth except for the impact damage to the aft center spar cap at Z_{FR} station 352. NDI checks during the test indicated that the damage in this location increased in size by approximately 40 percent over the initial damage by the end of 21,000 flights (1/2 lifetime). Post-test visual and NDI inspections indicated no further damage growth.

After the second life-cycle test was completed, the damage tolerance tests were run followed by the final residual strength test to structural failure. The damaged areas were not repaired for these tests.

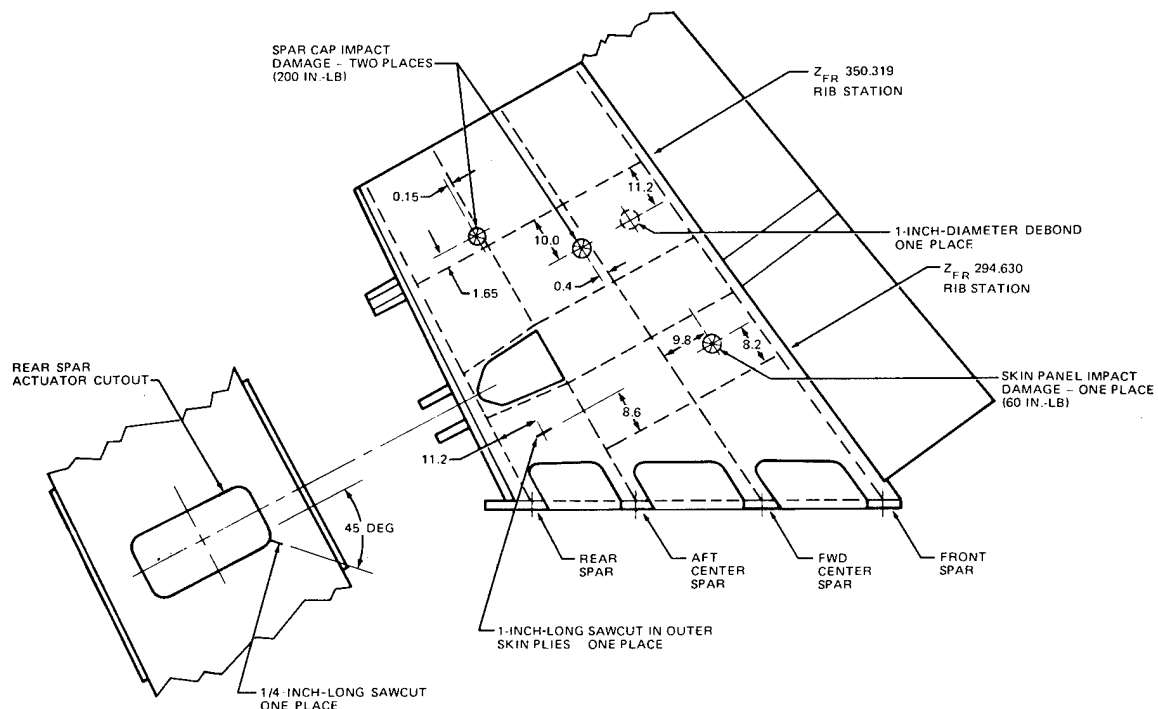


FIGURE 9.

RESIDUAL STRENGTH TEST

During the residual strength test, loading continued to 144 percent of design limit load (96 percent of design ultimate) when failure occurred suddenly on the compression side. Figure 10 shows the failures in the right skin and leading edge. Although there was no requirement to obtain any specific load level at failure, this failure was considered somewhat premature in that: (1) an undamaged structure would not be expected to fail before reaching 160 percent design limit load, and (2) none of the observed failures occurred through the damaged areas or in the high strain regions in the actuator cutouts.

Posttest investigations revealed that failure originated in the rear spar web at the lower access opening at Z_{FR} station 342. The failure was attributed to high stress concentrations at the edge of the access opening as a result of improper fit in the fasteners attaching the load-carrying access covers to the spar webs. This mode of failure as well as the sequence of failure through the structure were validated by finite-element analysis. The cause of failure was also verified by tests on a representative test panel.

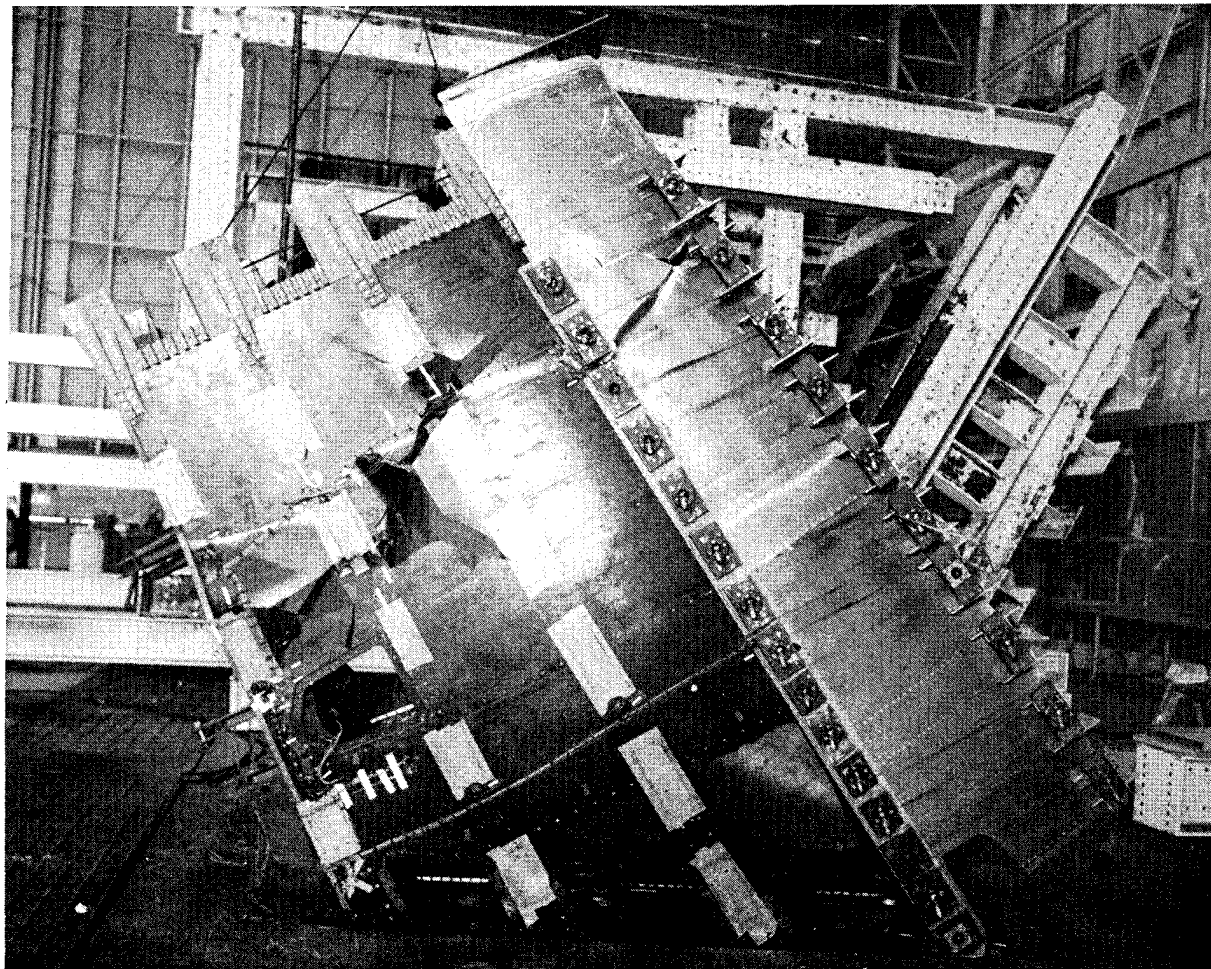


FIGURE 10.

FULL-SPAN GROUND TEST UNIT

The CVS ground test unit included the complete composite structural box, the aluminum leading edge fairing, VOR antenna panels, tip antenna assembly, and rudder hinge fittings. Trailing edge panels and internal control subsystems were not installed. Figure 11 shows the completed test article before it was transferred to the test laboratory.

This was the second full-span ground test article built under the CVS program. The first test article experienced a premature structural failure while undergoing the initial series of baseline limit load tests. The failure was attributed to high stress concentrations in the rear spar web at the edge of the lower access opening. The high-stress concentrations were caused by improper quality of fit in the fasteners attaching the load-carrying access cover to the spar web.*

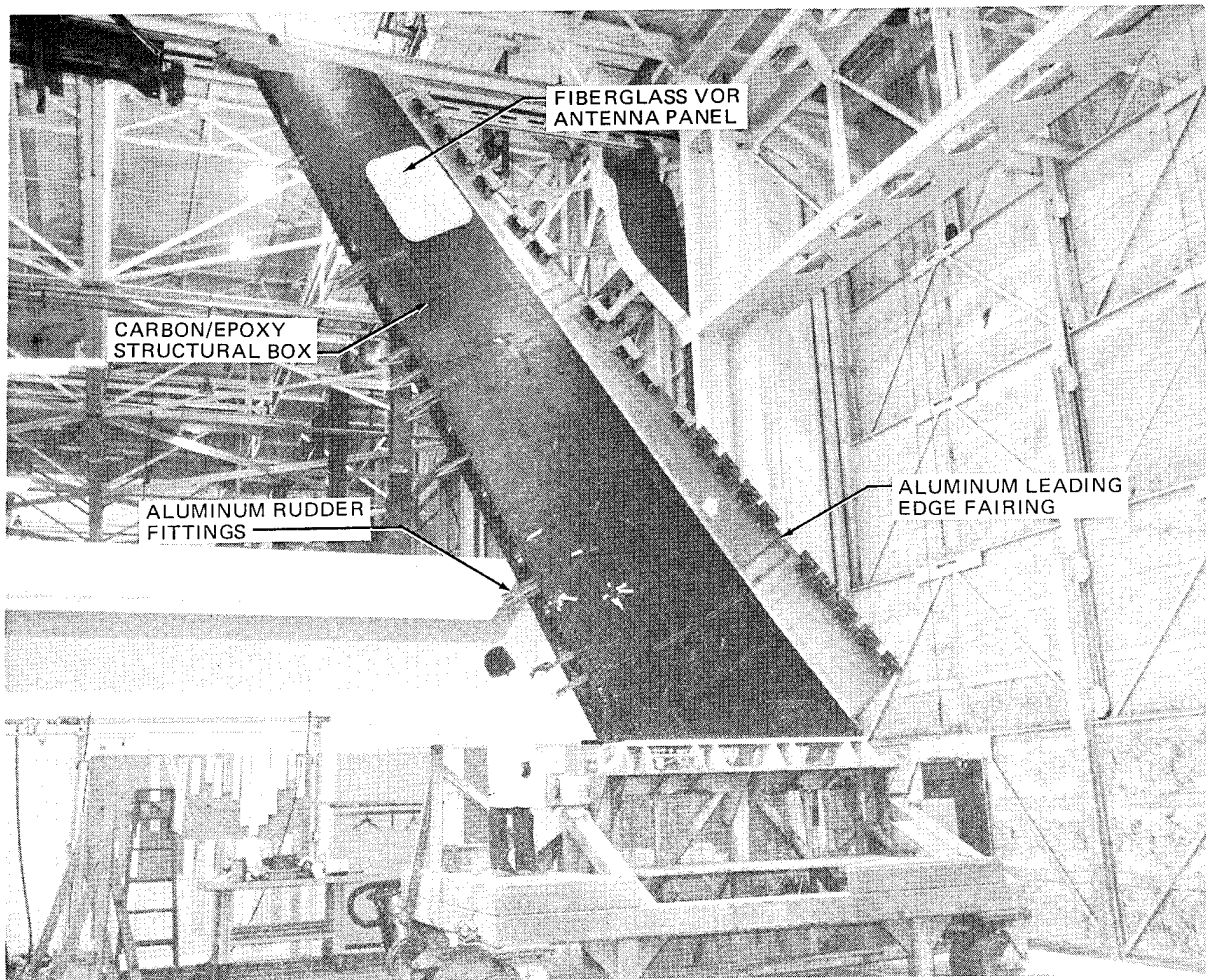


FIGURE 11.

* The failure investigation is covered in NASA Contractor Report 3715, "DC-10 Composite Vertical Stabilizer Ground Test Program", August 1983.

TEST SETUP

The test article was installed horizontally in the test fixture with the rear spar down and oriented parallel to the floor (Figure 12). This was the same orientation as for the stub box and was chosen to enable test loads to be applied to either side of the structure. The test article was bolted to the same root support structure in the test fixture used for the stub box testing.

A total of 29 load actuators (or load jacks) was used to apply loads to the test component. Sixteen load jacks (eight on each side) applied loads to the composite torque box through the compression whiffing system. The remaining 13 load jacks applied loads through the rudder hinge and tie-rod brackets and through the rudder actuator support brackets.

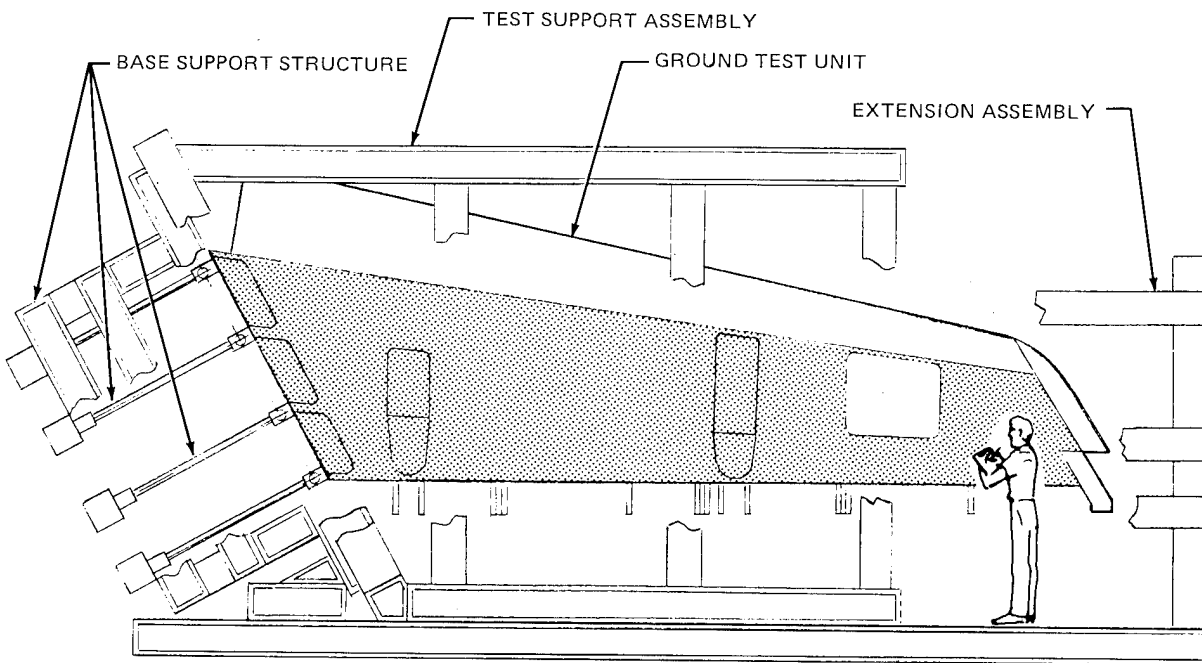


FIGURE 12.

TEST PROGRAM SUMMARY

All testing was conducted under laboratory ambient conditions. The completed structural test program is summarized in Table 2.

TABLE 2.

TYPE OF TEST	PURPOSE	LOADING
1. LIMIT LOAD TESTS	OBTAIN BASELINE DATA	MAXIMUM SHEAR, TORSION AND BENDING CASES
2. FIRST FATIGUE SPECTRUM TEST	DEMONSTRATE FATIGUE CAPABILITY	FATIGUE SPECTRUM TO 42,000 FLIGHTS
3. ULTIMATE LOAD TEST	DEMONSTRATE STRENGTH OF STABILIZER	MAXIMUM SHEAR CASE
4. SECOND FATIGUE SPECTRUM TEST (WITH DAMAGE)	DEMONSTRATE 2 LIFETIMES CAPABILITY	FATIGUE SPECTRUM TO 42,000 FLIGHTS
5. FAIL-SAFE TEST (WITH DAMAGE)	DEMONSTRATE LIMIT LOAD FAIL-SAFE CAPABILITY	MAXIMUM BENDING CASE
6. RESIDUAL STRENGTH TEST (DAMAGE REPAIRED)	DETERMINE RESIDUAL STRENGTH OF REPAIRED STRUCTURE	MAXIMUM BENDING CASE

INDUCED DAMAGE

Following the ultimate load test, the test setup was revised in preparation for the second life-cycle fatigue test. Before this test was conducted, impact damage was inflicted in the rear spar web at Z_{FR} station 370 and in the web of the AMC7880-5 rib in the upper actuator bay. These locations are indicated in Figure 13. The intent was to inflict a type of service-related damage that might occur in performing maintenance tasks on rudder actuators or hinge brackets.

Subsequent evaluation of strain data from the ultimate load test revealed that a failure (crack) had occurred in the front spar web approximately 7 feet from the tip. This was confirmed by a visual reexamination of the area after removal of the leading edge fairing at the conclusion of the test program. The data indicated that the failure had occurred at the time the noise was heard at 140 percent of design limit load. This failure is also shown in Figure 13.

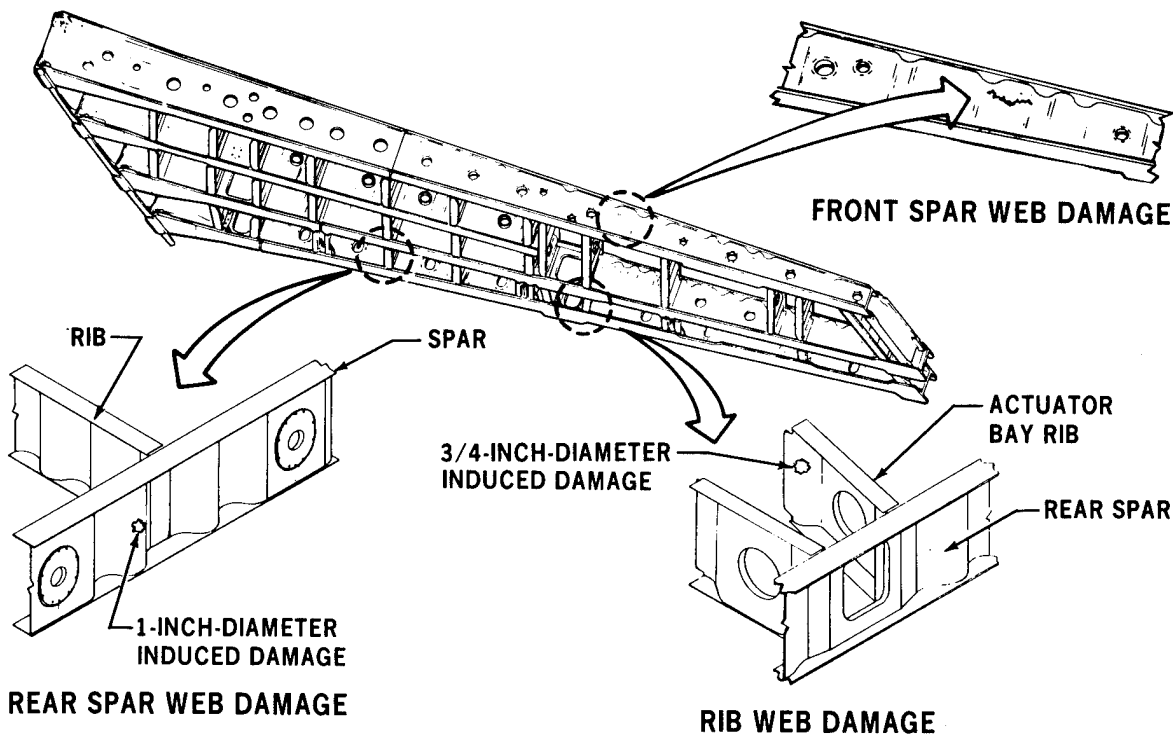


FIGURE 13.

REAR SPAR WEB DAMAGE

The rear spar web damage was caused by a 1-inch-diameter blunt impactor driven through the web using a rivet gun, which resulted in a 1 inch by 2-1/2 inch broken and delaminated area around the impact site. The spar web damage is shown in Figure 14. The spar web in this area consisted of four plies of carbon/epoxy cloth laid up in a pseudo-isotropic pattern.

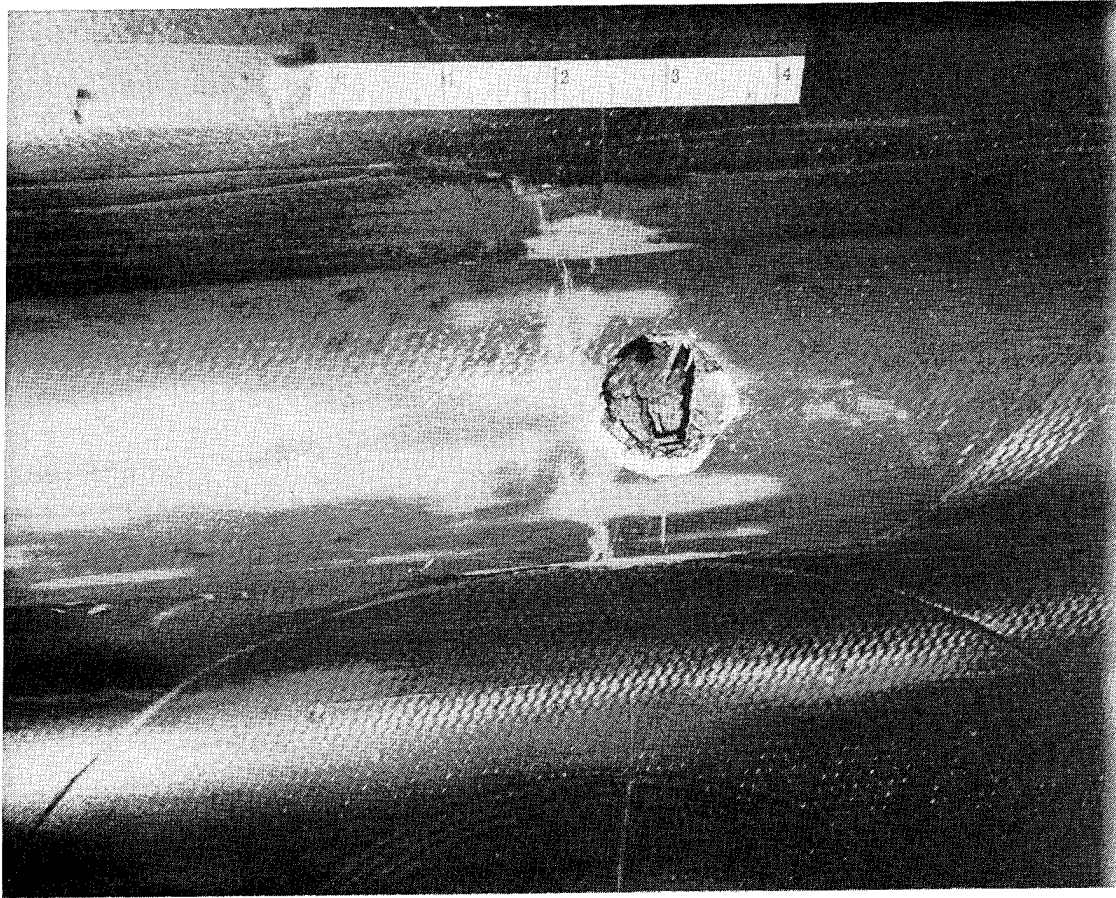


FIGURE 14.

ACTUATOR BAY RIB DAMAGE

The actuator bay rib damage was caused by a 3/4-inch-diameter sharp impactor. The rib web damage is shown in Figure 15. The rib web consists of two plies of carbon/epoxy cloth oriented at ± 45 degrees.

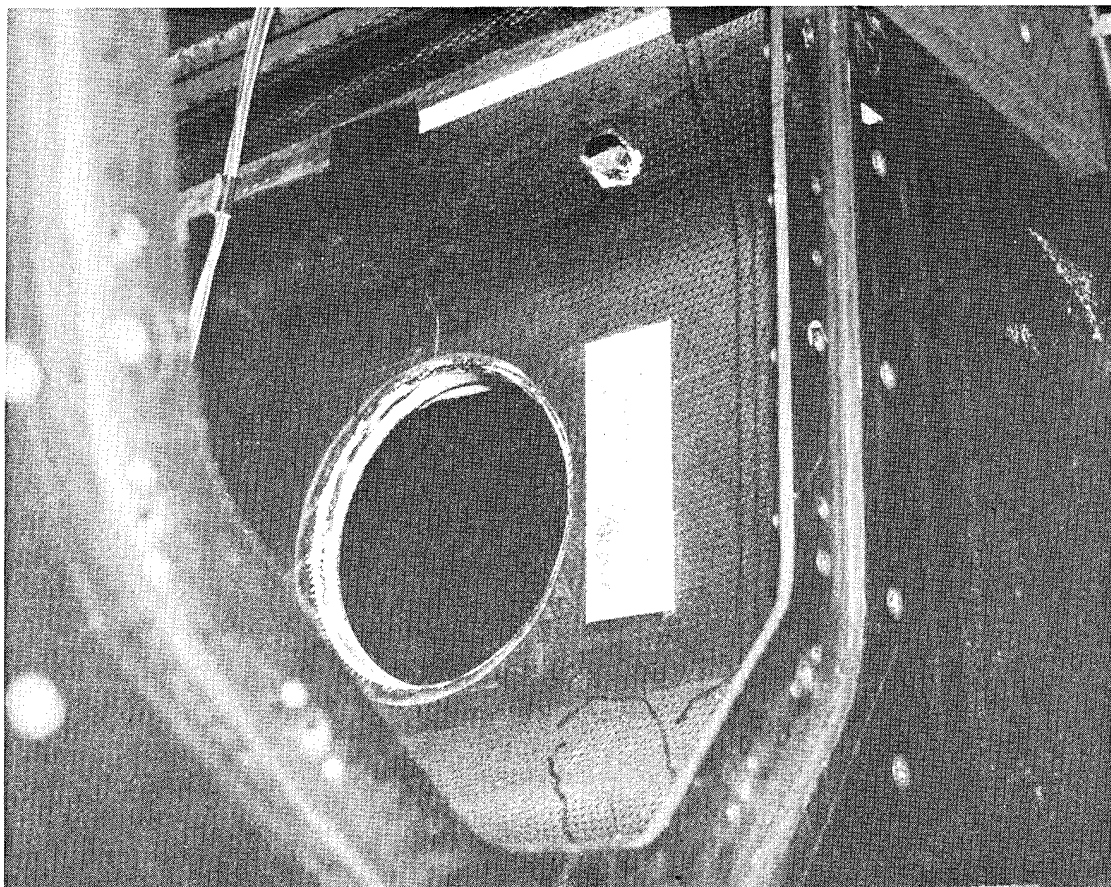


FIGURE 15.

FRONT SPAR WEB DAMAGE

Figure 16 shows the crack in the front spar web that occurred during the ultimate load test at 140 percent of design limit load.

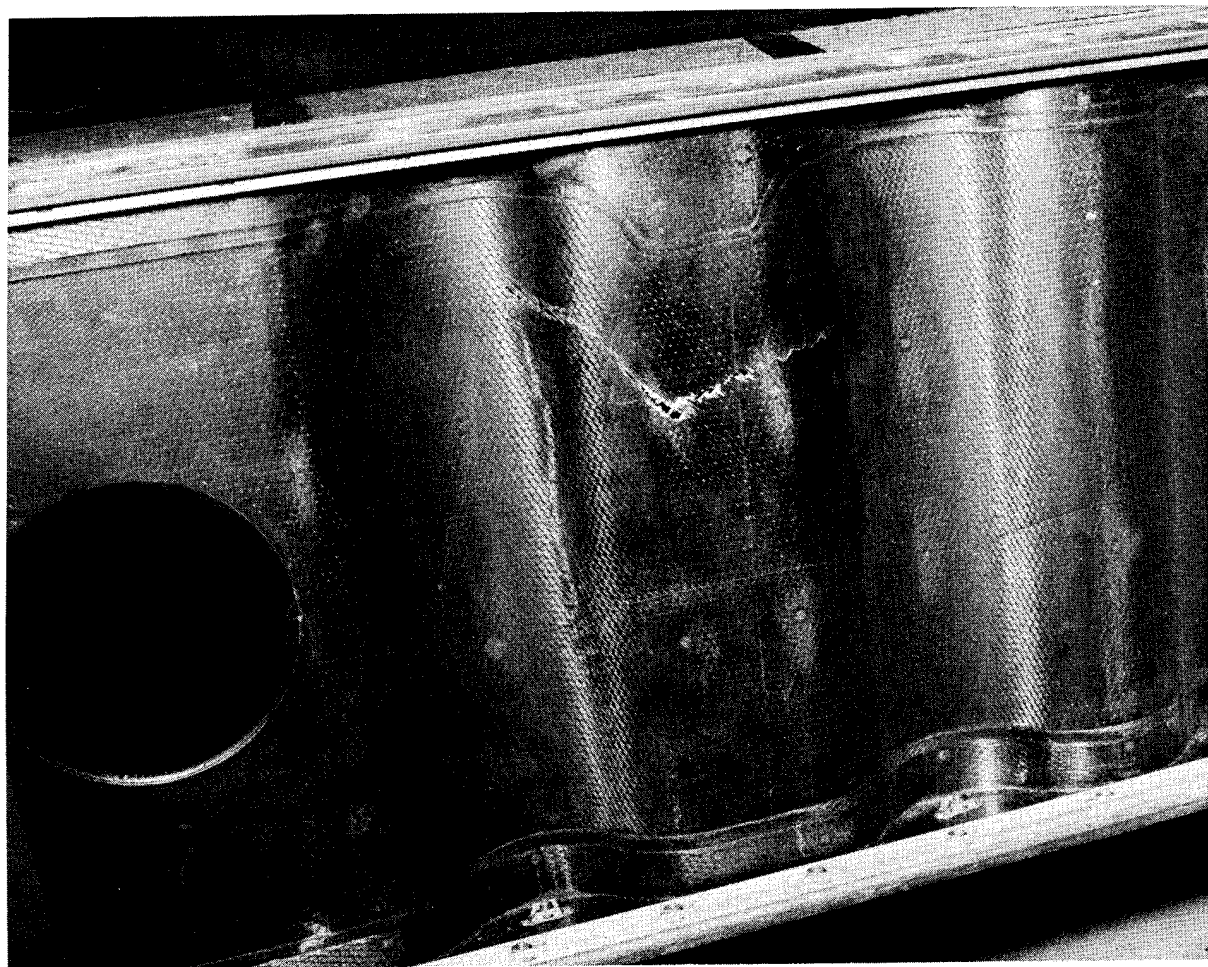


FIGURE 16.

CRACK GROWTH IN REAR SPAR AT 97 PERCENT
DESIGN LIMIT LOAD

The structure was loaded in a critical bending condition to 100 percent of limit load. At 97 percent of limit load, a fracture occurred through the damaged area in the rear spar. The loading was continued to 100 percent of limit load, then immediately removed so the crack could be inspected. The crack extended diagonally across the hole for approximately 8 inches. The upper crack tip arrested at the rib intersection and the lower crack tip stopped at a doubler buildup at an access hole. This damage is shown in Figure 17.

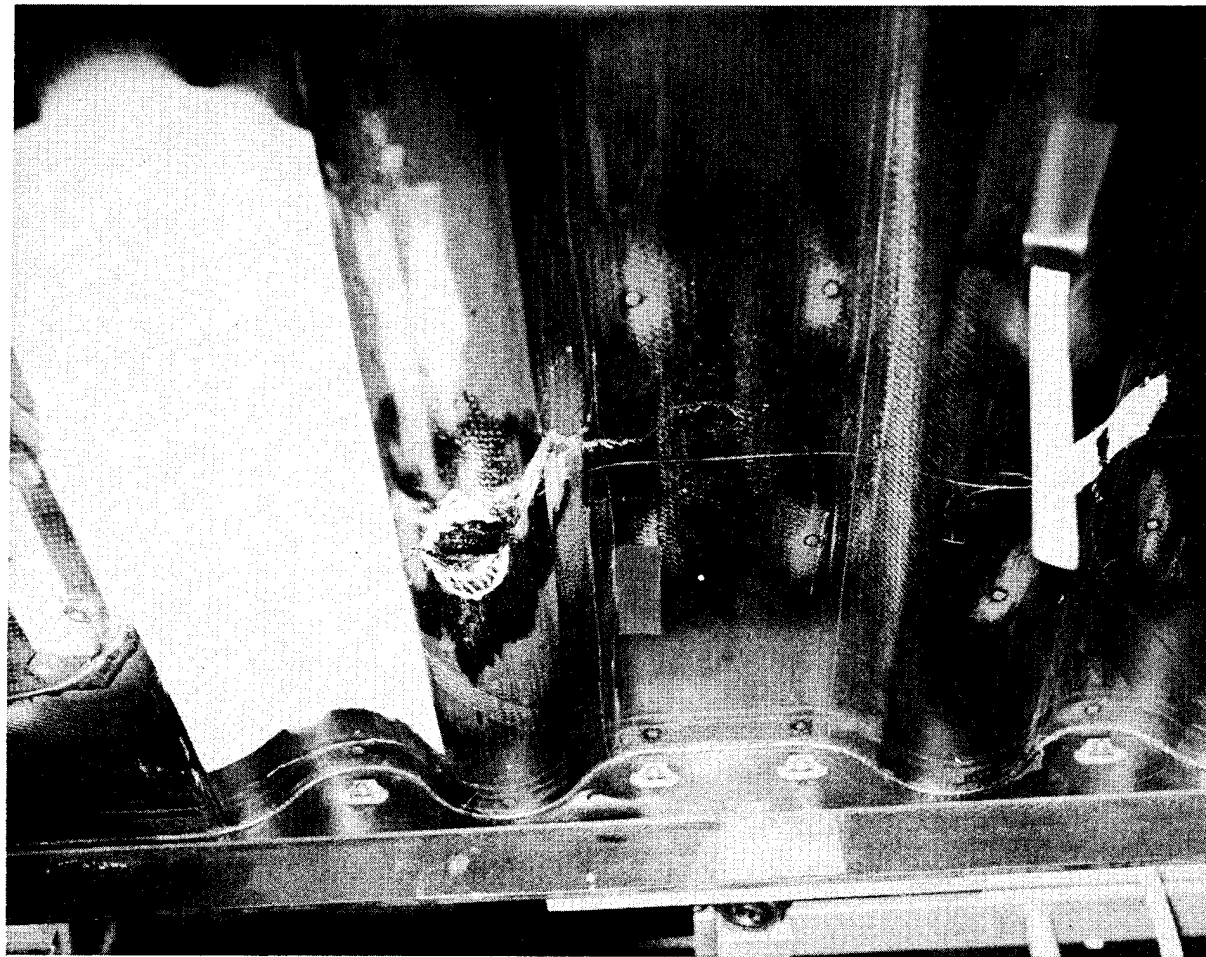


FIGURE 17.

CRACK GROWTH IN REAR SPAR AT 100 PERCENT DESIGN LIMIT LOAD

Since the load was immediately removed at 100 percent of limit load after the fracture occurred, the test did not comply with the FAA requirements of a 3-second hold with a full load, and it was necessary to rerun the test. The retest represented a very severe test of the fail-safe capability of the CVS with major damage. This time, full load was held for the required 3 seconds. The crack grew but self-arrested and was stable during the hold period. Posttest visual inspection revealed that the crack grew an additional 5 inches toward the tip past the rib intersection and self-arrested in the middle of the next bay.

Ultrasonic inspection revealed that there were delaminations in the region of the crack. Figure 18 shows the final spar web damage with the delaminated area outlined with white paint. The initial 3/4-inch hole in the actuator bay rib did not change in size during the tests.

The damage-tolerance tests demonstrated the durability of the composite structure when exposed to a realistic loading spectrum with preexisting damage. The fail-safe tests clearly demonstrated that the structure was able to sustain limit load even with severe damage.

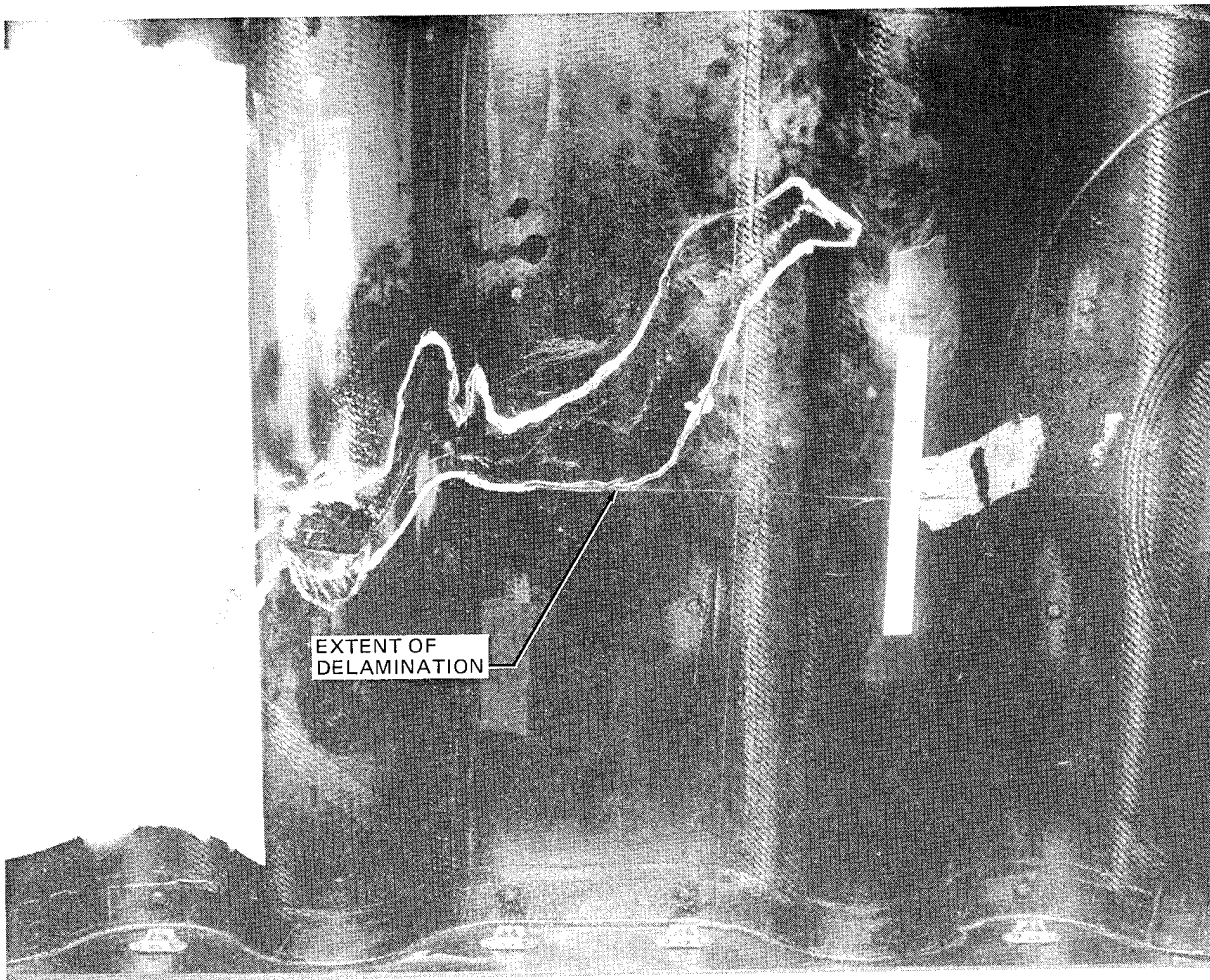
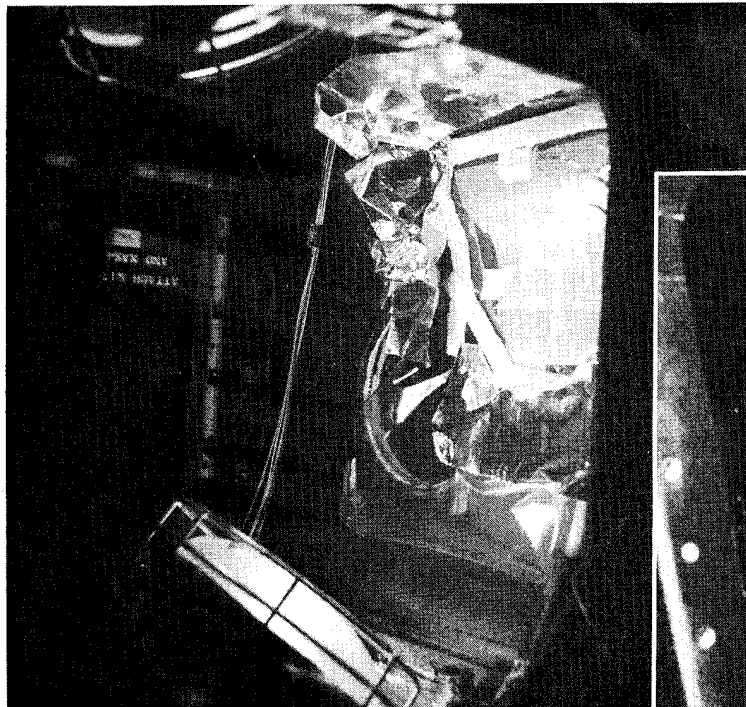


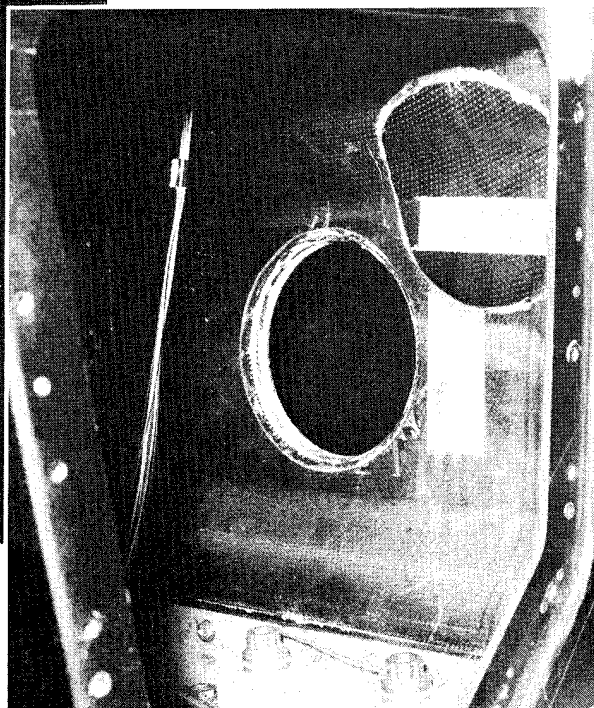
FIGURE 18.

RIB REPAIR

The delaminated area around the hole was trimmed away to provide a clean hole boundary. Prior to bonding, the surfaces were prepared by grit-blasting and a water wash. The bond surface preparation was verified by a water-break test. The patch was then bonded, with a scrim cloth backing used to maintain the bond thickness. The patch was bagged and cured under vacuum pressure. A portable vacuum pump and temperature-controlled heat lamp were used in the repair. Figure 19 shows the rib repair in progress and the completed repair.



(a) REPAIR IN PROGRESS



(b) COMPLETED REPAIR

FIGURE 19.

REAR SPAR REPAIR

The delaminated area around the crack was trimmed away, leaving an elongated slot which measured 12 inches by 2.5 inches (Figure 20). In addition to the visible damage, it was noticed that the rib-to-spar web attachment angle was separated away from the spar. To ensure that air would not leak through the bond line in this patch, a vacuum bag was used on both sides of the repair. This repair necessitated access to the back, so the two adjacent bonded and bolted access covers were removed, both above and below the damage. For convenience, these doors were subsequently replaced with aluminum doors.

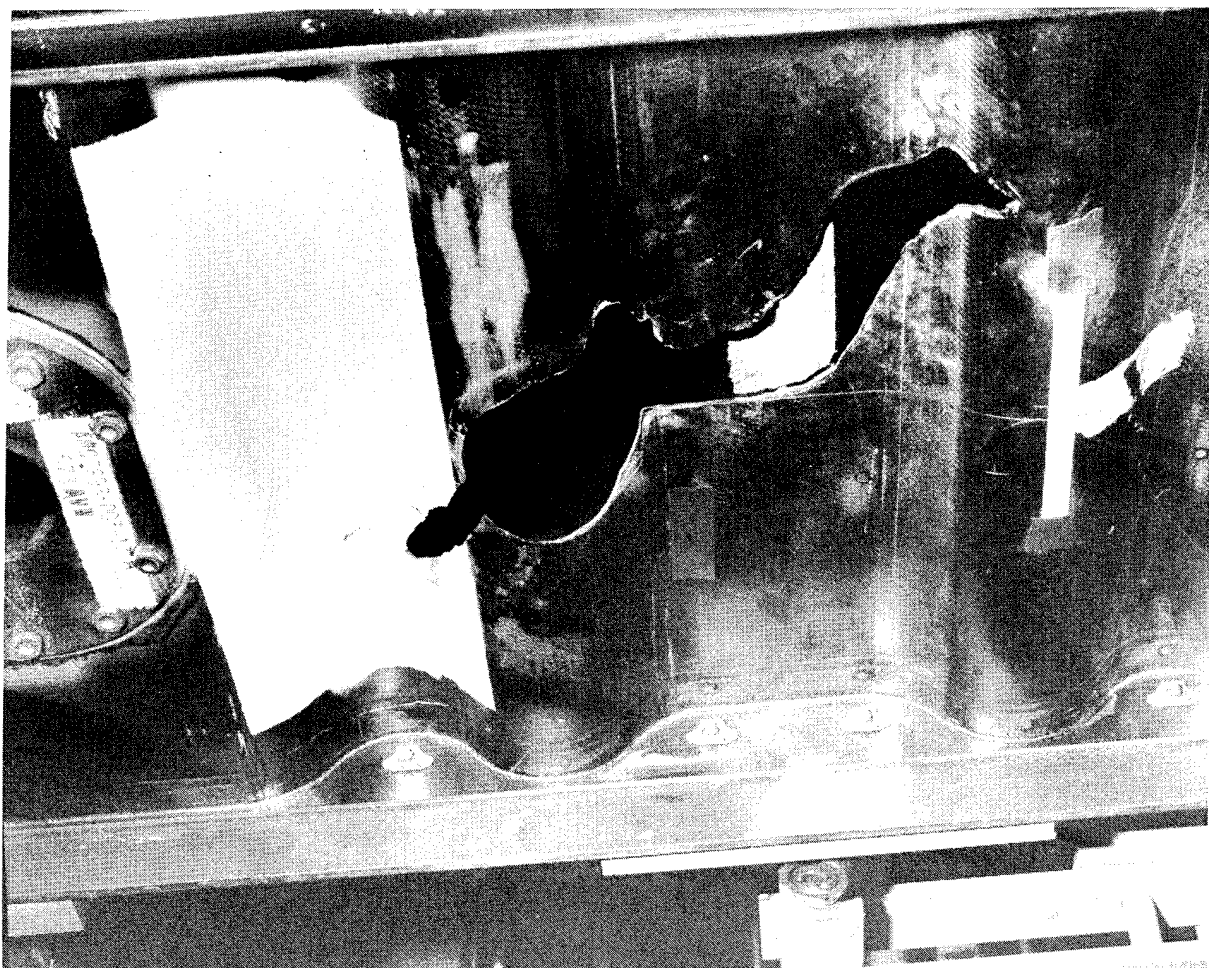


FIGURE 20.

REAR SPAR REPAIR PROCEDURE

Fiberglass angles impregnated with resin were laid over the delaminated rib-to-spar attachment angles and allowed to cure. These angles provided a vacuum seal for the inside bag. The vacuum bag setup was tested for leakage and then the structure was prepared for bonding. The patch was trimmed to a 19-inch by 13.5-inch size. Both the patch and the web were grit-blasted and washed with water. The surface preparation was verified by the use of a water-break test. The patch was then bonded, with a scrim cloth backing used to maintain the bond thickness. The outside vacuum bag was sealed and the patch was cured under vacuum pressure and heat. After the cure cycle, aluminum clamp-up plates were bolted through the delaminated rib-to-spar attachment angle to reinforce the angle and prevent further delaminations. Replacement doors were bonded and bolted over the access openings. The repair is shown in schematic form in Figure 21.

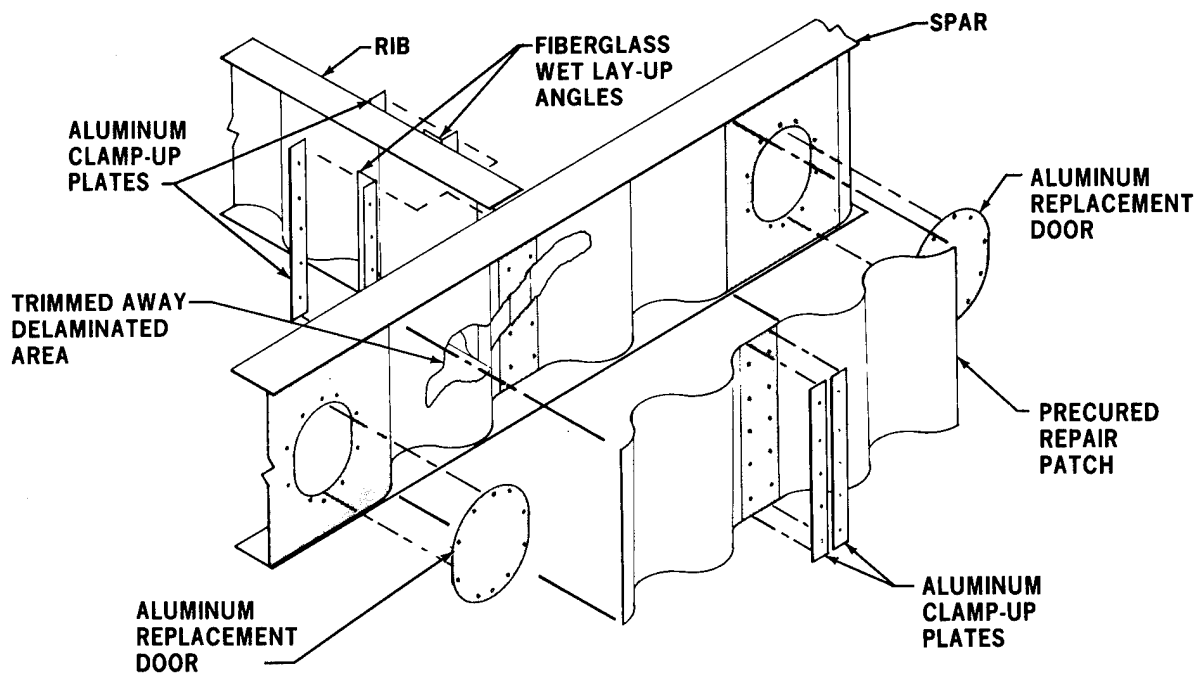


FIGURE 21.

COMPLETED REAR SPAR REPAIR

Figure 22 shows the completed rear spar repair.



FIGURE 22.

RESIDUAL STRENGTH TEST FAILURE

The final residual strength test was conducted on 1 July 1983. The objectives of this test were to determine the ultimate strength of the composite structure and to verify the structural adequacy of the two repairs.

In the test, loads simulating the critical bending condition were applied to the test article in a direction that placed the left side in compression. The loads were applied continuously to failure at a constant rate of approximately 1 percent of design limit load per second. Failure occurred in the left skin panel at 167 percent of design limit load. The skin panel spar cap material failed in compression, initiating at Z_{FR} station 329 (Figure 23). No failures were evident in the two repaired areas or in any of the rear spar access cover installations.

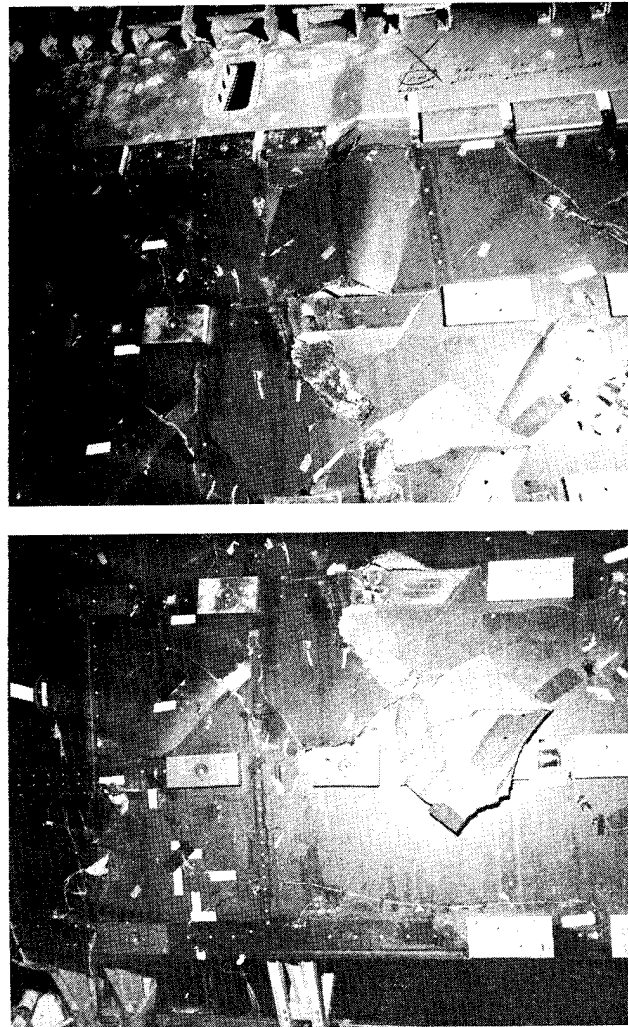
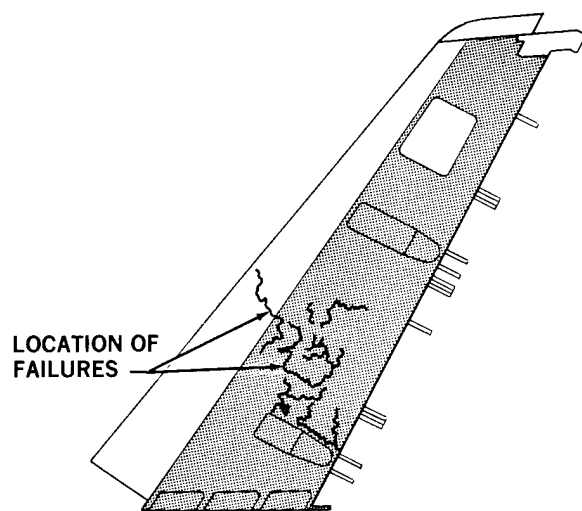


FIGURE 23.

BENDING MOMENT AT TEST FAILURE

A comparison of the applied (test) bending moment with the design bending moment at the time of structural failure (167 percent of design limit load) is presented in Figure 24. The applied bending moment at the failure location (Z_v station 300) compares well with the design bending moment.

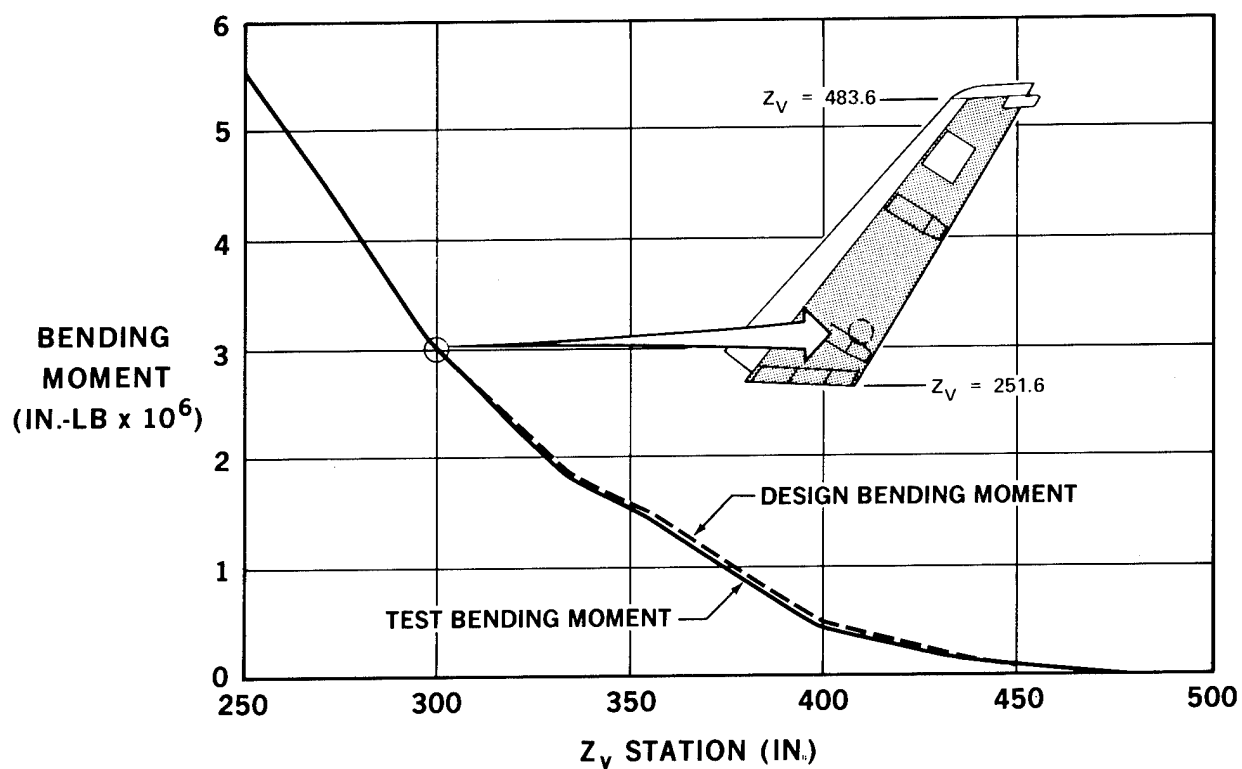
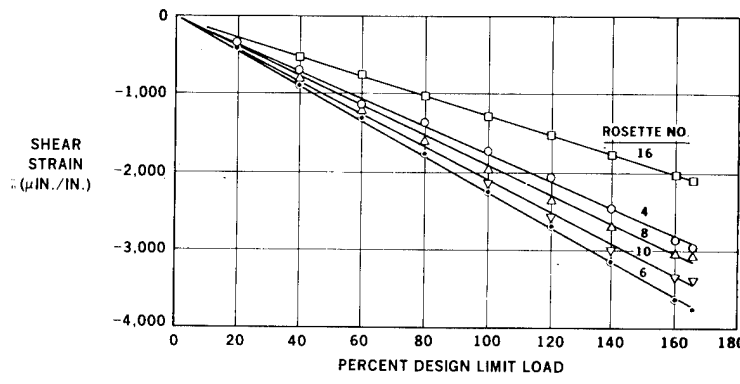
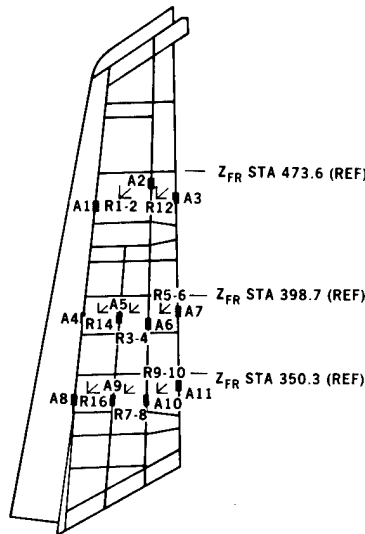


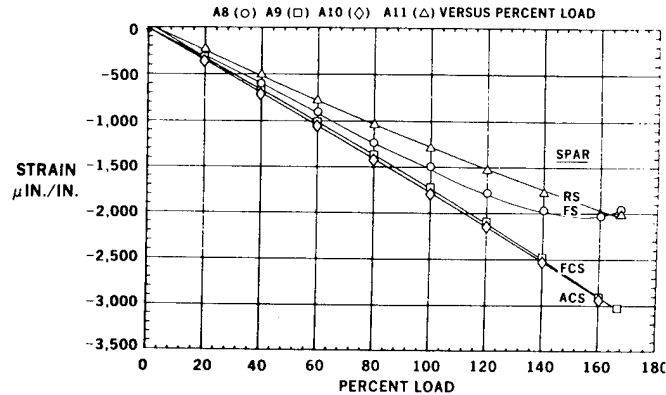
FIGURE 24.

STRAIN DATA FROM RESIDUAL STRENGTH TEST

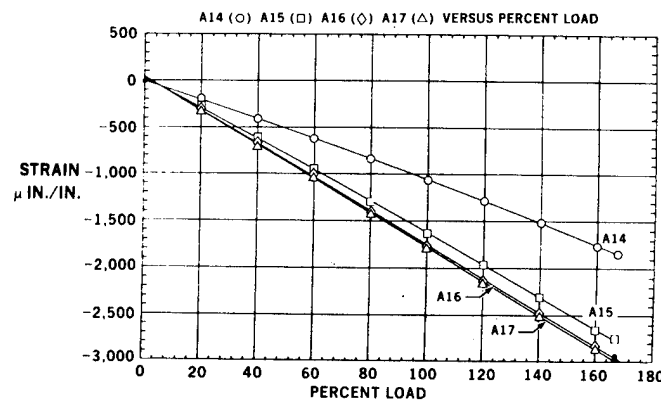
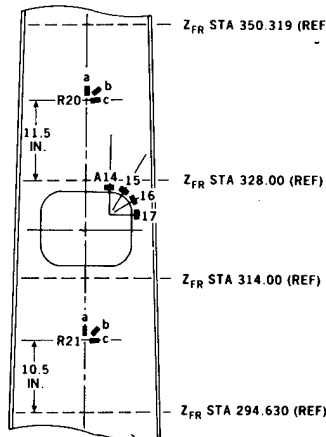
Some of the peak strain data are shown in Figure 25. The maximum skin panel shear strain at structural failure was $3,758 \mu\text{in./in.}$ and occurred in the aft skin panel bay at Z_{FR} station 387 (Figure 25a, Rosette No. 6). The maximum spar cap axial strain was $3,028 \mu\text{in./in.}$ compression and occurred in the forward and aft center spar caps at Z_{FR} station 339 and 336.7, respectively (Figure 25b, Strain Gages A9 and A10). The maximum strain in the aft center spar actuator cutout was $2,965 \mu\text{in./in.}$ compression (Figure 25c, Strain Gage A17). All strain levels were within expected limits.



(a) SKIN PANEL SHEAR STRAIN



(b) SPAR CAP AXIAL STRAIN



(c) ACTUATOR CUTOUT STRAIN

FIGURE 25.

FLIGHT LOAD/TEST LOAD/ANALYSIS CORRELATION

It was not practical to make an additional stress analysis of the complete structure for the test condition, but it was possible to allow the test to expose the minimum margin of safety. With the locations defined by the test failures, it was then possible to return to the detailed stress analysis, substitute the appropriate special test condition internal loads and room temperature material allowables, and recalculate the analytical margin of safety for the test condition (Figure 26).

This was done, and excellent correlation was obtained between this analytical solution and the test results, both in terms of failure mode (compression rupture) and load level (167 percent).

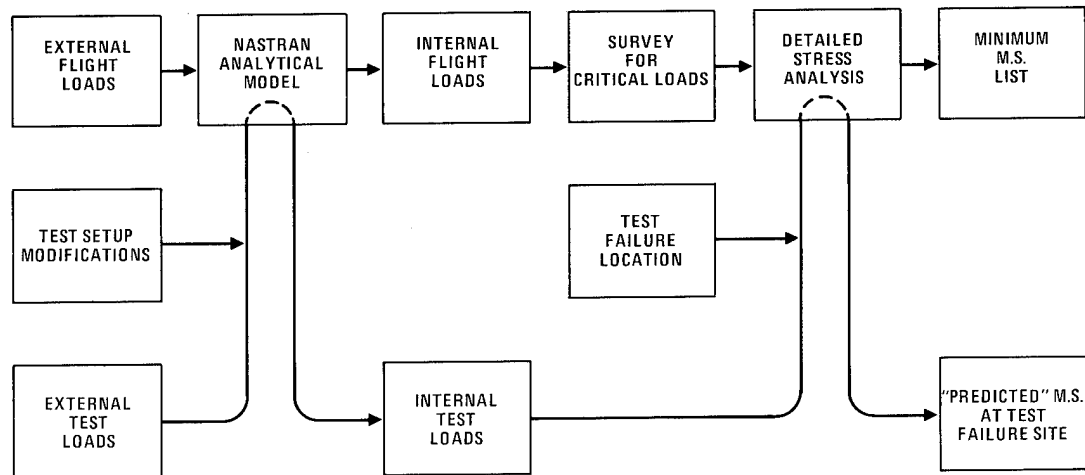


FIGURE 26.

NASTRAN ANALYSIS MODEL

The complete NASTRAN analysis model is shown in Figure 27. The front spar/leading edge thermal interface utilized a system of colinear bars at the joint plane.

The rudder segments were modeled as stick-and-web structures of appropriate stiffness and decreasing detail from the forward to the aft segments. All hinge, actuator, and tie-rod supports were modeled, and the rudder segments were modeled at the appropriate deflected positions for each analysis condition.

The structural box was modeled as a series of rib bulkheads, spars, and skin panels. Axial forces were carried by bar elements and quadrilateral plate elements, while shear forces were carried by shear panel and quadrilateral plate elements. Triangular plate elements were used in some instances. All elements were linearly elastic.

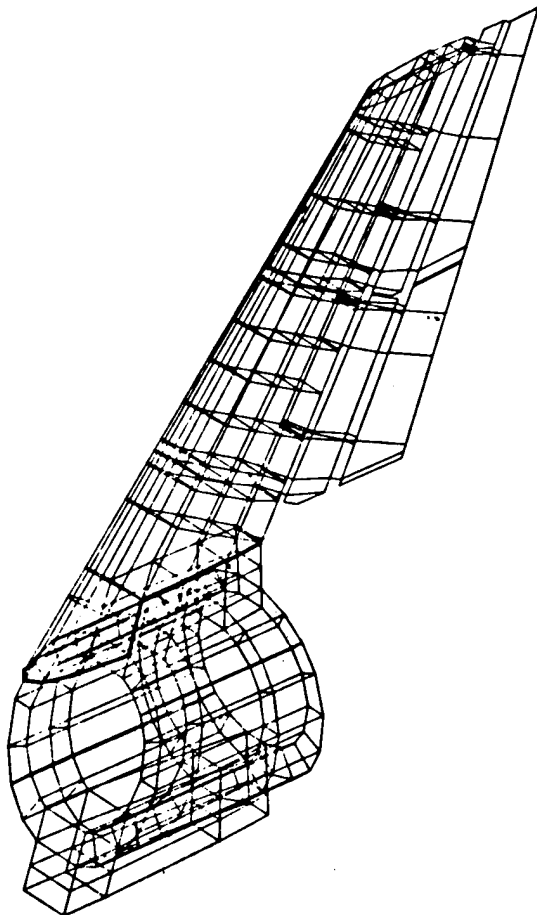


FIGURE 27.

SPANWISE STRAINS FROM GAGES R9A AND R10A

As the structure was loaded, the first sign of distress was a loud bang at approximately 153 percent of design limit load. There was no visible sign of damage to the structure. Subsequent examinations of the test instrumentation records showed only one anomaly corresponding to this noise. The spanwise leg of the inner surface rosette gage R9 showed an instantaneous loss of compressive strain, going to a $+1,300 \mu\text{in./in}$ tension strain (Figure 28). The opposite external surface rosette gage R10 showed only a very slight increase in strain and no other gages registered the event. Over the next 3 percent of applied load, the affected leg of R9 gradually recovered almost exactly back to the original strain loading rate and values. This strain gage record implies that the inner face sheet buckled away from the core, and by some as yet unexplained mechanism was persuaded to "reattach" itself. The general destruction of the specimen in this region as a result of the final failure made it impossible to clarify the issue by direct examination. This panel was analytically predicted to buckle at 150 percent of design limit load.

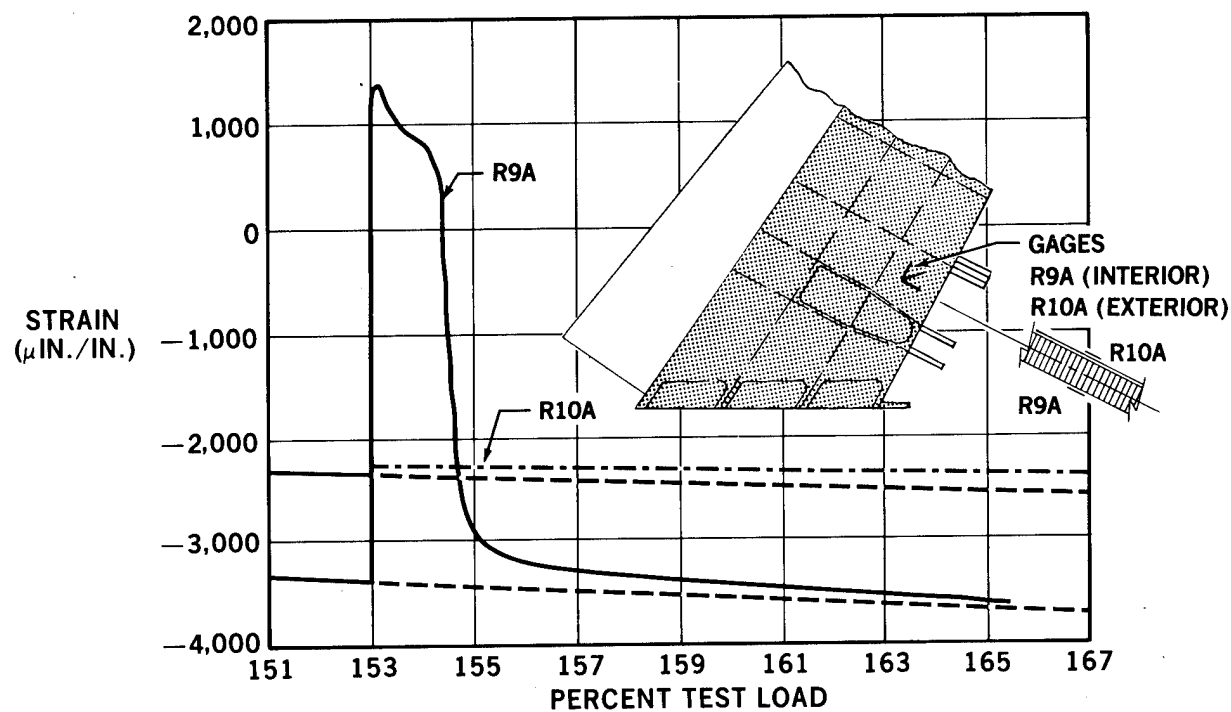


FIGURE 28.

MARGINS OF SAFETY WITH ALL STRUCTURE INTACT

At 167 percent of design limit load, a catastrophic failure occurred. Using the analysis method described previously, the analytical margins of safety in the region of the failure were derived and are shown in Figure 29.

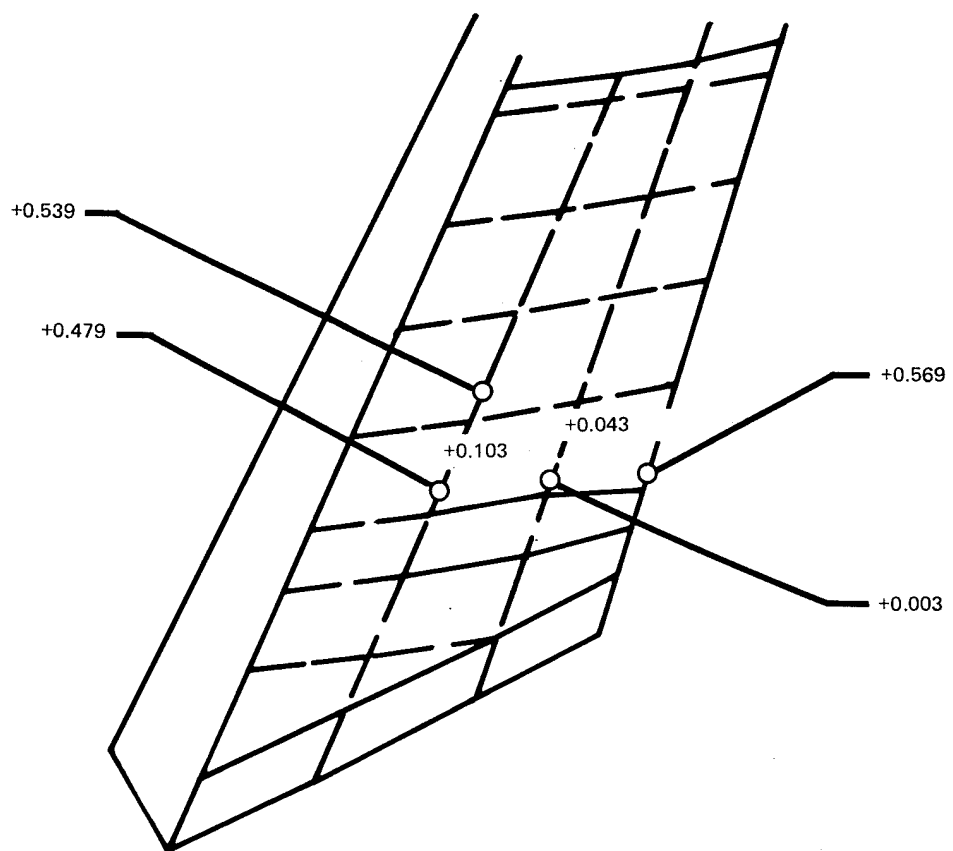


FIGURE 29.

LOCATION OF FAILURE IN AFT CENTER SPAR CAP

The analysis predicted that the failure would occur in the aft center spar cap, directly through a double row of attachments (Figure 30). The strain gage record and high-speed film showed that within one data scan (1/60th of a second) or one film frame (1/48th of a second), the aft center spar cap, the spar web at the same location, and the skin panel directly forward had all failed.

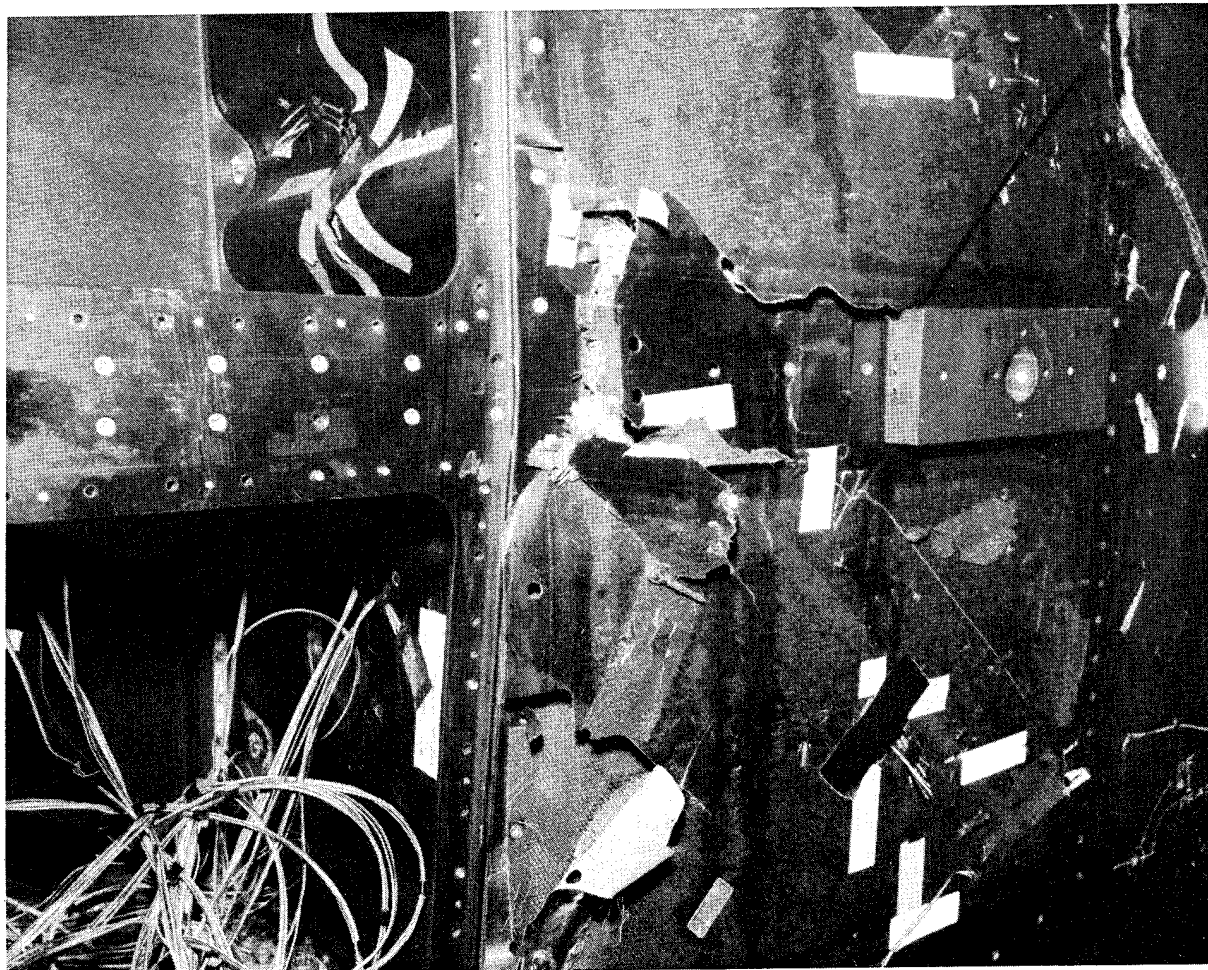


FIGURE 30.

MARGINS OF SAFETY WITH AFT CENTER SPAR CAP FAILED

The failure sequence was tested analytically by assuming the spar cap failed first and redistributing the internal loads to recheck the remaining margins of safety. Figure 31 shows the analytical margins of safety with the aft center spar cap failed. The redistribution of the spar cap axial load to the adjacent spar caps caused a considerable reduction in their margins of safety. However, that redistribution is accomplished by a large increment of shear flow, approximately 1,500 lb/in., in the skin panels to either side.

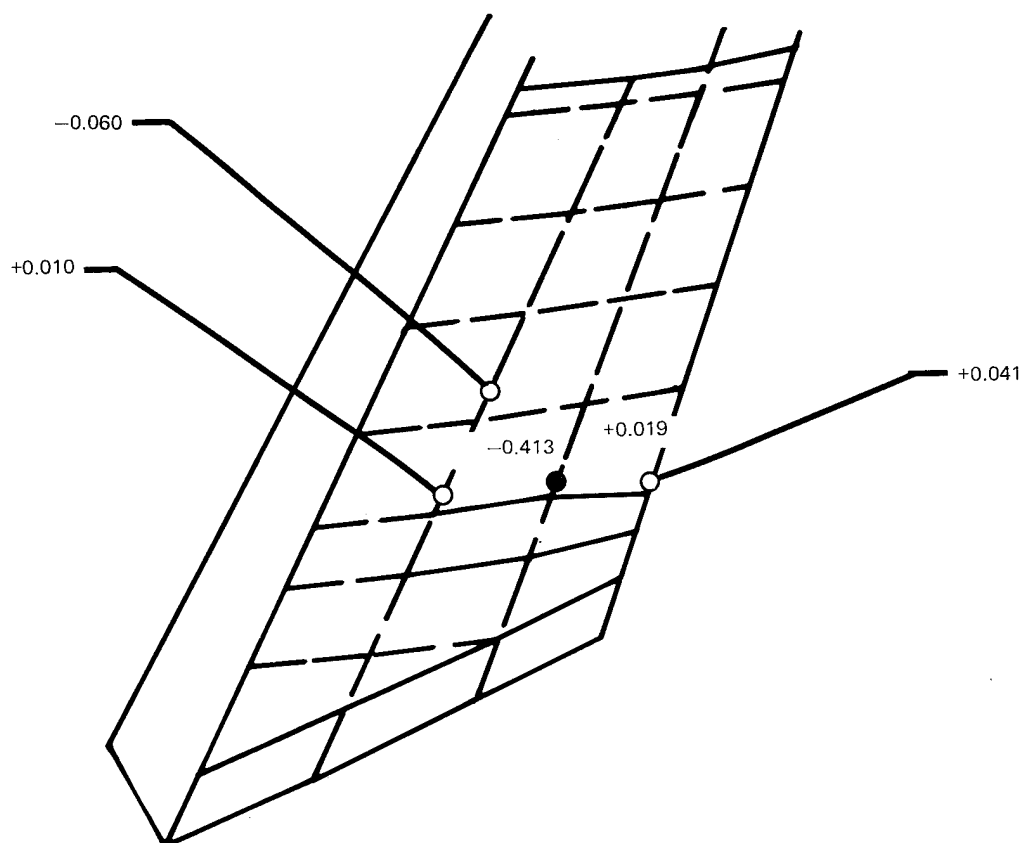


FIGURE 31.

SKIN PANEL TEST DAMAGE

Because of the direction of the shear flow already in the panels, each responds differently. The aft panel experiences essentially a reversal of its shear loading, with almost no effect on its margin of safety. The forward panel, on the other hand, experiences a tripling of its shear flow, which is instantly fatal. Figure 32 shows the central portion of this panel literally blown out of the structure, remaining attached only by the strain gage leads and the peel ply.

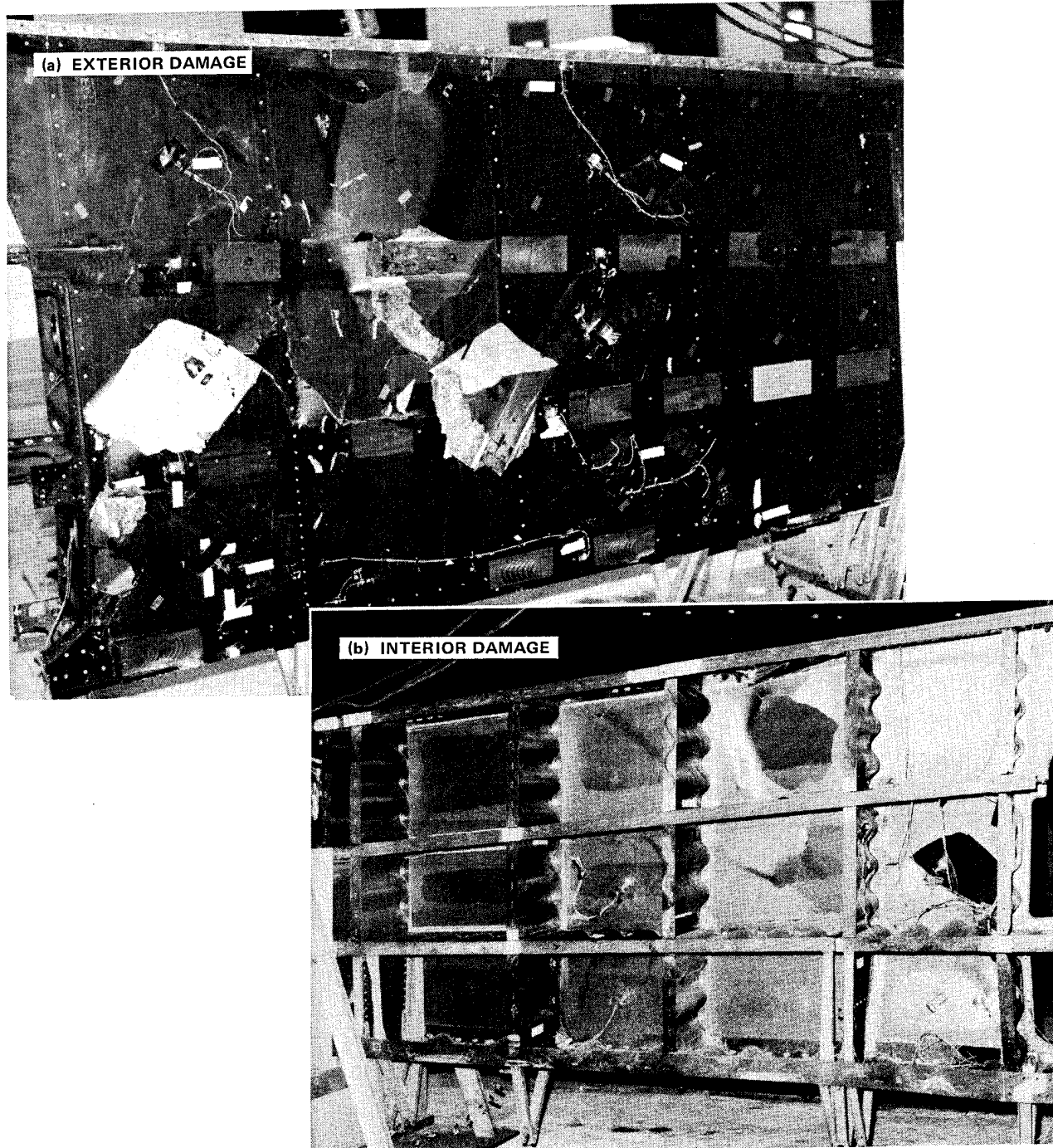


FIGURE 32.

LOCATIONS OF TEST DAMAGE

The final extent of the test damage to the specimen is shown in Figure 35.

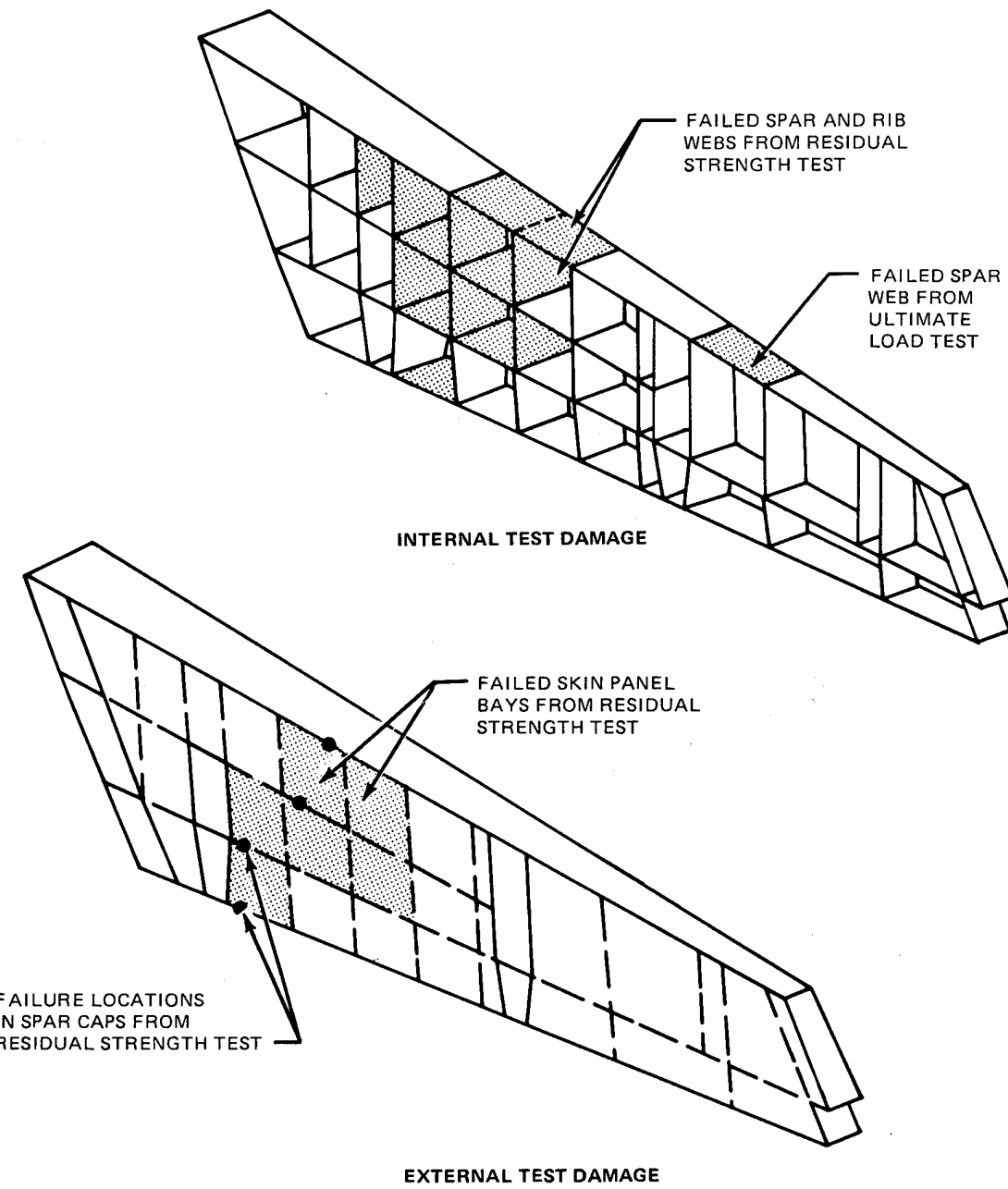


FIGURE 35.

MARGINS OF SAFETY WITH AFT CENTER SPAR CAP AND
SKIN PANEL FAILED

Assuming the spar cap and skin panel to be failed, the analytical margins of safety of the remaining structure were determined and are shown in Figure 33. Because of the failure of the skin panel, the rear spar becomes a stiffer load path, and the margin of safety decreases considerably.

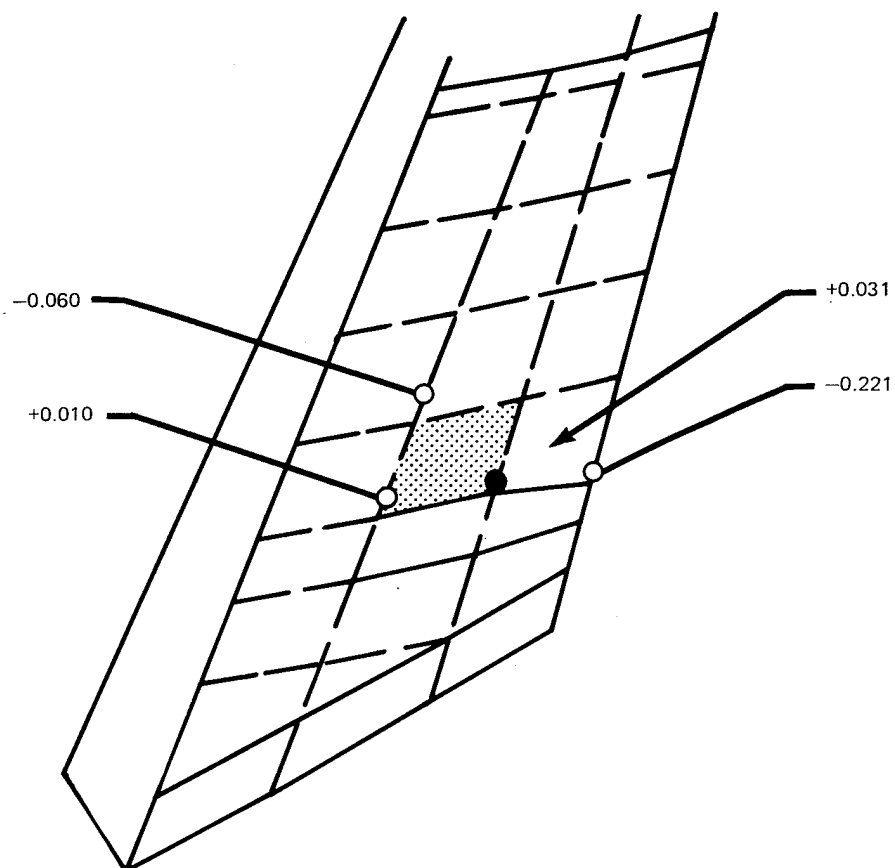


FIGURE 33.

FAILURE IN REAR SPAR CAP AND WEB

Analytically, the next failure in the sequence would be expected in the rear spar cap. The test record shows that no further failures occurred for approximately 0.06 second. This may be attributed to the lag time of the loading system. Again, in one data scan and one film frame, essentially all of the remaining structural damage occurred. Following the failure of the rear spar cap and web (Figure 34), the damage was so extensive that no further attempt was made to establish sequence.

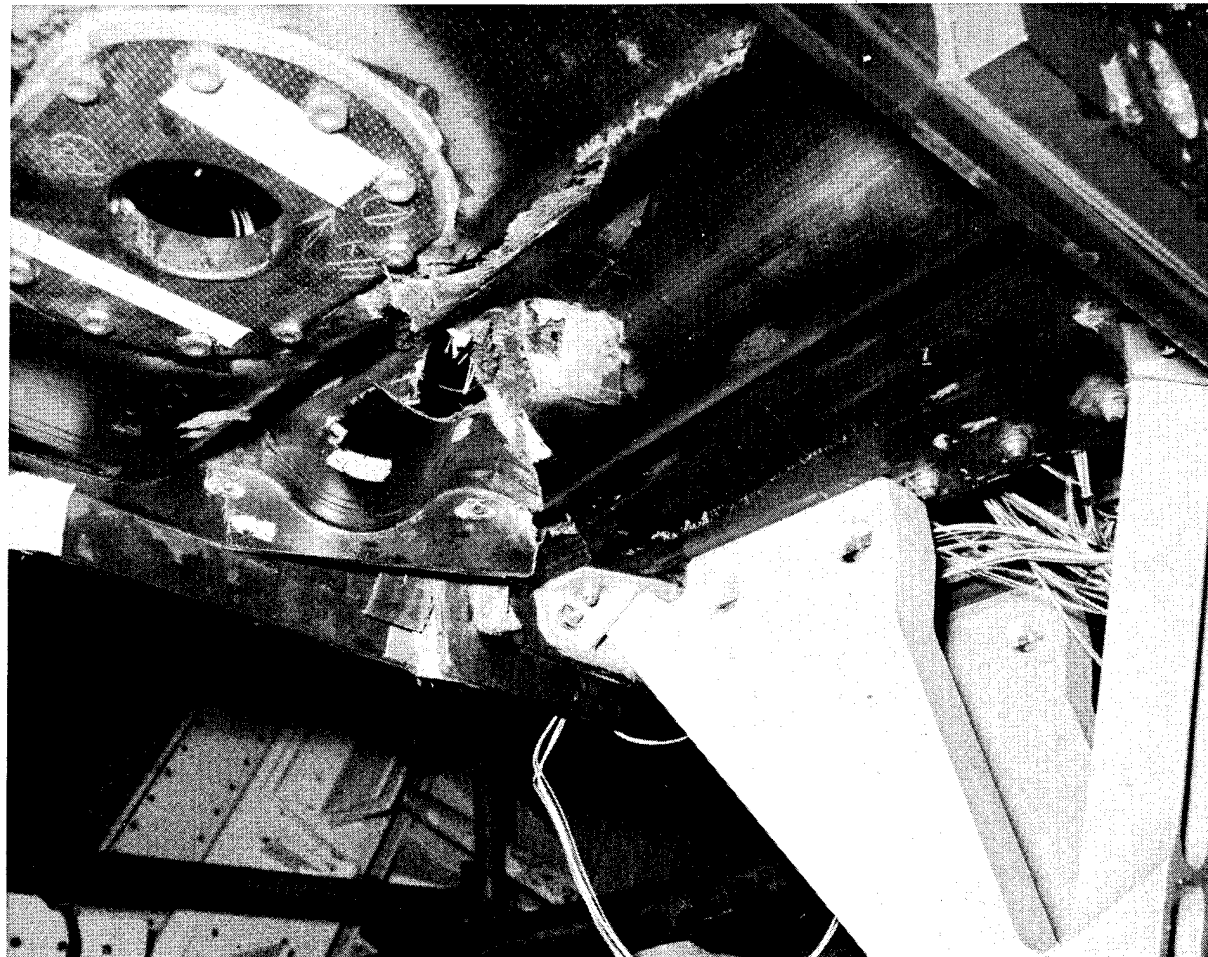


FIGURE 34.

THE FUTURE

COMPLETE FAA CERTIFICATION DOCUMENTATION

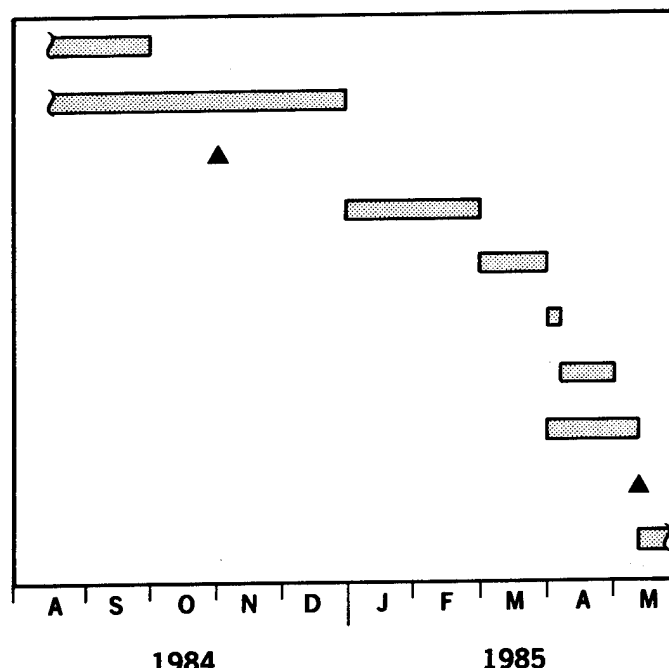
SELECT SERVICE EVALUATION AIRCRAFT

COMPLETE FLIGHT EVALUATION UNIT

CONDUCT FLIGHT TEST

OBTAIN FAA CERTIFICATION

FAA DOCUMENTATION — GROUND TESTS
FLIGHT ARTICLE ASSEMBLY
SELECT SERVICE EVALUATION AIRCRAFT
FLIGHT SYSTEMS INSTALLATION
STABILIZER INSTALLATION
GROUND VIBRATION TEST
FLIGHT TEST
FAA DOCUMENTATION — FLIGHT TEST
FAA CERTIFICATION
SERVICE EVALUATION



CONCLUSIONS

FATIGUE DAMAGE WILL NOT OCCUR

SMALL DAMAGE WILL NOT PROPAGATE

NO SPECIAL IN-SERVICE INSPECTIONS REQUIRED

PROPER FASTENER FIT CRITICAL

STRUCTURE IS DAMAGE-TOLERANT

FAIL-SAFE CAPABILITY DEMONSTRATED

STRUCTURAL ADEQUACY OF DESIGN FEATURES VERIFIED

THEORY AND ANALYSIS FOR OPTIMIZATION OF
COMPOSITE MULTI-ROW BOLTED JOINTS
CONTRACT NAS1-16857

Dr. L. J. Hart-Smith

Douglas Aircraft Company
Long Beach, California

ACEE Composite Structures Technology Conference
Seattle, Washington
August 13-16, 1984

THEORY AND ANALYSIS FOR OPTIMIZATION OF
COMPOSITE MULTI-ROW BOLTED JOINTS

ABSTRACT

This document reviews the key factors in the design and analysis of bolted composite joints. A consistent theory covers both single-row and multi-row joints. The analysis method relies on empirical modification factors that account for nonlinear behavior. Those factors, determined from single-bolt tests, have been found to apply to all practical structural joint configurations. The theoretical developments have occurred in parallel with an extensive test program that has verified the accuracy of the predictions. Optimum joint geometries have been identified. The joint strengths are predicted by the A4EJ computer program that models each fastener as a bi-elastic spring (to determine the load sharing) and uses appropriate bearing-bypass interactions to establish the failure criteria. Rules of thumb for design are included.

PROGRAM OBJECTIVES

**DEVELOP AND DEMONSTRATE THE TECHNOLOGY FOR
CRITICAL STRUCTURAL JOINTS IN TRANSPORT WING
COMPOSITE STRUCTURE**

- MEASURE AND EXPLAIN SINGLE-ROW BOLTED JOINT BEHAVIOR
- PERFORM PARAMETRIC STUDIES, ACCOUNTING FOR EACH OF THE VARIABLES IN MULTI-ROW JOINT DESIGN
- IDENTIFY OPTIMUM MULTI-ROW BOLTED JOINT PROPORTIONS
- ESTABLISH REALISTIC GROSS STRAIN LEVELS FOR MECHANICALLY-FASTENED COMPOSITE STRUCTURES

RELATIONSHIP BETWEEN STRENGTHS OF BOLTED JOINTS IN DUCTILE, FIBROUS COMPOSITE AND BRITTLE MATERIALS

The design of bolted joints in fibrous composite laminates cannot be based on a minor perturbation of either linear elastic or perfectly plastic analysis, as used for metal structures. A major fudge factor is required for all such analyses. All published composite bolted joint analysis methods depend on an empirical modification, based on test results. That correction is more evident in some theories than others. Perfectly elastic analyses are typically conservative by a factor of two, as shown in Figure 1. The McDonnell Aircraft BJSFM method successfully calculates limit load, by requiring the assessment to be offset by 0.020 inch from the edge of the hole. That characteristic length changes with bearing stress up to as much as 0.090 inch at failure, so the BJSFM program is not used by McAIR to predict ultimate strengths.

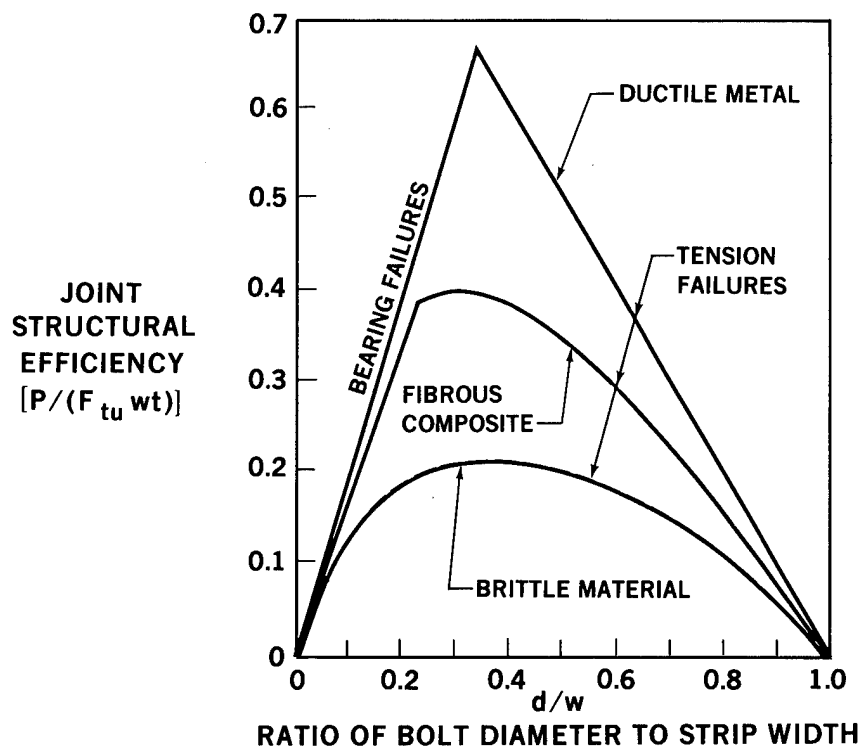


FIGURE 1.

RELATION BETWEEN STRESS CONCENTRATION FACTORS
OBSERVED AT FAILURE OF FIBROUS COMPOSITE LAMINATES
AND PREDICTED FOR PERFECTLY ELASTIC ISOTROPIC MATERIALS

The correlation factor used in the Douglas bolted composite analysis method is based on an alleviation of the purely geometric stress concentration factor. The lower apparent stress concentration factor at failure of composite laminates is found by test to be approximately proportional to the intensity of the elastic stress concentration. Selected testing can establish the alleviation factor, which can then be applied analytically to other joint geometries. Figure 2 shows also how to identify the geometries appropriate for testing: $w/d = 4$ to 5 for unloaded holes, $w/d = 3$ to 4 for loaded holes, and $w/d = 6$ to 8 for bearing stress cutoff.

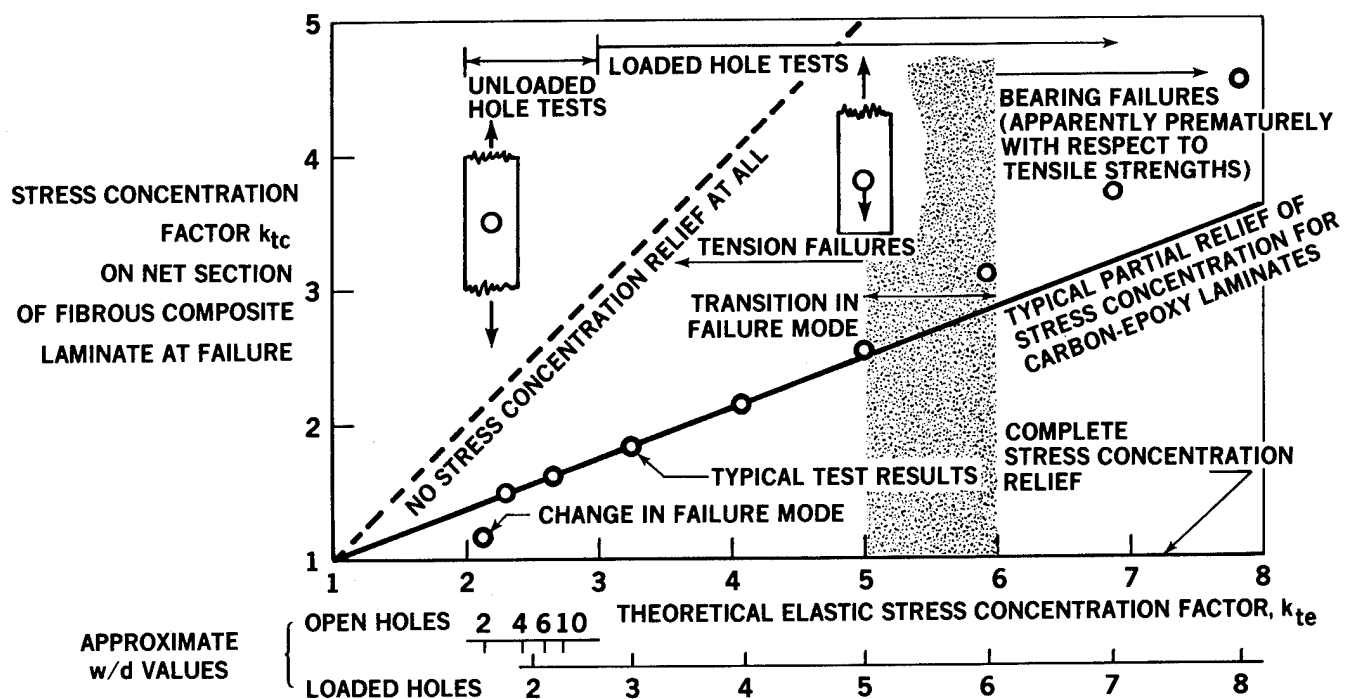


FIGURE 2.

STRESS CONCENTRATION RELIEF IN FIBROUS COMPOSITES BY DELAMINATIONS

The origin of the substantial stress concentration relief at bolt holes and cutouts in fibrous composite laminates is explained below in Figure 3. The key to this phenomenon is that the composites always behave like the distinctly two-phase materials that they really are, instead of as the one-phase homogeneous anisotropic material that is usually modelled. At high tensile stress gradients, the fibers parallel to the load pull out of the resin so that a sharp stress spike is replaced by a much lower average stress over a greater dimension. Also, there are intraply and interply delaminations that permit even more load redistribution before the first actual fiber breakage. The net effect of this softening of stress concentrations prior to failure is substantial, not minor.

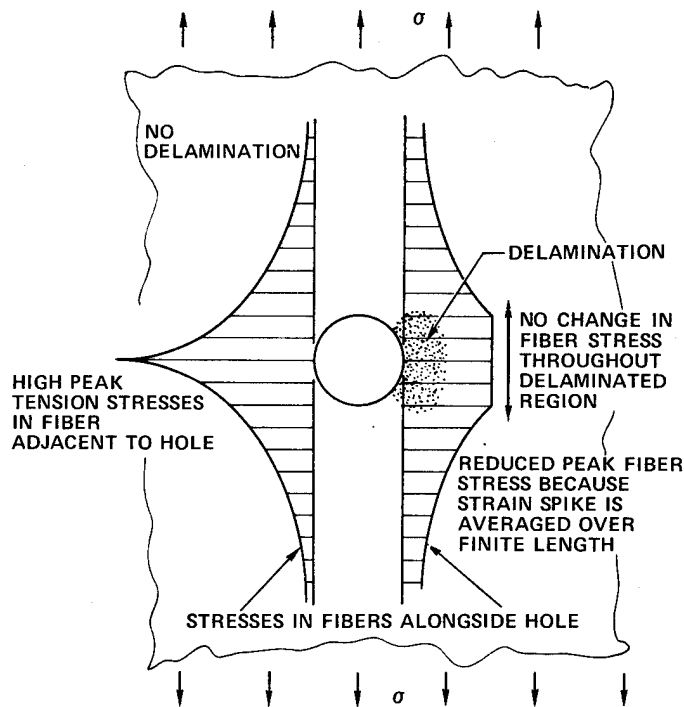


FIGURE 3.

STRESS CONCENTRATION RELIEF AT BOLT HOLES IN COMPOSITE LAMINATES

The amount of stress concentration relief appears to be dominated by the percentage of 0-degree plies in the laminate, with the softer laminates having proportionally more relief (Figure 4). The composite stress concentration factor for tension failure through a bolt hole (perpendicular to the load direction) is related to the geometric stress concentration factor for brittle elastic isotropic materials by

$$k_{tc} - 1 = C (k_{te} - 1).$$

Consequently, the stronger and stiffer laminates with a higher percentage of 0-degree plies are associated with stress concentration factors that increase almost (but not quite) as fast as the un-notched laminate strengths. The C-factor for unloaded holes is sometimes slightly lower than the test results shown for loaded holes. Specific test results should be used when available.

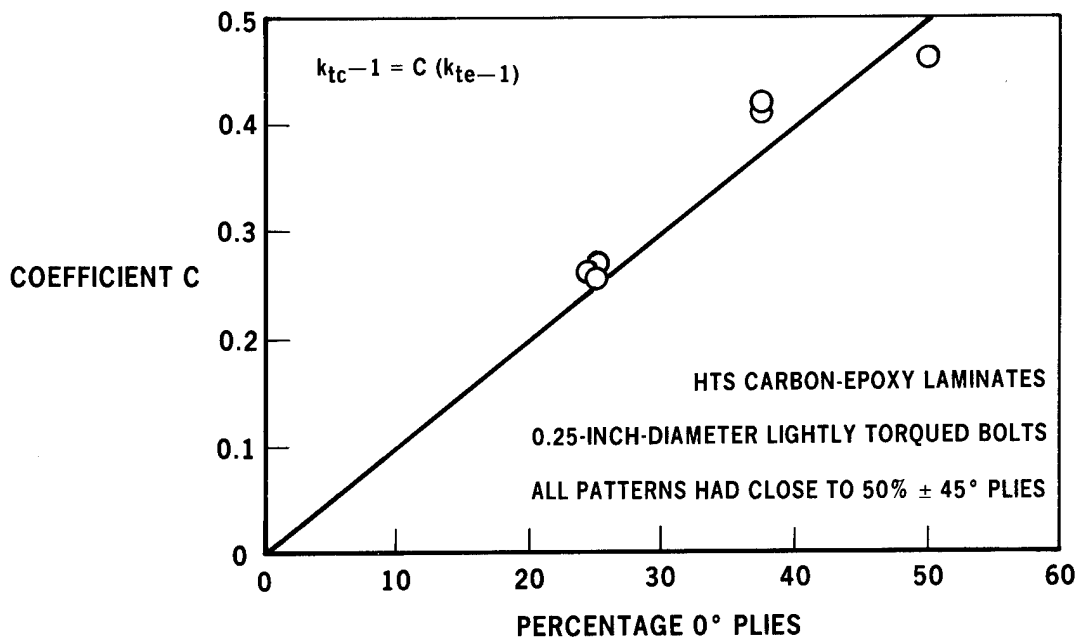


FIGURE 4.

BOLTED COMPOSITE JOINT EFFICIENCY CHART
(25 PERCENT 0-DEGREE PLIES)

For quasi-isotropic laminates (25,50,25) containing holes or bolted joints, the operating strains (and stresses) are limited as a function of the joint geometry shown below in Figure 5. The lowest curve represents the best that can be achieved with the entire load transmitted through a single row of fasteners; it peaks at a w/d ratio of about 3 to 1 and a structural efficiency just under 40 percent. The upper curve is the limiting case of an unloaded bolt hole. The intermediate curves represent the conditions in multi-row bolted joints where there is a combination of bearing and bypass loads. Maximizing the strength of multi-row bolted joints requires that the most critically loaded bolt operate in the upper left corner of this diagram, where the bearing stress is low.

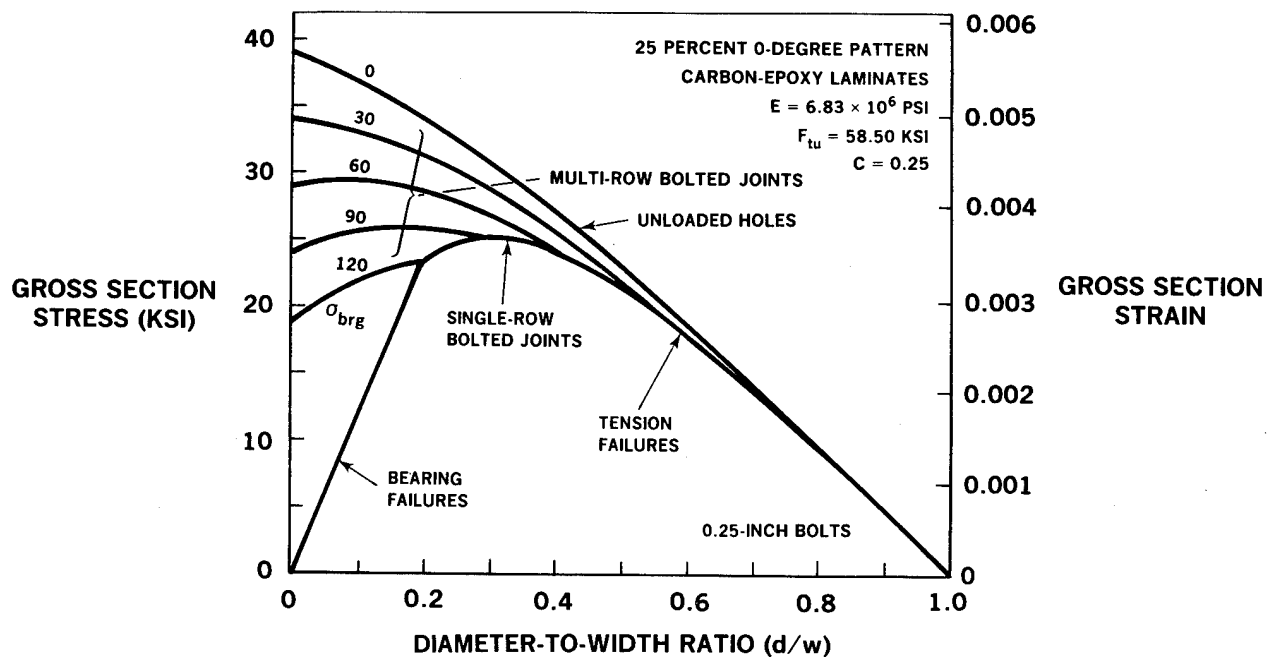


FIGURE 5.

BOLTED COMPOSITE JOINT EFFICIENCY CHART
(37.5 PERCENT 0-DEGREE PLIES)

The orthotropic laminate (37.5, 50, 12.5) selected for the Douglas composite wing skin studies permits slightly stronger bolted joints than in the quasi-isotropic pattern (25, 50, 25), by approximately 10 percent (Figure 6). This is the net tradeoff between the added strength due to 50 percent more 0-degree fibers and the increase in stress concentration factor by approximately the same value. However, for a high-aspect-ratio wing on a transport aircraft, this is a more suitable laminate than the quasi-isotropic one that is appropriate for the low-aspect-ratio wing on the AV-8B Harrier, that has a loading not dominated by the spanwise bending component.

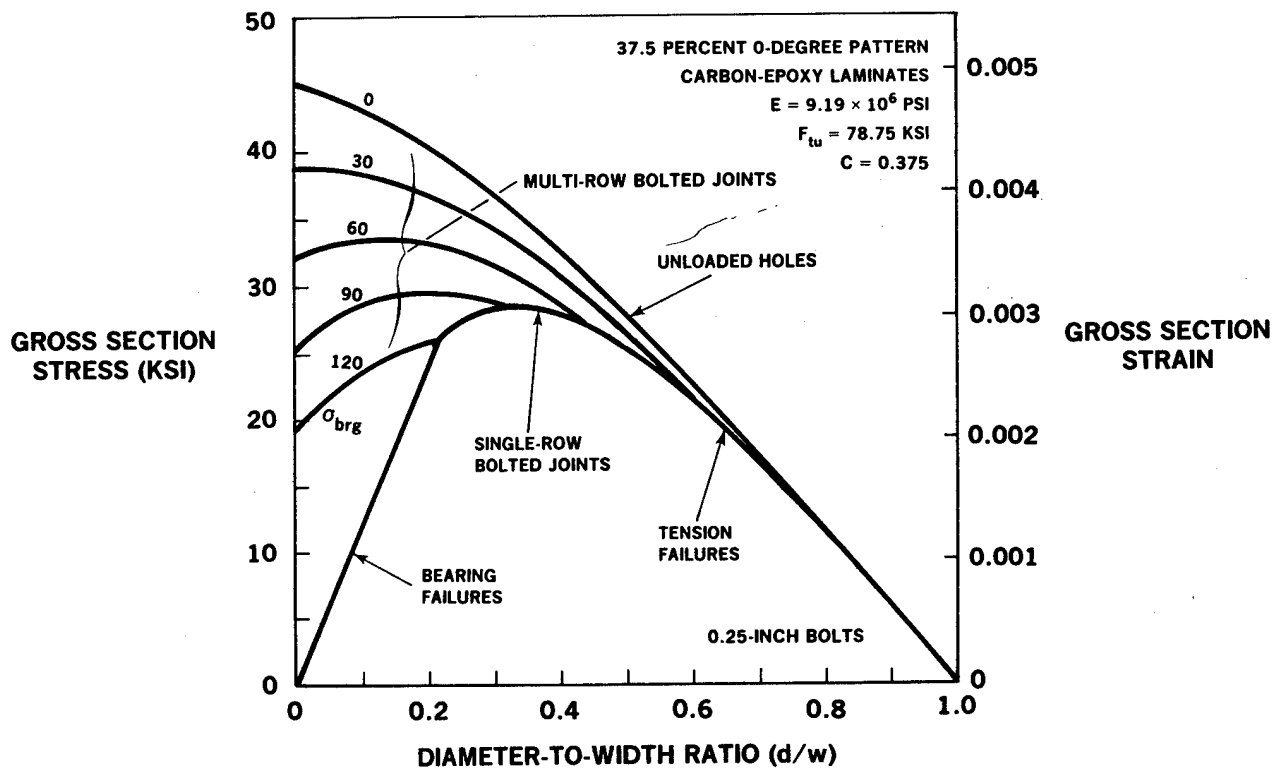


FIGURE 6.

BOLTED COMPOSITE JOINT EFFICIENCY CHART
(12.5 PERCENT 0-DEGREE PLIES)

The behavior of the (37.5, 50, 12.5) laminate under chordwise loading is represented by the (12.5, 50, 37.5) laminate (Figure 7). Despite having only half as many 0-degree fibers as the quasi-isotropic pattern (25, 50, 25), this laminate is more than half as strong, because of the lower stress concentration factors.

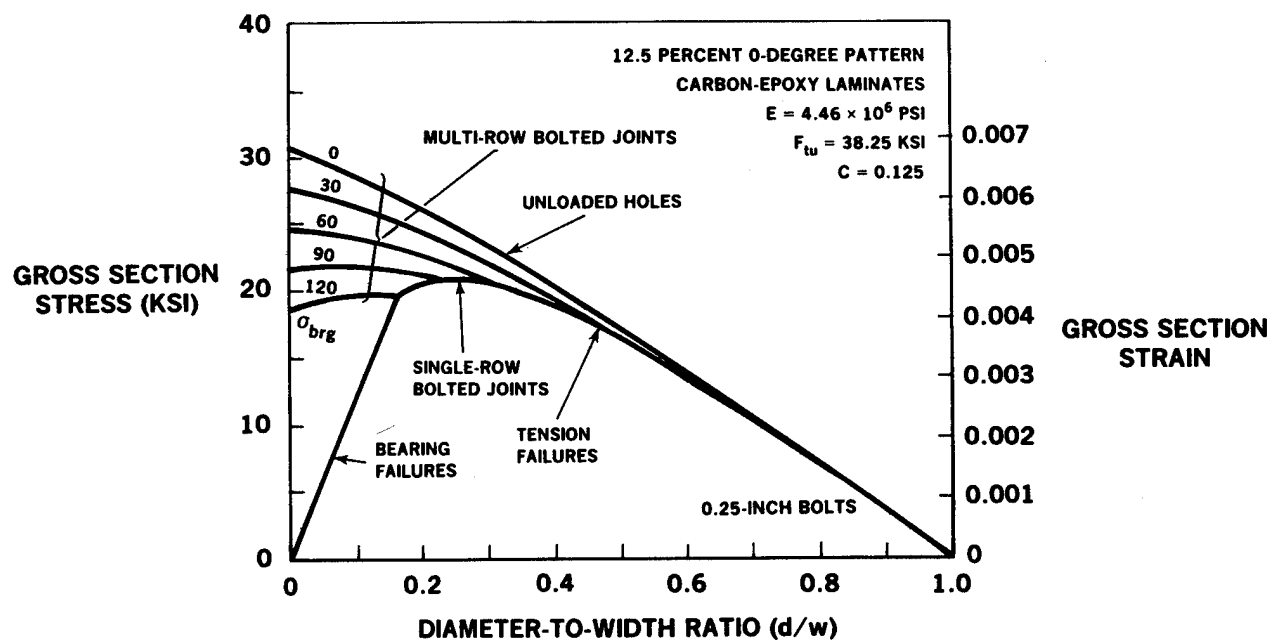


FIGURE 7.

BOLTED COMPOSITE JOINT EFFICIENCY CHART
(50 PERCENT 0-DEGREE PLIES)

The upper limit of 0-degree fibers in a composite laminate with bolt holes can be pushed as high as 50 percent (under some circumstances) before the law of diminishing returns takes over. Not only does the effective stress concentration factor for tensile failures increase, but there is a risk of premature failure by shearout. Shearout failures prevail for the (50, 50, 0) and (50, 0, 50) laminates. Only patterns near (50, 37.5, 12.5) laminates have a chance of developing the higher strengths shown below in Figure 8. Patterns with still higher 0-degree content are unsuitable for bolt holes and are excessively prone to failure by longitudinal splitting even without the bolt holes. Note that the failure strains are much lower than for the 12.5 percent 0-degree laminates.

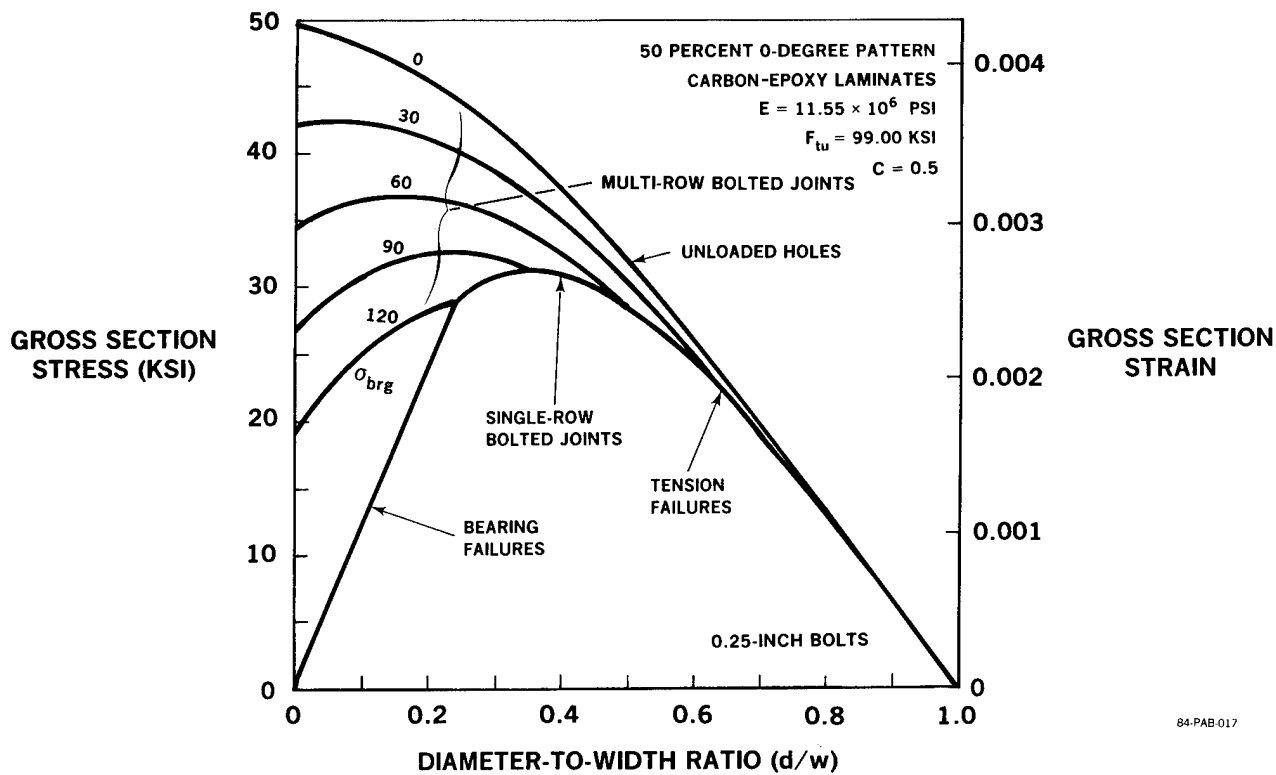


FIGURE 8.

GROSS SECTION DESIGN STRESSES FOR BOLTED COMPOSITE STRUCTURES
(CARBON-EPOXY LAMINATES)

The highlights of the preceding four sets of calculations are compared in Figure 9. It is immediately evident that the best multi-row bolted joints are approximately half as strong as the parent composite laminates. It is also clear that the bolted joint strengths are far less sensitive to the percentage of 0-degree plies than are the unnotched laminate strengths. The transverse strengths of bolted joints in the (37.5, 50, 12.5) pattern are two-thirds as high as the longitudinal strengths, even though the unnotched laminate strengths are only half as strong. All the calculations are in terms of the same B-basis allowables for T-300 carbon epoxy laminates. The test results are higher, but so are the associated average measured unnotched strengths. The ratios between notched and unnotched strengths are alike. The newer AS-4 fibers exhibit roughly equal increases in both unnotched and notched strengths.

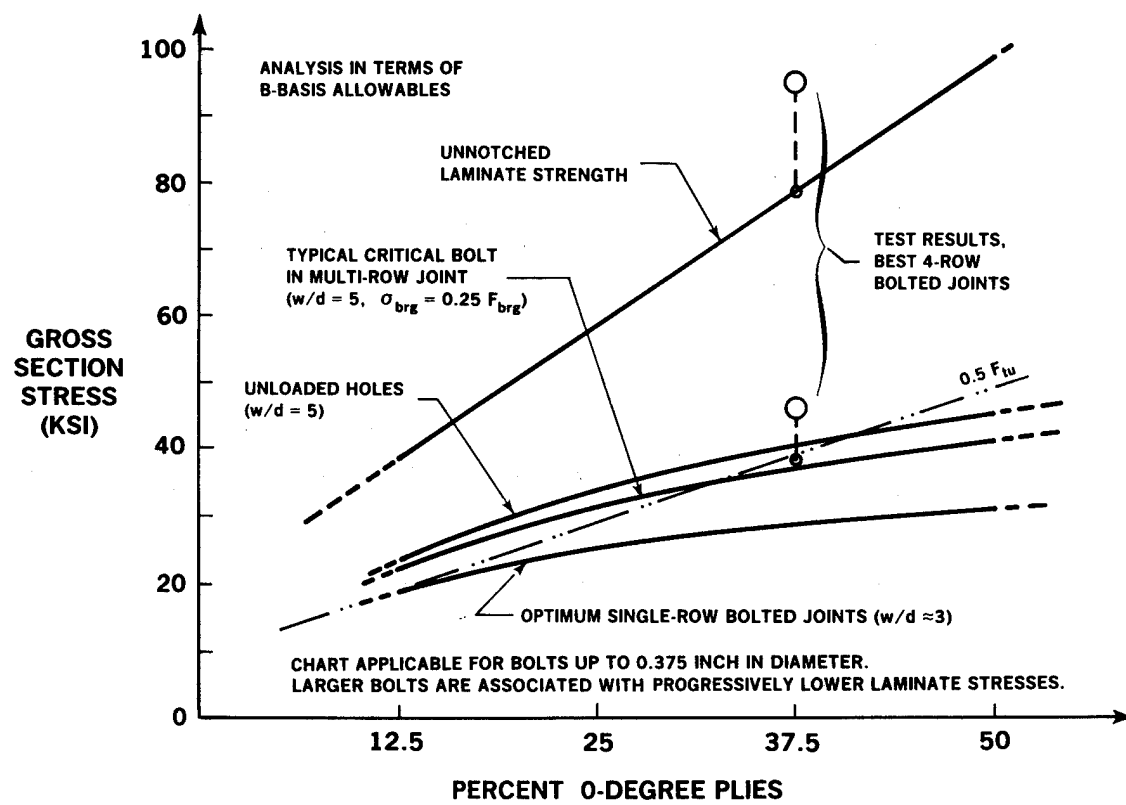


FIGURE 9.

SELECTION OF LAYUP PATTERN FOR
FIBROUS COMPOSITE LAMINATES

This diagram (Figure 10) shows the preferred laminate patterns for highly loaded, mechanically-fastened composite structures. The fiber layers should be interspersed as much as possible to maximize the number of effective resin interfaces. Bunching parallel plies together should be avoided if possible (to avoid overloading the small number of resin interfaces across which there is a change in fiber direction) and limited to 0.020-inch maximum stacks of parallel plies when not possible. Within the shaded area below, all bolted joints have similar strengths and there are no changes in failure modes.

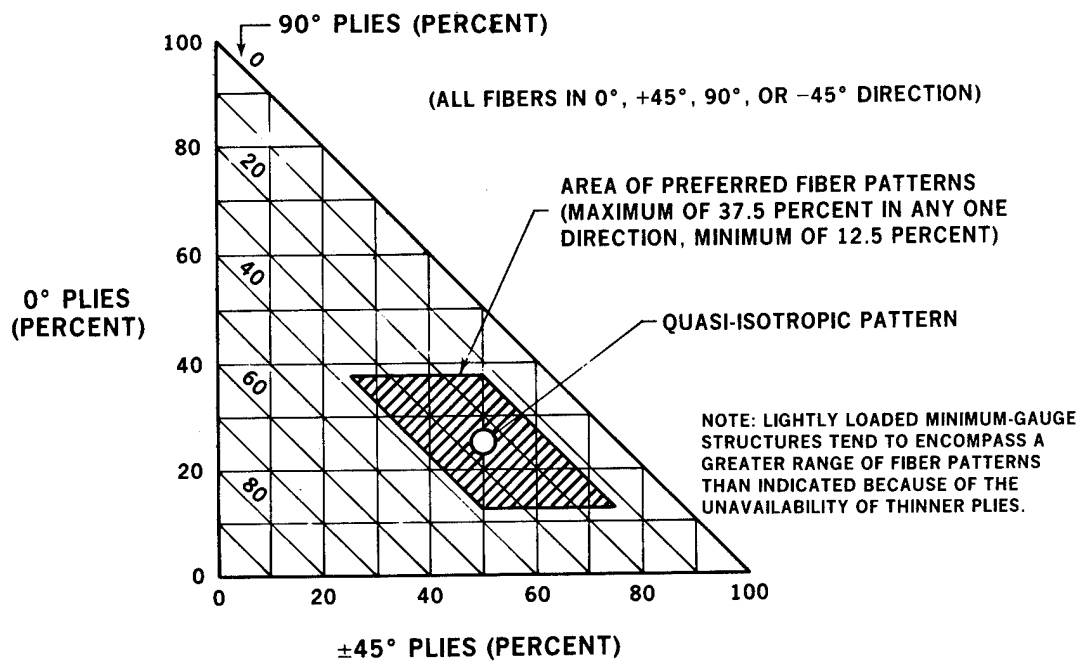


FIGURE 10.

DESIGN TECHNIQUE FOR BOLTED CARBON-EPOXY STRUCTURES

General-purpose design of simple bolted composite joints is customarily accomplished by use of the simple chart shown in Figure 11. The chart gives ultimate strains for double-shear bolts. The shaded area is available for general-purpose design, with the remainder of the enclosed area to be analyzed only by a very small number of experienced stress analysts. Charts very much like this were used for the Harrier and LearFan designs. For simplicity, the same universal chart is used for all laminates independently of the percentage of 0-degree plies, even though that is not strictly correct. The newer AS-4 fibers would permit higher operating strains.

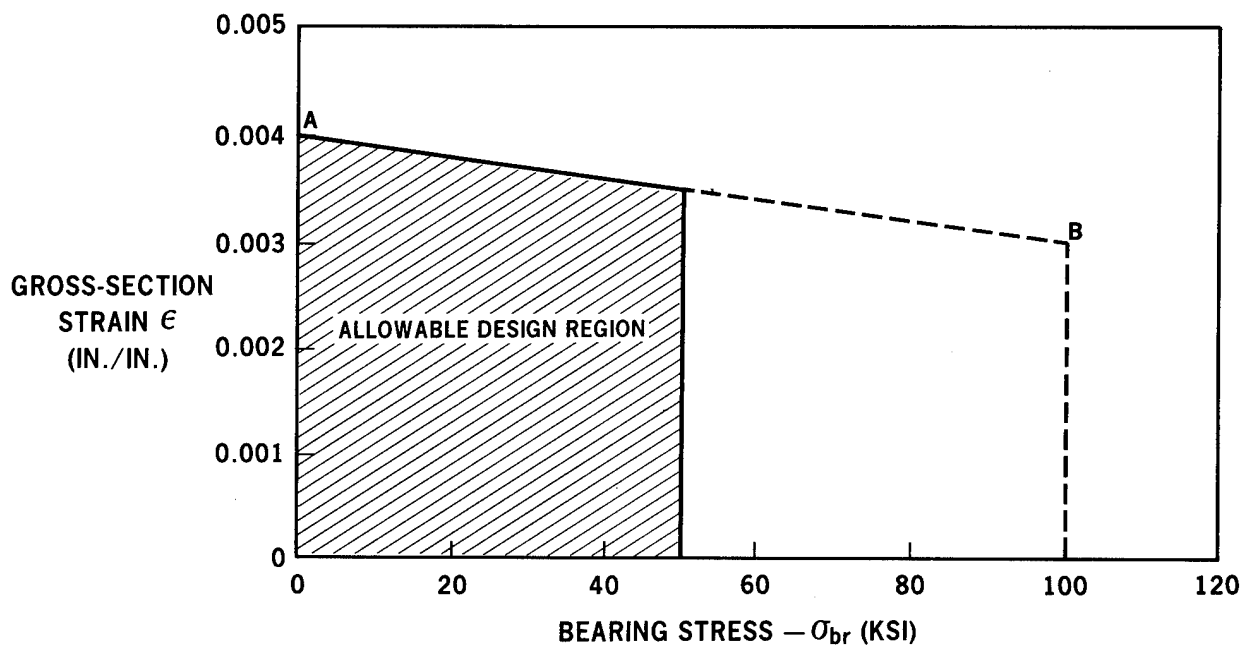


FIGURE 11.

EXPLANATION OF BEARING-BYPASS INTERACTION UNDER TENSION

Whether the load sharing between rows of bolts in a multi-row joint be established by the A4EJ computer program or by finite elements, it is necessary to have a failure criterion. The one built into the A4EJ program for tensile failures is illustrated below in Figure 12. Two failure modes - tension at a and bearing at b - are possible, depending on the geometry and bypass stress. The intercepts on the axes can be computed from the joint geometry, material allowables, and effective stress concentration factor k_{tc} . The bearing strength must be established by test. The total strength is the sum of the coordinates and is always maximized in the regime of high bypass loads combined with only low bearing stresses.

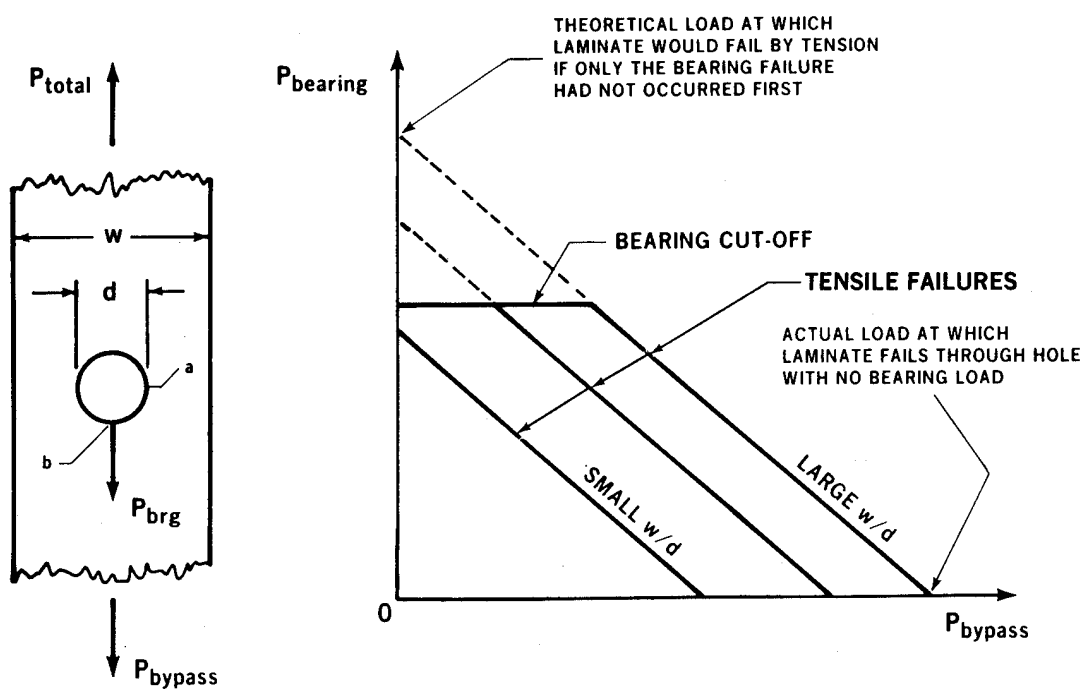


FIGURE 12.

EXPLANATION OF BEARING-BYPASS INTERACTION UNDER COMPRESSION

For compressive loading, the bearing-bypass interaction encoded in A4EJ is as shown in Figure 13. There is a difference between filled and unfilled holes and the former is always stronger despite the first impression from the diagram below. The total strength is the sum of the two coordinates. The testing on this NASA program has shown that the bearing strength actually developed is particularly sensitive to the effective through-the-thickness clampup, particularly if the bolts bend under load. Such bending tends to relieve clampup on splice plates, resulting in premature failure due to delaminations.

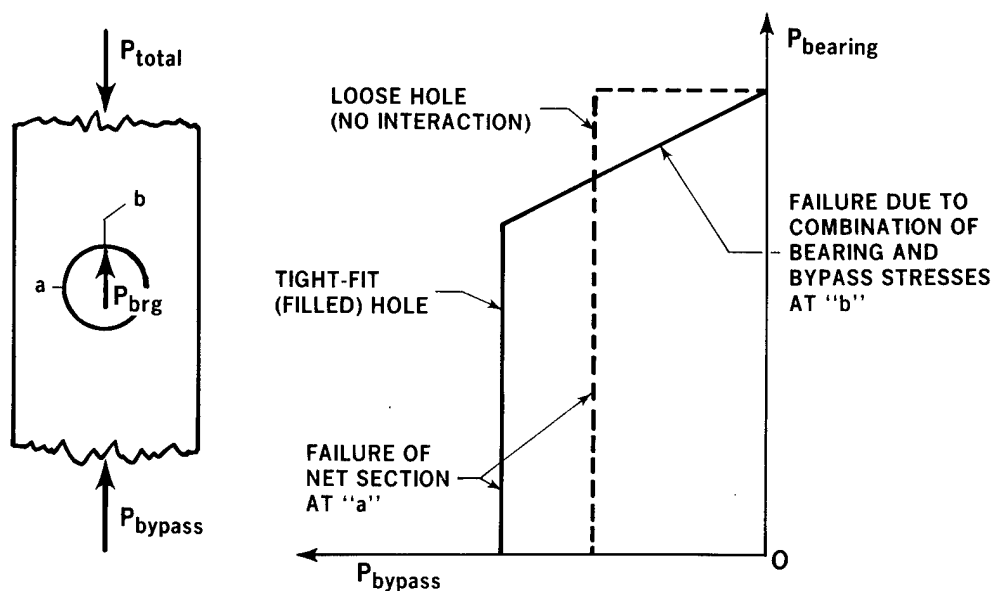


FIGURE 13.

EFFECT OF BOLT TORQUE ON BEARING STRENGTH
OF FIBROUS COMPOSITE LAMINATES

The bearing strength of bolted composite joints is very sensitive to the through-the-thickness clampup (Figure 14). Pin-loaded bolt holes (no clampup) are barely half as strong as finger-tight bolts with protruding head fasteners. Single-shear or countersunk fasteners develop bearing strengths between those limits. It is standard practice not to rely on the added strength from clampup. That is not due to fear of creep relaxation, which is minimal, but because an under-torqued bolt would impose a loss of static strength and not just a reduction in fatigue life.

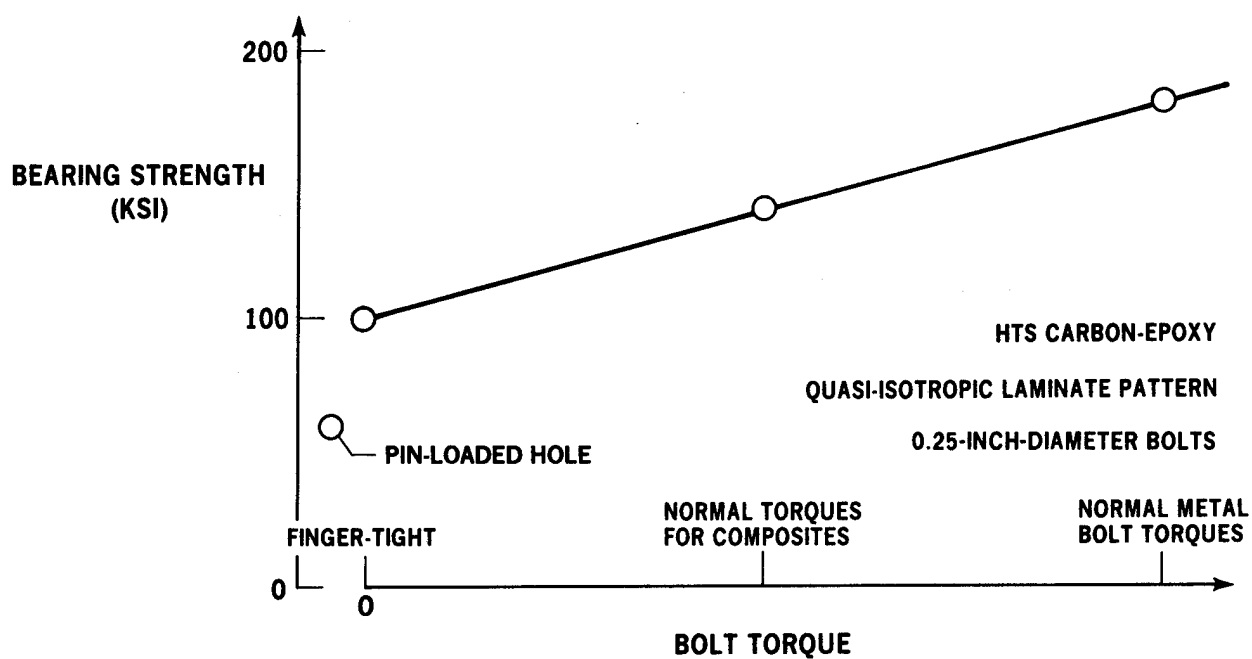


FIGURE 14.

NEED FOR REINFORCEMENT OF COMPOSITE SPLICE PLATES

Composite splice plates need to be reinforced because they exhibit lower allowable strengths than the skin sandwiched in the middle. The primary reason for this is the bending of the bolts, as shown in Figure 15. The Douglas ACEE wing program is now using metal splice plates for this reason. The most recent test failures have been in the skin at higher loads than those at which the composite splice plates delaminated in the earlier testing. The small weight penalty in the splice plates is more than offset by the associated large weight saving in the skin.

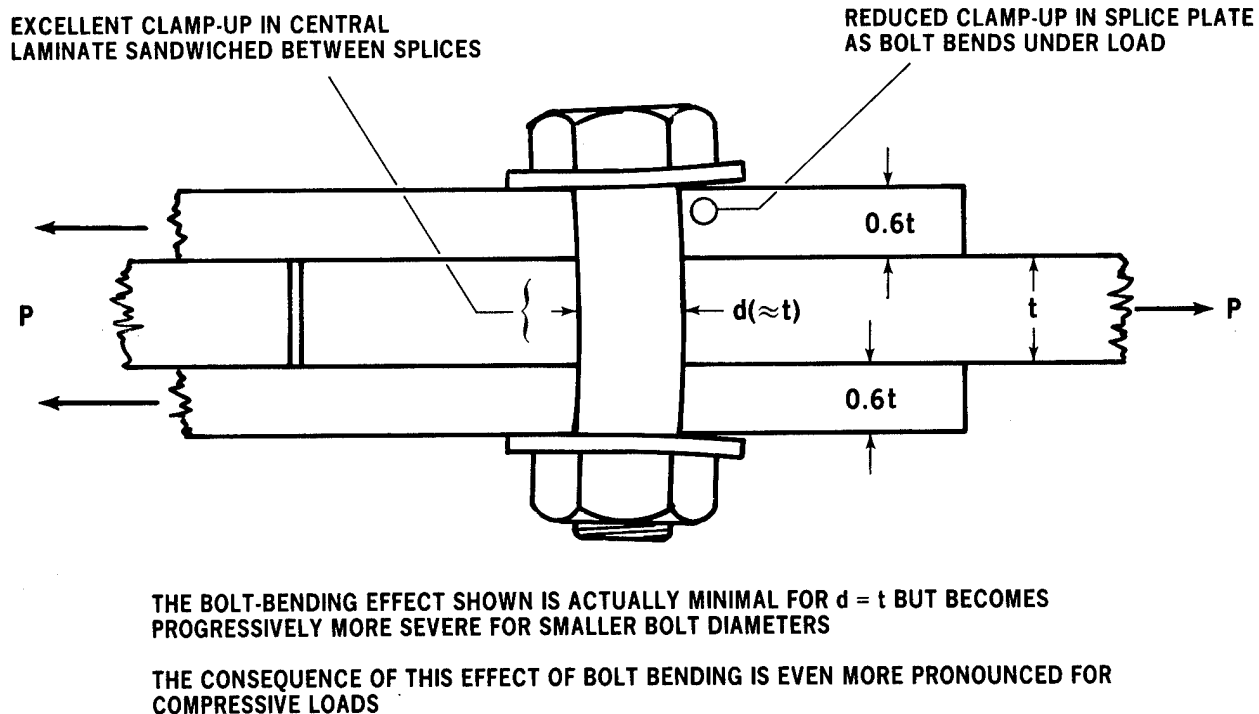


FIGURE 15.

EFFECT OF JOINT CONFIGURATION ON BOLT LOAD DISTRIBUTION

The keys to the design of efficient bolted composite splices are shown in the comparison between the strengths of various joint configurations (Figure 16). The strongest, configuration 4, was built and tested. It failed within 5 percent of the before-the-fact prediction of 50,000 pounds per inch strength. The combination of tapering and reinforcing of the splice plate minimizes the bearing load at station 1 where the bypass load is highest, and maximizes it at station 4 where there is no bypass load. In addition, the bolt diameter at station 1 is only one-fifth of the strip width, to make it more flexible, while a much larger bolt is used at station 4 - $w/d = 3$ there. These refinements reduce the bearing stresses at the outermost stations. The other two interior bolts had a w/d ratio of four. The taper and thickness were established by parameteric studies with the A4EJ multi-row bolted joint computer program.

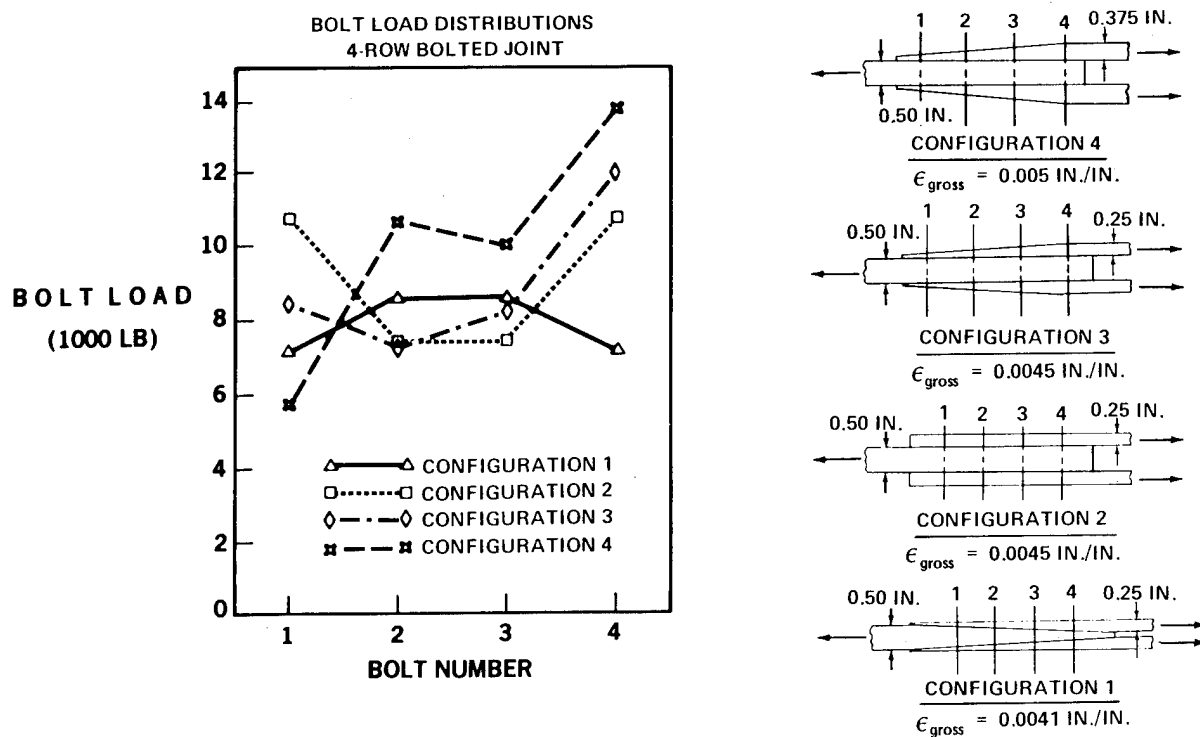


FIGURE 16.

EFFECTS OF SPLICE PLATE TAPER AND TIP THICKNESS

The strengths of multi-row tapered-splice bolted joints are influenced significantly by the proportions of the tapered splices. In particular, the thin tip at the first bolt row and the reinforcement at the last bolt row are vital to the attainment of maximum joint efficiency. No universal design rules have been recognized yet. However, those parametric studies that have been run have identified clearly peak strengths that are identified with certain values of each variable. While the optimum thicknesses at each end are not independent of each other, there are clear losses of strength associated with excessively thick as well as excessively thin ends and the middle of the splice plates.

RELATIVE THICKNESSES OF SPLICE PLATE AT TIP AND MIDDLE AFFECT LOAD SHARING IN MULTI-ROW BOLTED JOINTS

RATIO OF SKIN THICKNESS TO MAXIMUM SPLICE PLATE THICKNESS ALSO AFFECTS JOINT STRENGTHS

OBJECTIVE OF TAPERING SPLICE PLATE IS TO MINIMIZE BOLT LOAD AT TIP AND TO MAXIMIZE THE LOAD TRANSFERRED THROUGH THE LAST BOLT IN THE SKIN

ANALYSIS AND TESTS HAVE BOTH SHOWN THAT SUITABLE TAPERING OF SPLICE PLATES CAN ENHANCE JOINT STRENGTHS SUBSTANTIALLY IN COMPARISON WITH UNIFORM SPLICES

A4EJ COMPUTER PROGRAM IS USED TO DETERMINE LOAD SHARING AND JOINT STRENGTH

PARAMETRIC STUDIES TO DATE HAVE YET TO IDENTIFY ANY UNIVERSAL PROPORTIONS LIMITING THE LOAD IN THE END FASTENER BY DESIGNING FOR A BEARING FAILURE IN THE SPLICE PLATE TIP SEEMS TO BE A USEFUL TECHNIQUE

FIGURE 17.

EFFECT OF ABSOLUTE BOLT SIZE ON
STRESS CONCENTRATION RELIEF AT HOLES IN COMPOSITE LAMINATES

The effect of absolute bolt size on the stress concentration alleviation in fibrous composites must vary between complete relief for a pin hole and zero relief for a huge hole. A suggested formula is given here in Figure 18. The constant coefficient, that is independent of joint geometry, still reflects the effects of orthotropy as well as relief, with the exponent k characterizing the size effect. Such a hypothesis is consistent with the notion that any stress concentration relief is confined to a narrow zone around a cutout or bolt hole. That zone is proportional to the ply thickness and not to the size of the hole. The relief diminishes asymptotically to zero for very large cutouts. The use of the square root of the bolt diameter d is based on the frequent use of the same quantity in residual strength formulae. This aspect of the work is still in its preliminary stages.

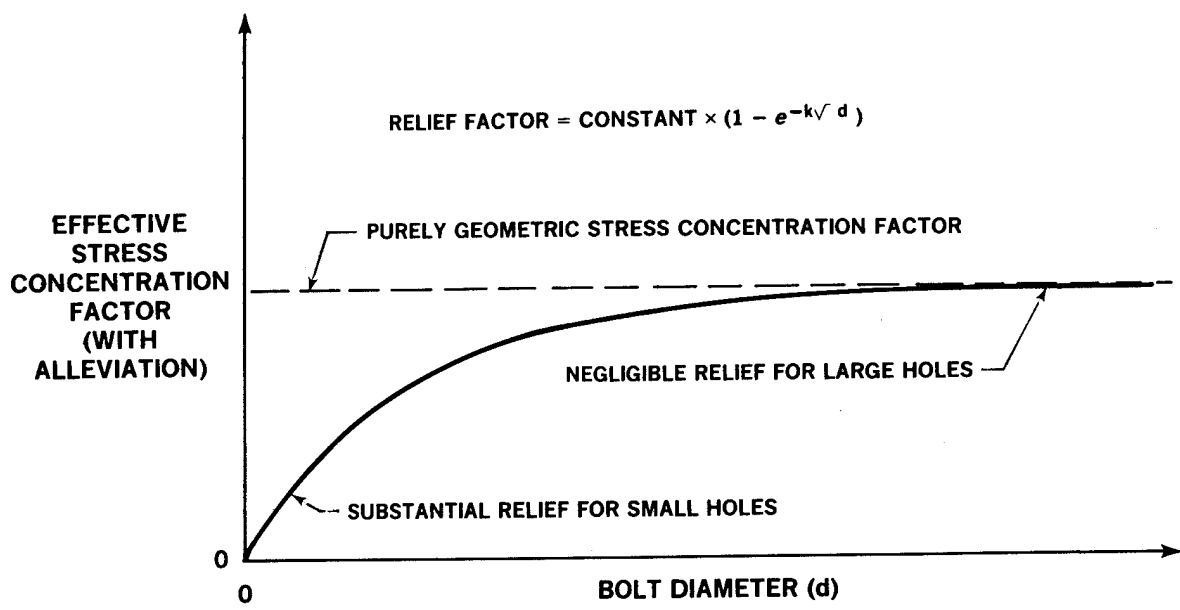


FIGURE 18.

EFFECT OF BOLT DIAMETER AND SPLICE PLATE THICKNESS
ON STRENGTH OF SINGLE-ROW BOLTED COMPOSITE JOINTS

The optimum bolt diameter should be determined by the strength of the laminate in the area of the joint, even though doing so usually results in very high margins on the shear strength of the bolt. Bolt bending is much more significant than for metallic structures because laminated composite components are usually thicker. Excessive bolt bending causes both bolt failures and premature laminate failures because of highly nonuniform bearing stresses. For single-row joints, the optimum d/t ratio is approximately 1, based on the central laminate thickness, as shown in Figure 19.

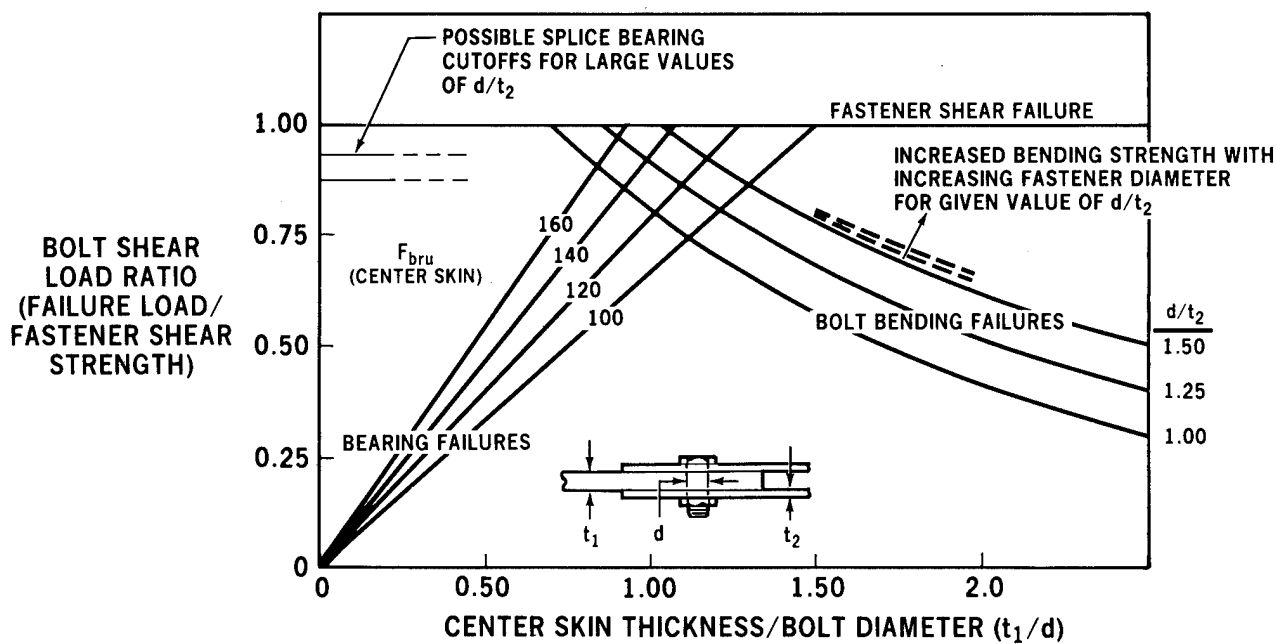


FIGURE 19.

PREDICTED ELASTIC SPRING RATES
FOR DOUBLE-SHEAR BOLTED COMPOSITE JOINTS

The stiffness of bolted composite joints depends on both the bolt diameter to skin thickness ratio and splice plate to skin thickness ratio. Very thin splice plates, as at the tip of tapered doublers, create a low stiffness fastener installation because of high stresses in the splice plate laminate. Very thick splice plates cause a low stiffness because of excessive bolt bending. There is a maximum stiffness geometry somewhere in between, as shown in the diagram in Figure 20. That maximum occurs roughly where the bolt diameter equals the skin thickness and the splice plates are each half as thick. In multi-row joints, the geometry can be tailored at each row to maximize the total joint strength, which is not achieved by having all of the details the same as for the optimum single-row joint.

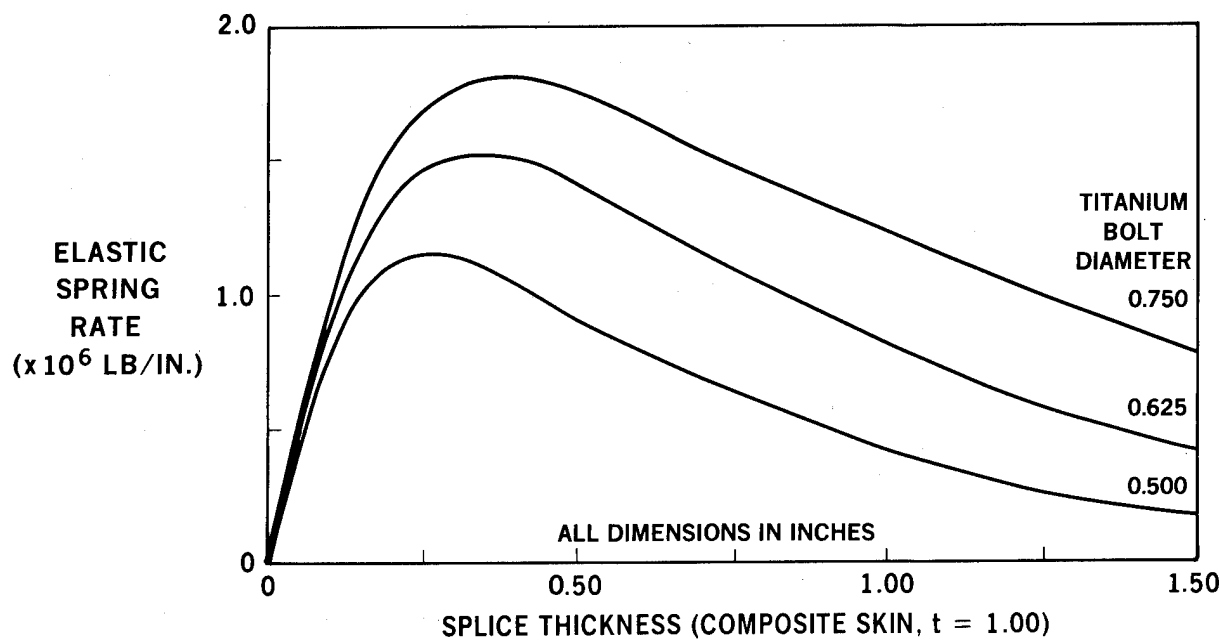


FIGURE 20.

RULES OF THUMB FOR DESIGNING BOLTED COMPOSITE JOINTS

DESIGN THE JOINTS FIRST AND FILL IN THE GAPS AFTERWARDS — OPTIMIZING THE "BASIC" STRUCTURE FIRST COMPROMISES THE JOINT DESIGN AND RESULTS IN LOW OVERALL STRUCTURAL EFFICIENCY

THE BEST BOLTED JOINTS CAN BARELY EXCEED HALF THE STRENGTH OF UNNOTCHED LAMINATES

OPTIMUM SINGLE-ROW JOINTS HAVE APPROXIMATELY THREE-FOURTHS OF THE STRENGTH OF OPTIMUM FOUR-ROW JOINTS

JOINTS DESIGNED TO FAIL IN TENSION ARE STRONGER THAN THOSE DESIGNED TO FAIL IN BEARING

MANY BOLTED COMPOSITE JOINTS CONTAIN TOO FEW BOLTS, SPACED TOO FAR APART, AND THE DIAMETERS ARE TOO SMALL TO PERMIT MAXIMIZING THE STRENGTH OF THE LAMINATE

RATED SHEAR STRENGTH OF FASTENERS SHOULD NOT BE A FACTOR IN DESIGN — BOLTS NEED TO BE SIZED TO RESTRICT BEARING STRESSES IN LAMINATES

PEAK HOOP TENSION STRESS AROUND BOLT HOLES IS ROUGHLY EQUAL TO THE AVERAGE BEARING STRESS

BOLT-BEARING STRENGTH IS SENSITIVE TO THROUGH-THE-THICKNESS CLAMPUP OF LAMINATES

SPlice PLATE STRESSES SHOULD BE LOWER THAN IN SKINS TO PREVENT DELAMINATIONS

BOLT BENDING IS MUCH MORE SIGNIFICANT FOR COMPOSITES THAN FOR METALS, BECAUSE COMPOSITE MEMBERS ARE THICKER (FOR A GIVEN LOAD) AND MORE SENSITIVE TO NONUNIFORM BEARING STRESSES (BECAUSE OF BRITTLE FAILURE MODES)

BOLT DIAMETER SHOULD TYPICALLY BE ABOUT THE SAME SIZE AS THE SKIN THICKNESS

OPTIMUM w/d RATIO FOR SINGLE-ROW BOLTED JOINTS IS ABOUT 3 TO 1

OPTIMUM w/d RATIO FOR MULTI-ROW BOLTED JOINTS VARIES ALONG LENGTH OF JOINT — w/d = 5 AT FIRST ROW TO MINIMIZE LOAD TRANSFER AND w/d = 3 AT LAST ROW TO MAXIMIZE TRANSFER, WITH w/d = 4 FOR INTERMEDIATE BOLTS

BOLTED JOINT STRENGTH VARIES FAR LESS WITH PERCENTAGE OF ZERO-DEGREE PLIES IN FIBER PATTERN THAN DOES UNNOTCHED LAMINATE STRENGTH

BEST FIBER PATTERNS ARE FULLY INTERSPERSED (PARALLEL PLIES NOT BUNCHED TOGETHER) AND HAVE AT LEAST 12.5 PERCENT OF THE PLIES IN EACH OF THE FOUR DIRECTIONS — 0°, +45°, -45°, AND 90°

CONCLUSIONS

OPTIMUM SINGLE-ROW BOLTED JOINTS DEVELOP ABOUT 3/8 OF THE UNNOTCHED LAMINATE STRENGTHS

OPTIMUM SINGLE-ROW BOLTED JOINTS HAVE A w/d RATIO OF ABOUT 3

JOINTS WITH GEOMETRIES THAT CAUSE TENSILE FAILURES ARE STRONGER THAN THOSE THAT FAIL IN BEARING

BOLTED COMPOSITE JOINT BEHAVIOR CANNOT BE EXPLAINED BY A MINOR PERTURBATION OF LINEARLY ELASTIC OR PERFECTLY PLASTIC ANALYSES

EMPIRICAL DATA ARE NEEDED TO GENERATE THE FAILURE CRITERIA (BEARING-BYPASS INTERACTIONS)

USEFUL PARAMETRIC STUDIES OF BOLTED COMPOSITE JOINTS CAN BE PERFORMED EASILY
BOLTED JOINT STRENGTHS ARE FAR LESS SENSITIVE TO FIBER PATTERN VARIATIONS THAN ARE THE UNNOTCHED MATERIAL STRENGTHS

LOAD SHARING IN MULTI-ROW JOINTS CAN BE COMPUTED RELIABLY BY THE A4EJ PROGRAM IN STANDARD GEOMETRIES AND BY FINITE ELEMENTS FOR COMPLEX STRUCTURAL JOINTS

OPTIMUM MULTI-ROW JOINT PROPORTIONS HAVE BEEN IDENTIFIED AND VERIFIED BY TEST
GROSS SECTION STRESS LEVELS IN MULTI-ROW BOLTED COMPOSITE JOINTS CAN BARELY EXCEED HALF THE UNNOTCHED LAMINATE STRENGTHS

DESIGN AND TEST OF LARGE WING JOINT

DEMONSTRATION COMPONENTS

CONTRACT NAS1-16857

Bruce L. Bunin

Douglas Aircraft Company

Long Beach, California

ACEE Composite Structures Technology Conference

Seattle, Washington

August 13-16, 1984

DESIGN AND TEST OF LARGE WING JOINT

DEMONSTRATION COMPONENTS

ABSTRACT

Current research conducted under a NASA-sponsored program on the design, analysis, and testing of highly loaded bolted joints in composite structures is reviewed. The purpose of this NASA program is to develop the technology for critical joints in composite wing structure of large transport aircraft. Program objectives and the results of the Phase I effort are reviewed. The Phase II test program began with additional single-bolt coupon tests, continued with several subcomponent tests, and will culminate in a large technology demonstration test. Development of analytical methodology beyond that of Phase I was required to properly account for the geometric complexities of representative wing joint structure.

This review covers the Phase II test program to date, along with the methodology development and correlation of analysis and test. The testing and analysis of a wing skin-stringer transition specimen is discussed. Results are presented for a subcomponent of the lower rear spar at the side of fuselage joint. In each case, finite-element analyses were combined with semiempirical methods to make accurate strength predictions. The upcoming technology demonstration test and the associated design and analysis effort are reviewed.

CRITICAL JOINTS PROGRAM OVERVIEW

The Critical Joints program is in progress at Douglas Aircraft Company under NASA-Langley Contract NAS1-16857. Phase I of the program began in November 1981 and was completed in January 1983. The most notable accomplishments included the development of analysis methods that give reliable strength predictions for multirow bolted joints in composites, and the successful testing of composite joint specimens that verified the analysis methodology and showed considerable improvement in structural efficiency over the previous state of the art. This review centers on Phase II of the program during which representative composite wing joint structure will be tested to demonstrate the present level of technology. The methodology development, structural test program, and correlation between test results and analytical strength predictions are reviewed.

PROGRAM OBJECTIVES

PHASE I OVERVIEW

METHODOLOGY DEVELOPMENT

STRUCTURAL TEST PROGRAM

ANALYSIS/TEST CORRELATION

SUMMARY/CONCLUSIONS

PROGRAM OBJECTIVES

The major objective of this investigation was to develop and demonstrate the technology for critical structural joints of a composite wing structure that meets all the design requirements of a 1990 commercial transport aircraft. To fulfill this objective, analytical procedures were developed for joint design and analysis. Specimen tests were conducted on single-bolt joints to provide empirical data for the analytical procedures, which were then used to predict the strength and performance of multirow bolted joints. The analytical methods were also used to evaluate various design concepts in an effort to maximize joint efficiency. Structural tests were conducted on multirow bolted joints in several configurations, and the results were compared with analytical predictions. Multirow specimens ranged in size from relatively small, two-row joints to large, full-scale specimens representative of actual structure.

The objective of Phase II of the program is to demonstrate the technology developed in Phase I with structural tests of representative wing joint structure and to correlate these results with analytical predictions.

DEVELOP AND DEMONSTRATE THE TECHNOLOGY FOR CRITICAL STRUCTURAL JOINTS OF COMPOSITE TRANSPORT WING STRUCTURE

- **CHARACTERIZE SINGLE-ROW JOINT PROPERTIES**
- **DEVELOP ANALYTICAL METHODS**
- **EVALUATE DESIGN CONCEPTS**
- **VERIFY METHODOLOGY BY STRUCTURAL TEST**
- **DEMONSTRATE THE TECHNOLOGY FOR REPRESENTATIVE STRUCTURE**

CRITICAL JOINT TECHNOLOGY FOR LARGE COMPOSITE AIRCRAFT STRUCTURE

The Phase I program began with the preliminary design of a composite wing for a high-technology commercial transport. This effort was conducted to the level required for the conceptual design of major joint areas. An internal loads analysis was performed to establish ultimate load intensities at selected locations, and the skin-stringer thicknesses and spacing were designed and optimized accordingly. At the same time, analytical methods were developed for multirow bolted joints in composites.

The methodology developed in this program was based primarily on the results of prior research contracts with NASA-Langley Research Center (Reference 1) and the U.S. Air Force Flight Dynamics Laboratory at Wright-Patterson AFB, Ohio (Reference 2), in which the failure mechanisms of composite bolted joints were characterized and A4EJ analysis program for load-sharing in multirow bolted joints was developed. The material system selected for the program was the Ciba Geigy 914 resin with Toray T-300 fibers, one of the newer toughened resin systems. A series of ancillary tests was then conducted to characterize the strength and stiffness properties of bolted joints for the new material and selected fiber patterns. These tests provided the data base required to perform accurate strength predictions for multirow joints. Large composite subcomponent joints were tested, and in most cases, excellent correlation was obtained between analysis and test results (Reference 3). The Phase II program presently underway continues the development of analytical methods and will conclude with a series of technology demonstration tests.

The flow of technology development for the Critical Joints program is described in Figure 1.

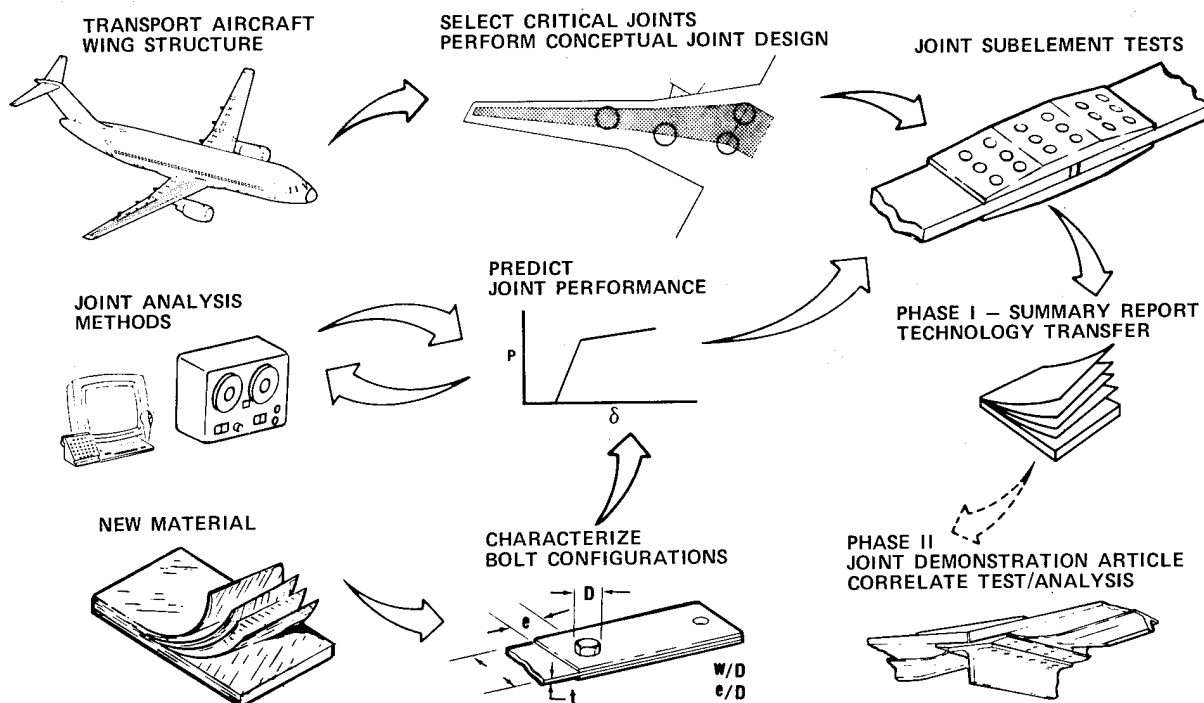


FIGURE 1.

PHASE II ANCILLARY TESTS SINGLE-ROW PROPERTIES

Phase II of the program began with a series of ancillary tests to further characterize single-row joint properties (Figure 2). These tests were conducted on specimens with joint geometries that were not tested in Phase I, or where data were inconclusive in previous tests. Net-section tension strengths and the associated stress concentration factors were measured for both loaded and unloaded hole specimens. Wider specimens were tested in the loaded hole configuration to establish bearing strength cutoffs, including the initial point of nonlinearity as well as an ultimate bearing stress level. Of particular interest were measurements of the variations in bearing strength between laminates that were fully clamped in double shear and those that were external to the joint with clamp-up afforded only by the fastener head and washer. Differences in bearing strength of as much as 60 percent were observed between these configurations.

An additional consideration is the potential for fastener bending failures, the severity of which is often underestimated or overlooked. While bolt shear allowables have proven to be quite consistent, several Phase I joint specimens suffered bolt bending failures at load levels substantially below the fastener rated shear strength. In addition, load-deflection measurements were taken for all loaded hole tests. The elastic spring rates for joints consisting of several materials with asymmetric thicknesses were tested and compared with analytical predictions using methods developed in Phase I.

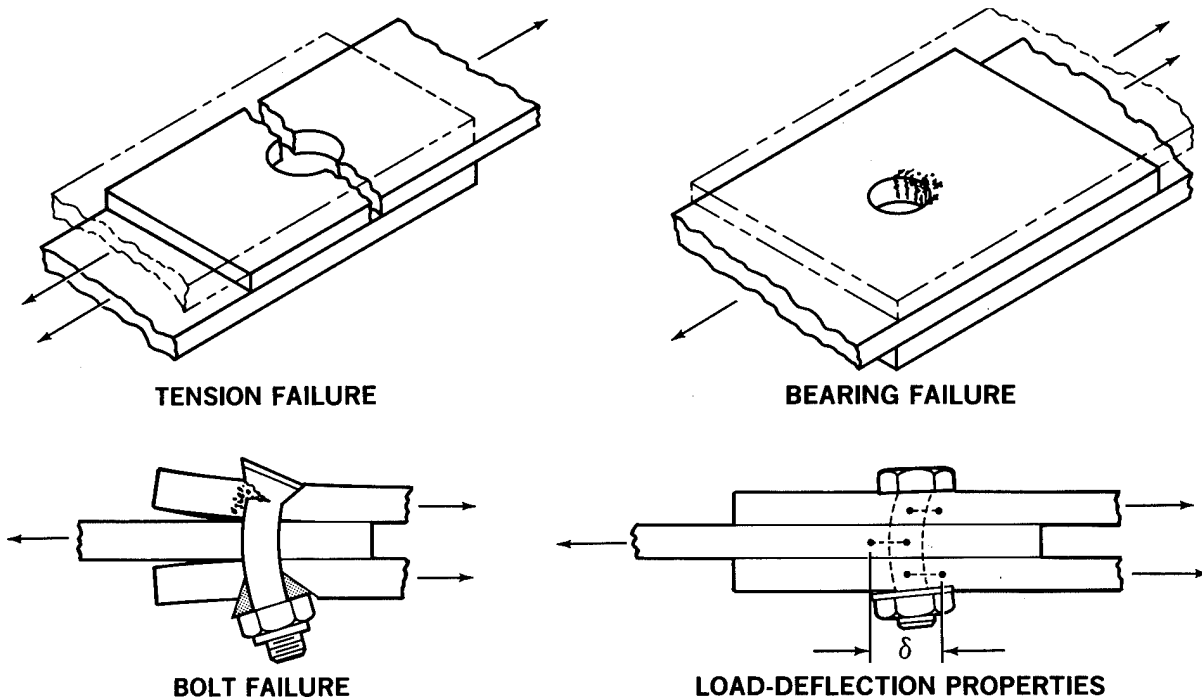


FIGURE 2.

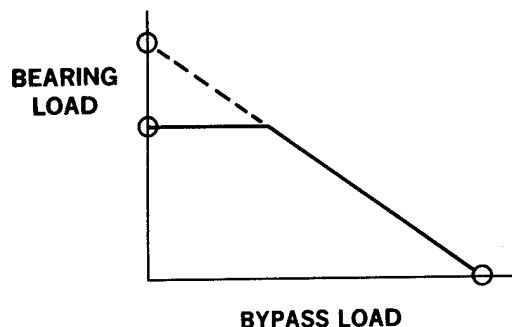
METHODOLOGY DEVELOPMENT SEMIEMPIRICAL METHODS

The data obtained from single-bolt coupon tests provide the load-sharing properties and strength envelopes required to perform multirow joint analyses, as shown in Figure 3. The strength of bolted joints in composites is limited by the bearing-bypass interactions that result from the associated stress concentration factors at failure. Single-bolt coupon tests can be used to characterize the loaded and unloaded hole section strengths for a given material system and fiber pattern. By establishing a relationship between the calculated elastic stress concentration factors and the observed factors at failure for composites, the section strengths of various geometries can be predicted. Single-bolt tests are also used to determine bearing strengths, the third element required to construct a complete bearing-bypass interaction curve.

The loaded hole tests also provide the load-deflection properties that are necessary to determine bolt load distributions throughout a multirow joint. Elastic spring rates for various geometries were measured and correlated with analytical predictions. The limits of elastic behavior including bearing yield and (plastic) bolt bending were also measured.

STRENGTH PROPERTIES

- STRESS CONCENTRATION FACTORS
- SEMIEMPIRICAL METHODS
- BEARING STRENGTHS



BOLT LOAD DISTRIBUTIONS

- ELASTIC SPRING RATE
- PLASTIC DEFORMATION
- BOLT BENDING

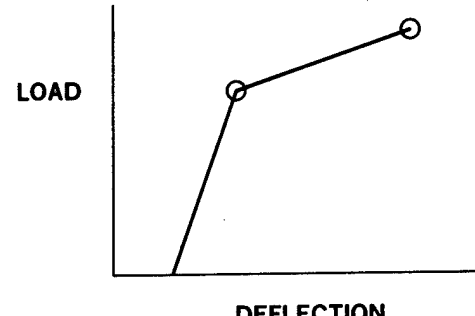


FIGURE 3.

SUBCOMPONENT TESTS ANALYSIS VERIFICATION

Twenty large, multirow joints were tested in Phase I of the program to verify the accuracy of the analytical methods (Reference 4). Various configurations of two-row and four-row bolted joints were tested in tension and compression. All joints consisted of constant-thickness center laminates with uniform or tapered composite splice plates. The specimens were equipped with strain gages to monitor the load distribution among joint members and between rows of fasteners.

The types of correlations that were achieved for both strength predictions and bolt load distributions are shown in Figure 4. In most cases, the strength predictions were accurate to within a few percent of the test results. In some cases, the observed mode of failure was different than expected because of premature bolt bending or tapered splice failure. Nevertheless, the subcomponent tests of Phase I demonstrated the ability to achieve gross-section failure strains on the order of 0.005, and to perform reliable strength predictions for multirow joints of relatively simple geometries. Having reached these initial objectives, it is a goal of the Phase II program to develop and apply this technology to the more complex joint geometries of actual structure.

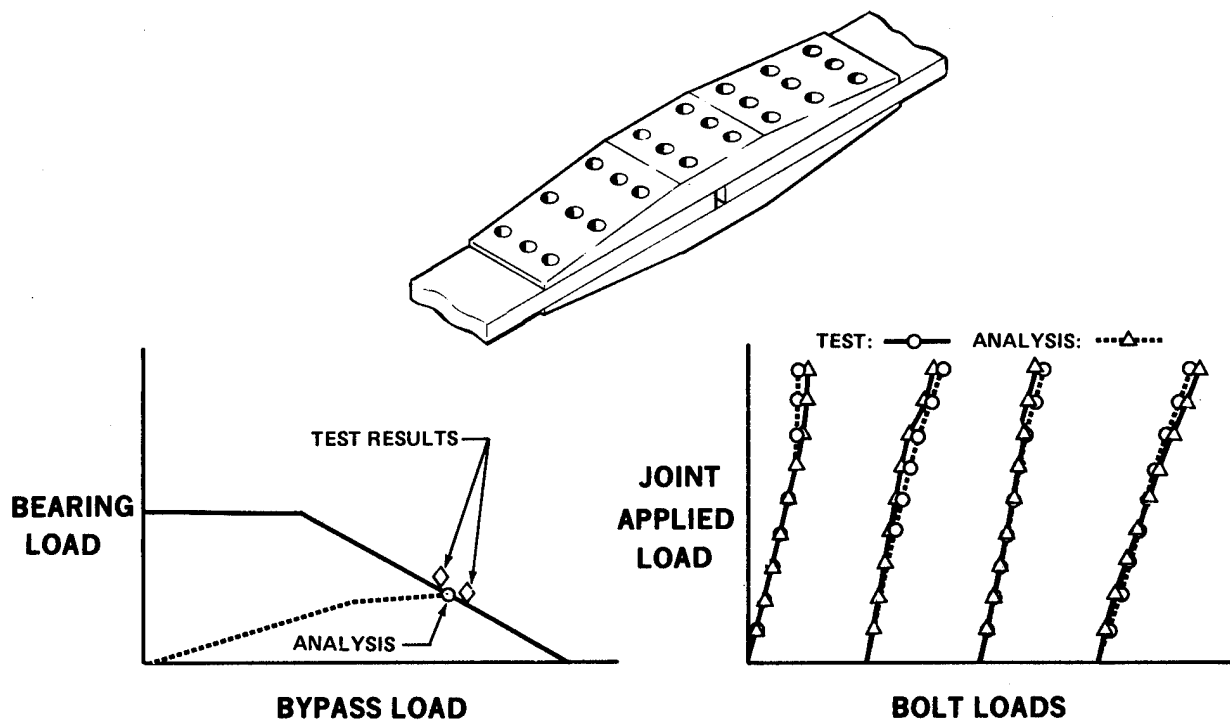


FIGURE 4.

COMPOSITE WING STRUCTURE
LOWER REAR SPAR AND STRINGER CONCEPTUAL JOINT

The conceptual design of several critical joint locations throughout the wing was completed during Phase I. For the purposes of technology demonstration in Phase II, the lower rear spar at the side of fuselage attachment was selected, as shown in Figure 5. This joint presents a relatively complex problem for structural analysis and includes a stringer transition joint concept. As a result of this complexity, the test program was formulated to investigate portions of this area individually. The stringer transition was tested as a separate specimen, while portions of the corner joint representing the skin-spar cap and spar web splices were tested as subcomponents. The program will culminate in a test of a large specimen representing the skin and spar cap corner splice without including the stringer transition.

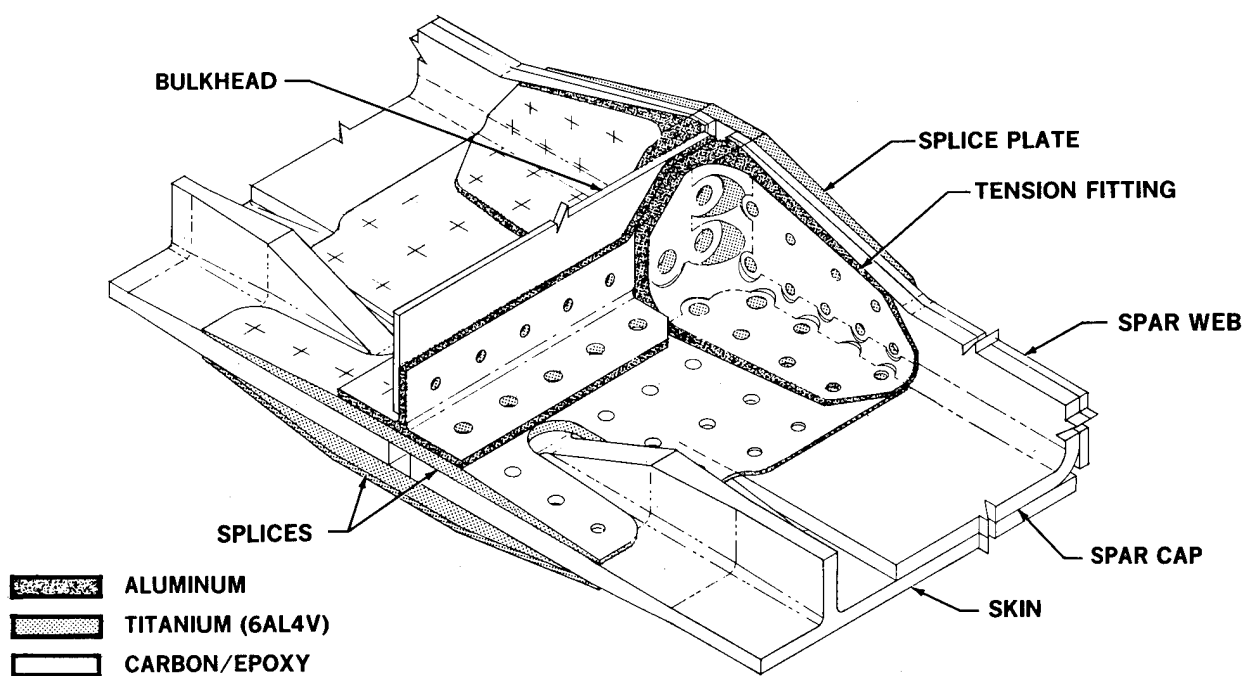


FIGURE 5.

JOINT TRANSITION SPECIMEN

The stringer transition joint was the first of several large multirow joints to be tested in Phase II. The concept shown in Figure 6 represents the lower wing skin with an integral blade stringer which transitions into a bolted shear joint at the side of the fuselage. The stringer blade is scarfed off along the length of the joint while a thickness buildup is introduced in both the skin and stringer. This transition is initiated beyond the first row of fasteners to maximize the bypass load and minimize the bearing load at the critical location in the skin.

The fiber pattern was (37.5% 0°, 50% +45°, 12.5% 90°) throughout, with nominal thicknesses of 0.504 inch and 0.426 inch for the skin and blade, respectively. Tapered titanium splice plates transferred the load while the titanium fasteners varied in diameter from 7/16 inch at the thin end of the splice to 5/8 inch at the thick end. These features were incorporated in the design in an effort to optimize the bolt load distribution and maximize the load transfer. The skin-stringer combination was designed to an ultimate strain level of 0.005 inch/inch for the wing lower surface.

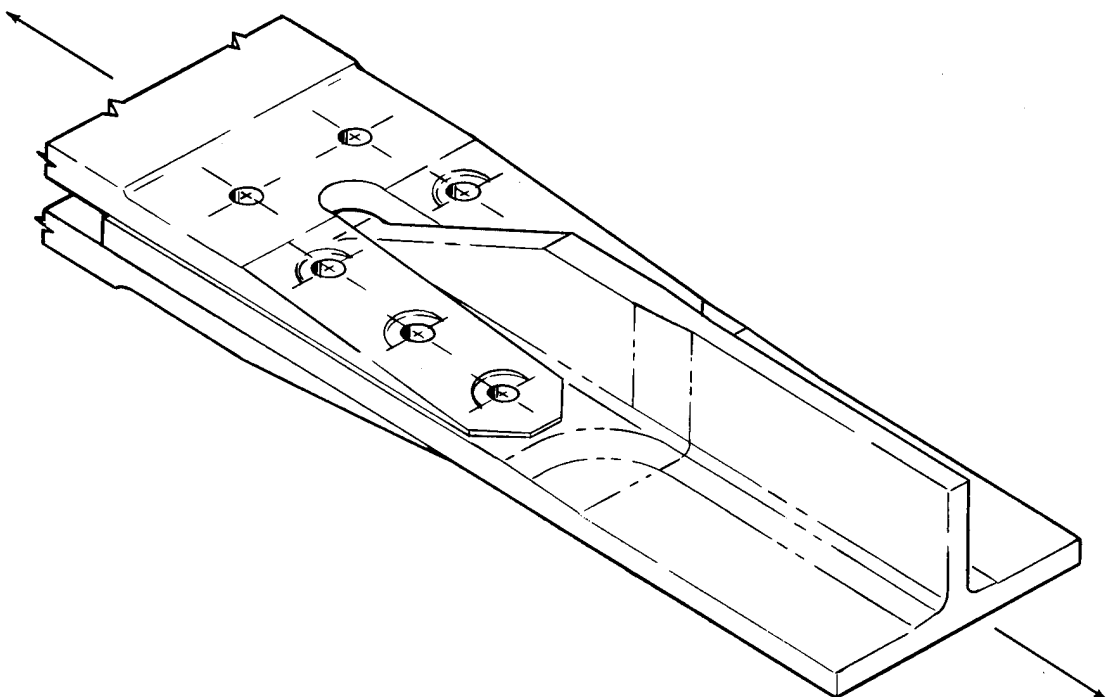
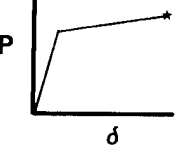
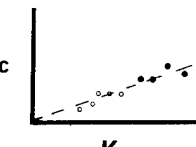
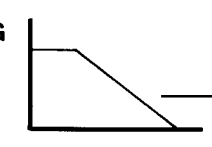


FIGURE 6.

JOINT TRANSITION SPECIMEN ANALYSIS METHODOLOGY

The load-sharing analytical methods developed in Phase I were sufficient to analyze multirow joints of uniform cross section, and were proven to be accurate for load distribution and strength predictions. The more complex joints of Phase II required a more versatile analysis approach. In this case, the load transfer from the stringer runout into the bolted joint had to be accounted for. The selected approach was to combine finite-element analysis with the semiempirical methods developed in Phase I (Figure 7). Strength and stiffness properties including joint load-deflection data are incorporated in a finite-element model which is used to determine bolt load distributions. Bearing-bypass load combinations determined by the model are then compared to calculated interaction curves for failure prediction. Nonlinear effects are accounted for through successive iterations with altered stiffness properties. There is often a tendency to use finite-element analysis methods at excessive levels of detail, resulting in unnecessarily high costs. It was therefore an objective of the analysis development effort to perform accurate strength predictions while minimizing the complexity of the approach.

GIVEN:

- **GEOMETRY**
- **(%0, %±45, %90)**
- **PROPERTIES**
- 
- 
- **BEARING LOAD** 
- **BYPASS LOAD** 

- **NASTRAN FINITE ELEMENT MODEL**
- **SEMIEMPIRICAL METHODS**

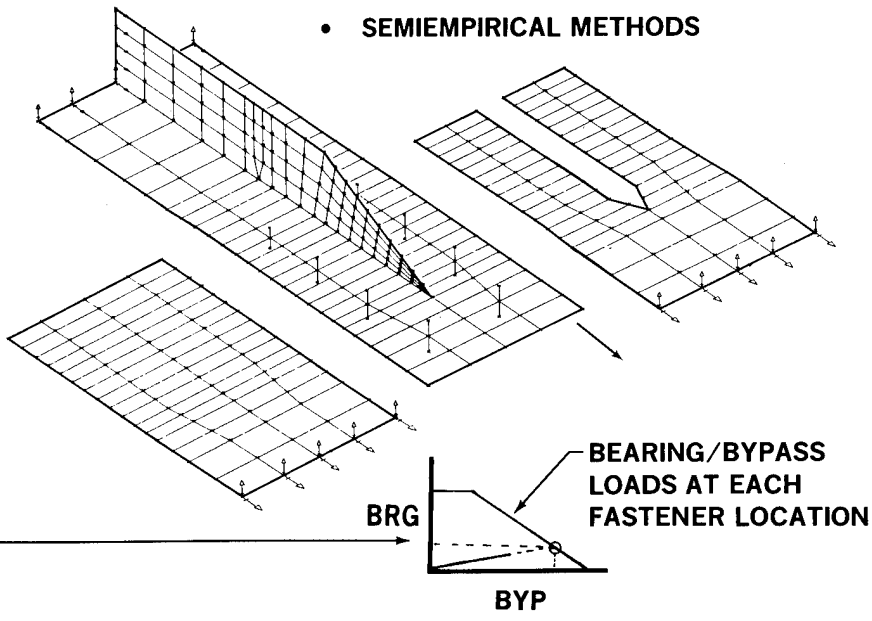


FIGURE 7.

JOINT TRANSITION SPECIMEN
PHOTO-ELASTIC SURVEY

The stringer transition specimen consisted of a single composite member with a test section containing the thickness buildup, blade transition, and a multirow bolted joint at both ends. Test loads were transferred to the composite part directly from the test machine through the titanium splices. One end of the specimen was equipped with strain gages to monitor joint behavior, while the other end was coated with photo-elastic material to provide a qualitative assessment of the structural response. Photographs of the coated areas were taken at specified load levels throughout the test (Figure 8). The photograph of the stringer transition section to the left indicates the variation in strain level from the skin surface to the top of the blade. The change in direction or "bend" in the distribution pattern results from an increase in thickness occurring simultaneously in the skin and stringer. Strain gages mounted at the other end of the specimen confirm the trends as indicated by the photo-elastic coating.

The photograph of the bolted joint to the right shows the strain distribution on the surface of the tapered titanium splice plate and along the stringer blade edge. It would be desirable to place strain gages on the splice member in a manner that would provide an accurate measurement of bolt load distributions throughout the test and at failure. The difficulty in accomplishing this is illustrated by the complex strain distributions that are visible on the surface of the splice, which result from the combined effects of stress concentrations and hole shadowing. The buildup of high stresses at the tip of the stringer transition is also visible in this view.



FIGURE 8.

JOINT TRANSITION TEST RESULTS

The joint transition specimen was tested to static failure at an ultimate load of 197,200 pounds, or at a running load intensity of 34,300 pounds per inch. This corresponds to an average gross-section stress and strain of about 50,000 psi and 5,300 microstrain in the basic section, prior to the thickness buildup outside the joint. These are only average values, however, and as shown by the photo-elastic coating, the specimen was not under a state of uniform stress through the section. Strain gage data indicated a strain level in the skin prior to the buildup of about 5,900 microstrain, which corresponds to a strain level at the bolted joint of roughly 4,700 microstrain. (Young's modulus equals 9.3×10^6 psi.) A net-section tension failure occurred through the first row of fasteners at a high-bypass, low-bearing load combination, followed by a tension failure through the minimum section of the stringer blade, as shown in Figure 9. This was precisely the failure mode that was anticipated and analytically predicted. Strain readings were taken throughout the test, with continuous readings taken from approximately two-thirds of the predicted strength to failure. The specimen failed, as shown, through the end which was equipped with the photo-elastic coating.

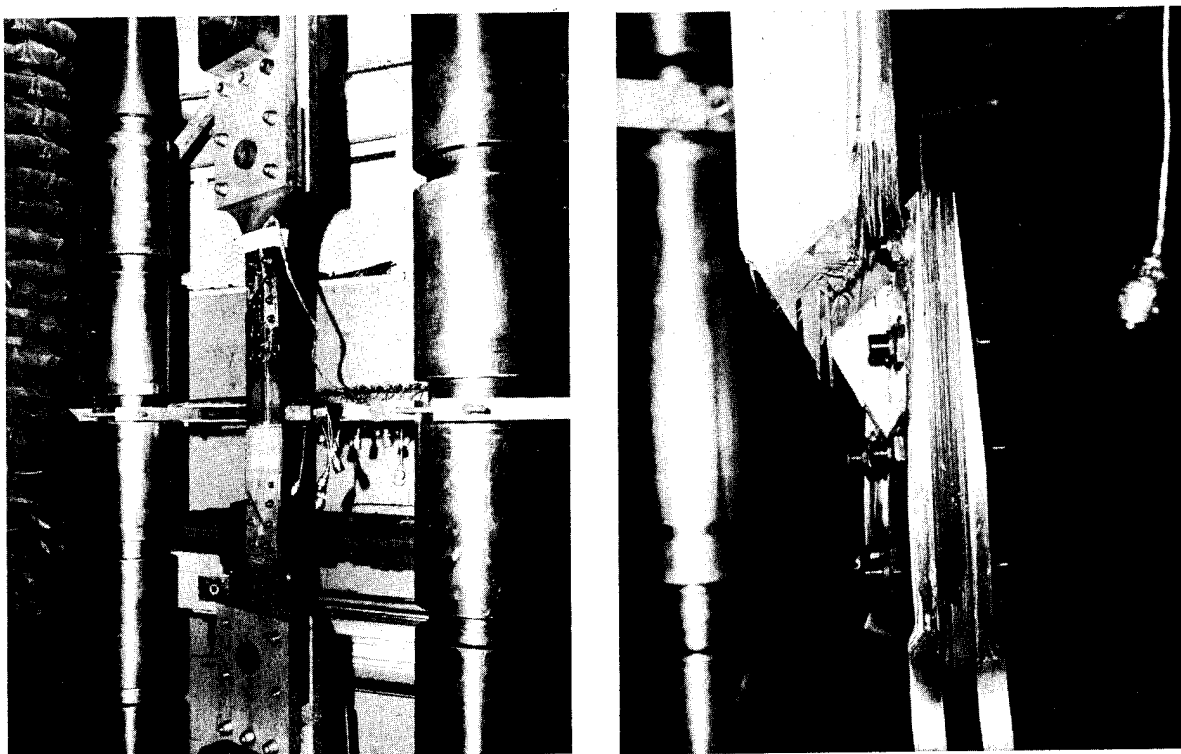


FIGURE 9.

JOINT TRANSITION SPECIMEN ANALYSIS/TEST CORRELATION

The joint transition specimen analysis consisted of a NASTRAN finite-element model which was used to determine the load distribution in the composite skin and blade, and to solve for the load-sharing between rows of fasteners. A second iteration was required to account for the change in stiffness due to a predicted bearing yield in the titanium splice at the first row of fasteners, prior to ultimate load. The bearing-bypass loads determined by the model were then compared with calculated interaction curves for each row of fasteners (Figure 10). The resulting prediction was a net-section failure through the first row of fasteners, as previously described, at an ultimate load of 183,700 pounds. This predicted strength is roughly 3 percent below the tested value of 193,200 pounds. The strain level in the composite skin away from the joint (and prior to thickening) was measured throughout the test, and the strain at failure of 5,891 microstrain is quite close to the predicted value of 5,945 microstrain.

The key to this analysis prediction is the accurate determination of the bearing-bypass conditions at the first row of bolts. This solution must also account for the difference (if any) in the load passing around either side of the bolt holes because of the substantial difference in net area and stress concentration effects between the inner and outer edges. While the accuracy of the present strength prediction is certainly acceptable, a more detailed analysis is in progress to more fully account for these effects and to ensure the validity of the initial approach.

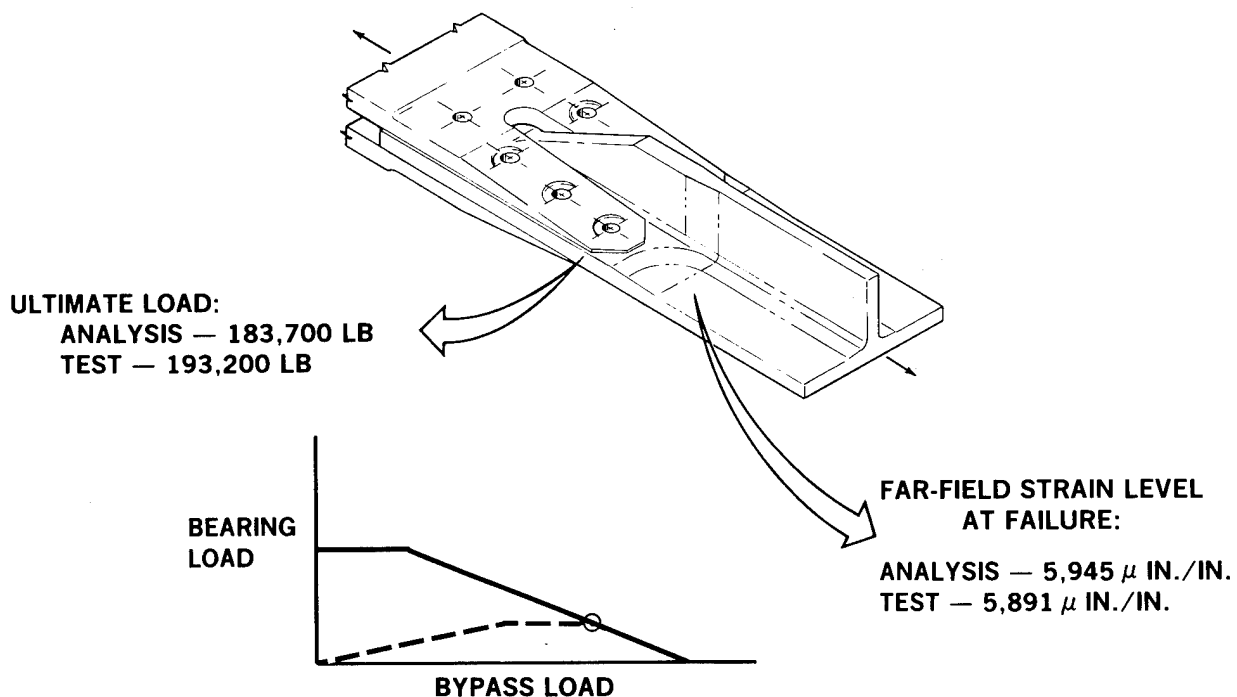


FIGURE 10.

DEMONSTRATION SUBCOMPONENT TESTS

The technology demonstration joint selected for the program presents a reasonably complex problem for strength analysis. To provide some insight into the performance of this joint and to develop additional confidence in the analytical approach, two specimens were built and tested which were representative sections of the large corner joint. The specimen shown in Figure 11 represents the portion of the skin and spar cap splice below the aluminum corner fitting. Member thicknesses, fastener sizes, and overall geometry of the subcomponent joints were identical to the corresponding portions of the technology demonstration specimen. The same analytical approach was used for this specimen as for the joint transition specimen with some changes only in modeling the bolted connections, which must, in this case, account for the load-sharing between four rows of fasteners and four or five layers of material.

An additional subcomponent specimen (not shown) tested in the program represented the spar and stiffener web sections that were spliced externally by a titanium splice and internally by the aluminum corner fitting. These specimens also used the (37.5% 0°, 50% +45°, 12.5% 90°) fiber pattern.

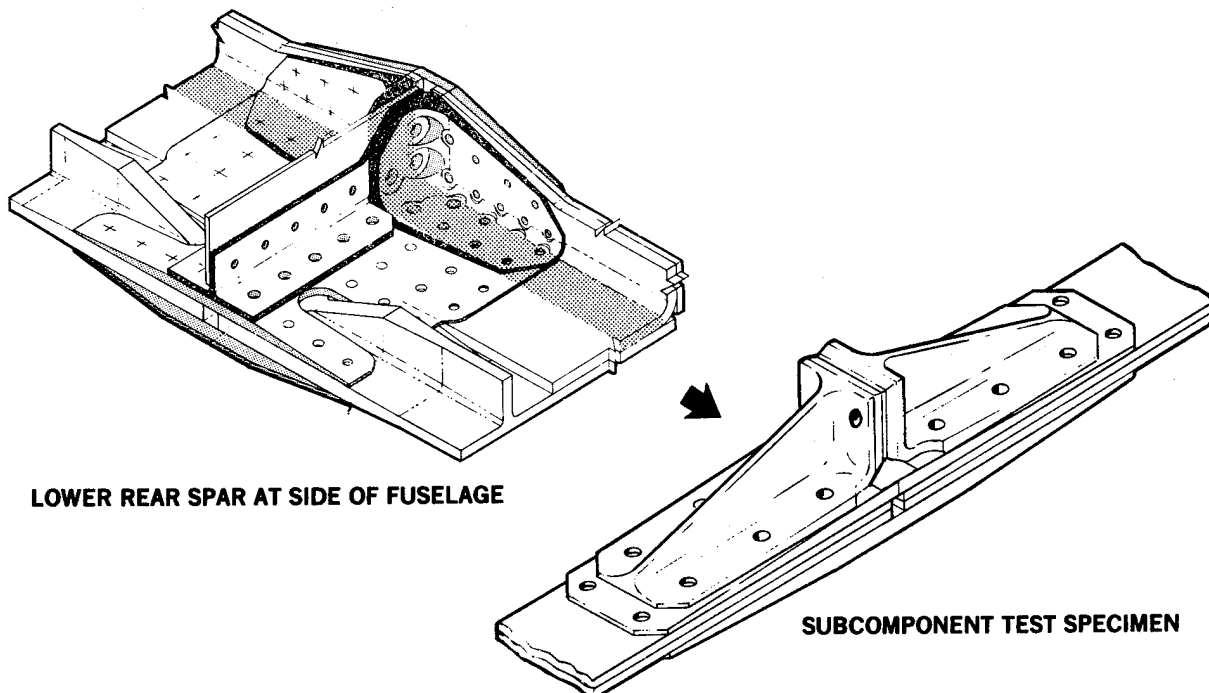


FIGURE 11.

DEMONSTRATION SUBCOMPONENT JOINT TEST RESULTS

The subcomponent specimen was loaded in axial tension to static failure at an ultimate load of 270,000 pounds. This corresponds to an average gross-section stress and strain level of about 47,500 psi and 5,100 microstrain for the composite members. The laminates, which represented the wing skin and spar caps, were each 0.5-inch thick and no thickness was added prior to the bolted connection. The failure mode was a net-section tension failure through the first row of fasteners in the composite panels, as shown in Figure 12.

The specimen was equipped with 15 strain gages to provide data on the load distribution throughout the joint. Load-indicating tension bolts were used at the attachment between aluminum fittings to monitor the load transfer at that point. A side restraint equipped with a load cell was used to react and measure the kick force at the specimen centerline which results from the shifting center of mass. The ultimate stress and strain levels achieved in the test were the highest to date for a multirow joint with this particular fiber pattern and overall configuration.

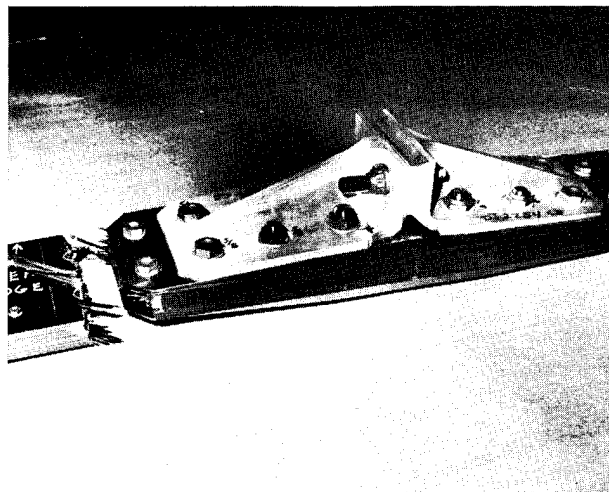
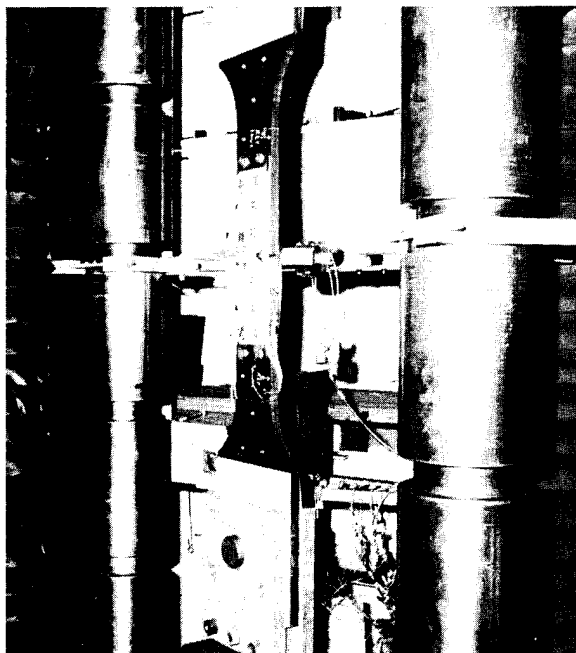


FIGURE 12.

DEMONSTRATION SUBCOMPONENT JOINT
ANALYSIS/TEST CORRELATION

A NASTRAN finite-element model was constructed with each joint member represented in its actual geometry. Fastener holes were modeled in a gross sense to properly represent member stiffnesses and facilitate the revised approach to modeling the bolt load transfer. The revised approach features bending elements representing the fasteners, with axial bars used to react the shear load transfer to the joint members. The local stress concentration effects are not measured by the model, but are accounted for in semiempirically derived bearing-bypass interaction curves.

By taking the bearing and bypass loads from the model and comparing them with the calculated strength envelopes at each row of fasteners, an ultimate load of 260,000 pounds was predicted (Figure 13). This falls within 4 percent of the tested failure at 270,000 pounds, and is easily within the range of strengths that may result from variations in material properties and fastener hole tolerances. Strain readings were taken at selected locations throughout the joint and compared with predicted strains from the analytical model with generally good correlation. These results provided a sufficient level of confidence in the analysis methodology to use the same approach for the technology demonstration specimen.

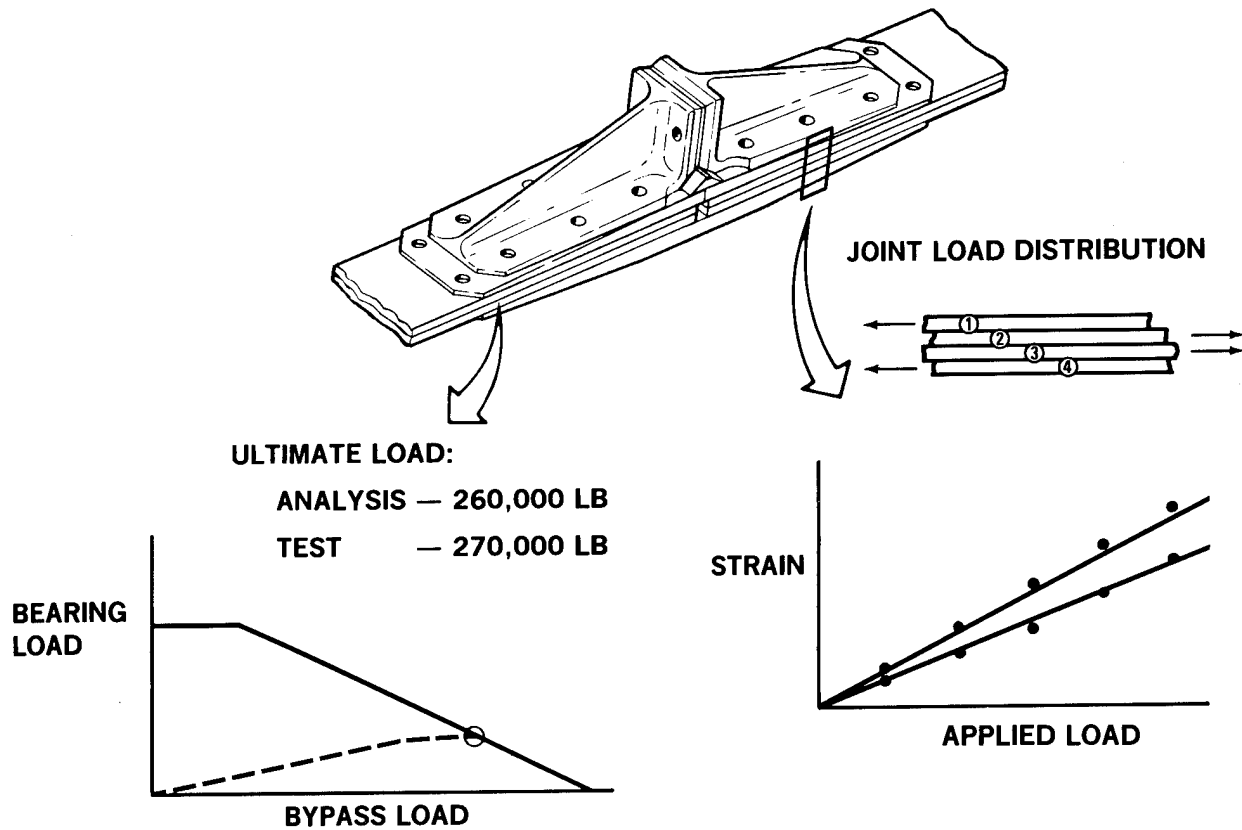


FIGURE 13.

TECHNOLOGY DEMONSTRATION JOINT

The Phase II test program culminates in a static tension test of a large bolted joint representing the lower rear spar and wing skin splice at the side of fuselage attachment, as shown in Figure 14. The wing skin, spar cap, and stiffener web members are all composite parts, fabricated with the (37.5% 0°, 50% +45°, 12.5% 90°) fiber pattern. The lower surface wing box structure away from the joint was designed to ultimate strain criteria of approximately 5,250 microstrain, with a skin-stringer load intensity of 30,000 pounds per inch. Due to the potentially high out-of-plane forces, the two tee splices and the lower skin splice were made of titanium, while the two corner fittings were aluminum.

Splice members were tapered and fastener sizes were tailored in an attempt to optimize the bolt load distribution for maximum load transfer. This specimen presents a challenging task for stress analysis because of the multiple layers and types of materials, resulting in a more complex load distribution. The dihedral and sweep break that would be present in actual structure has not been included for this specimen, but the asymmetric nature of the specimen itself induces out-of-plane deflections and nonuniform load transfer that must be accounted for analytically.

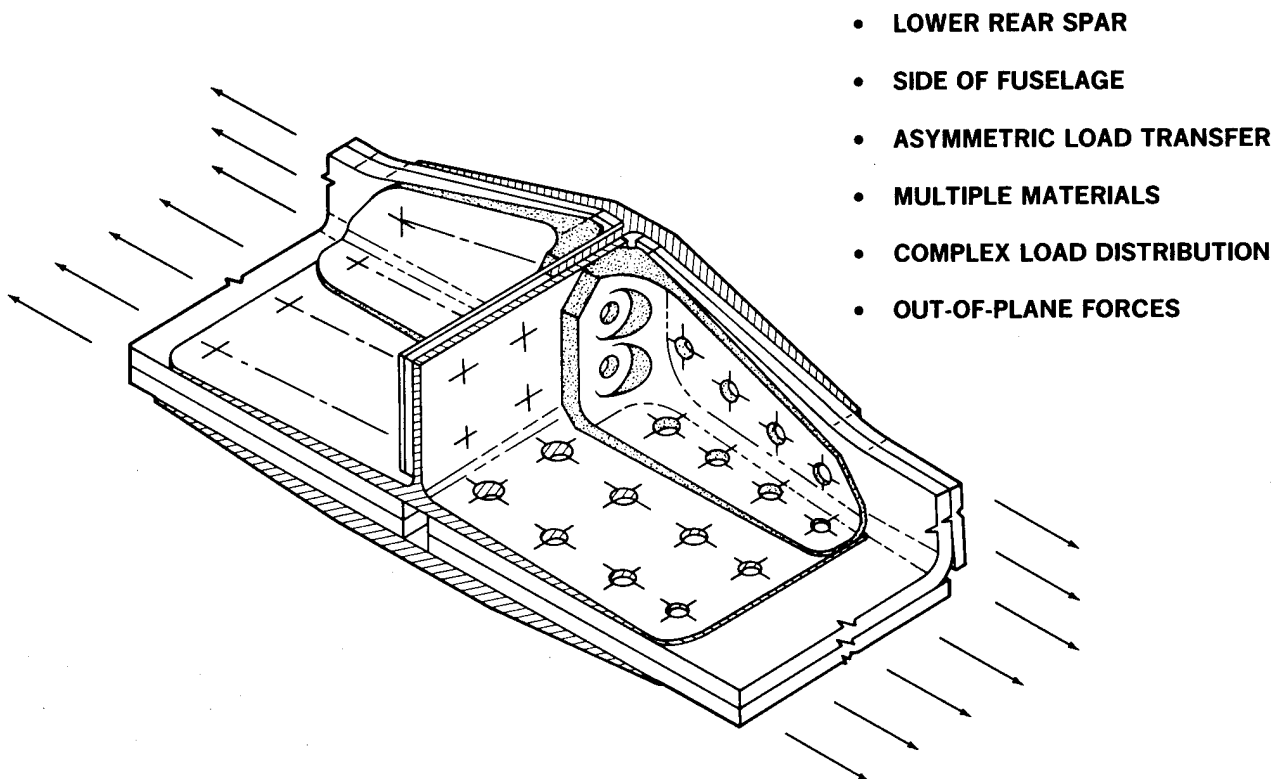


FIGURE 14.

TECHNOLOGY DEMONSTRATION SPECIMEN
ASSEMBLY

The technology demonstration test article is shown in Figure 15 in the process of being assembled. The specimen is pictured with one side of the center joint test section fully assembled in the foreground, while the background shows the various parts of the assembly as separate pieces. Most of the laminates that make up the joint are flat plates except for the spar cap members. These are angle sections which are fabricated on an aluminum male tool with thickness transitions machined into the tool surface. In all cases, the laminate quality was excellent. Large aluminum end fittings are used to transfer the applied tension load from the test machine. The composite parts are increased in width and thickness before the member is attached to the end fittings. Despite the large number of components, the assembly of the center test section was completed without the use of shims in any portion of the joint.

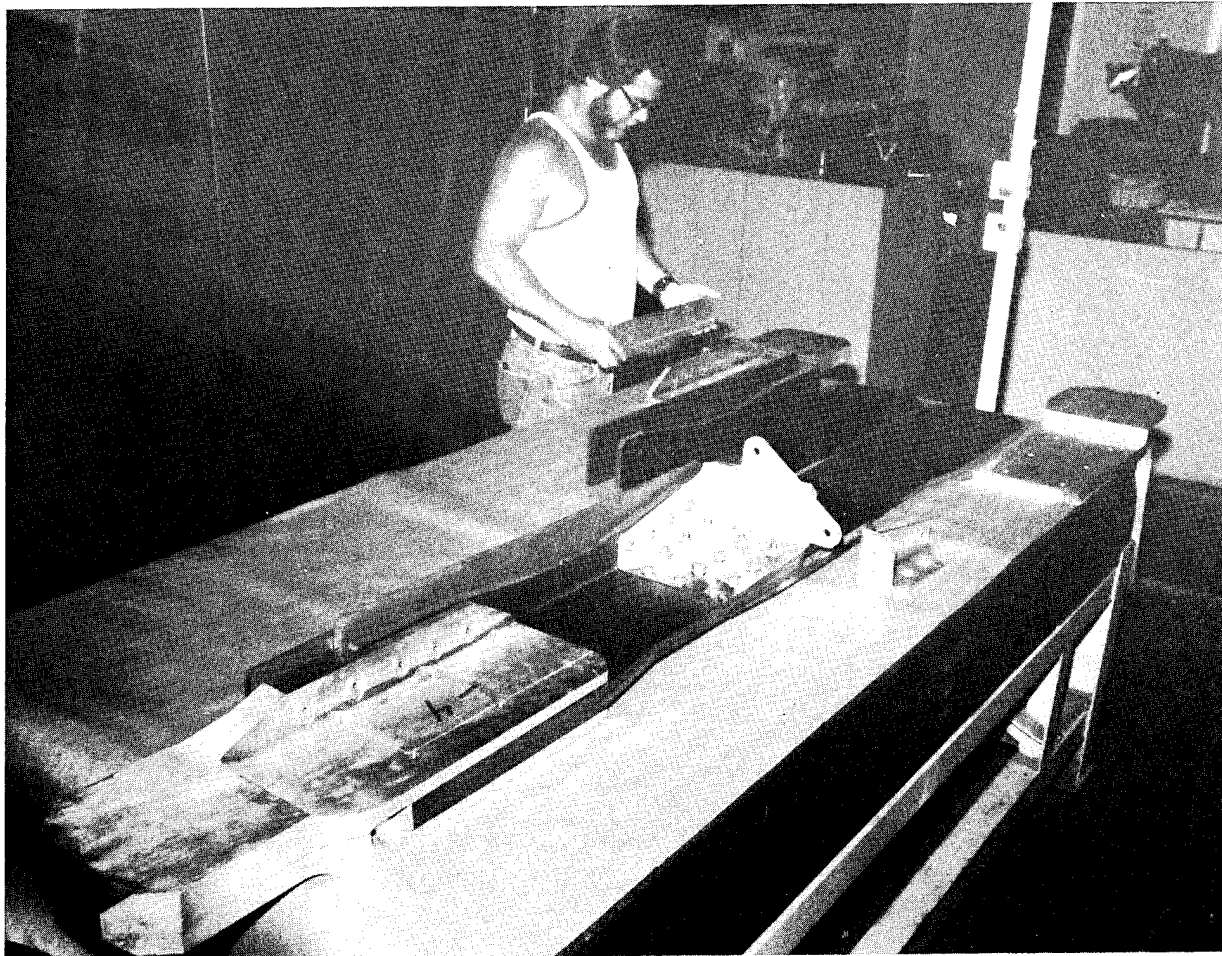


FIGURE 15.

TECHNOLOGY DEMONSTRATION JOINT

A close-up of the joint test section is shown in Figure 16. One noticeable difference between the actual specimen design and the line drawing previously shown is the portion of each aluminum corner fitting that was removed on the lower surface at the first row of fasteners. This design change was made in an attempt to decrease the load transfer at that point, causing a higher ratio of bypass load to bearing load, which results in a higher overall joint strength.

Testing of the specimen is scheduled for August 1984. The anticipated ultimate strength is approximately 435,000 pounds, pending the completion of the detailed stress analysis.

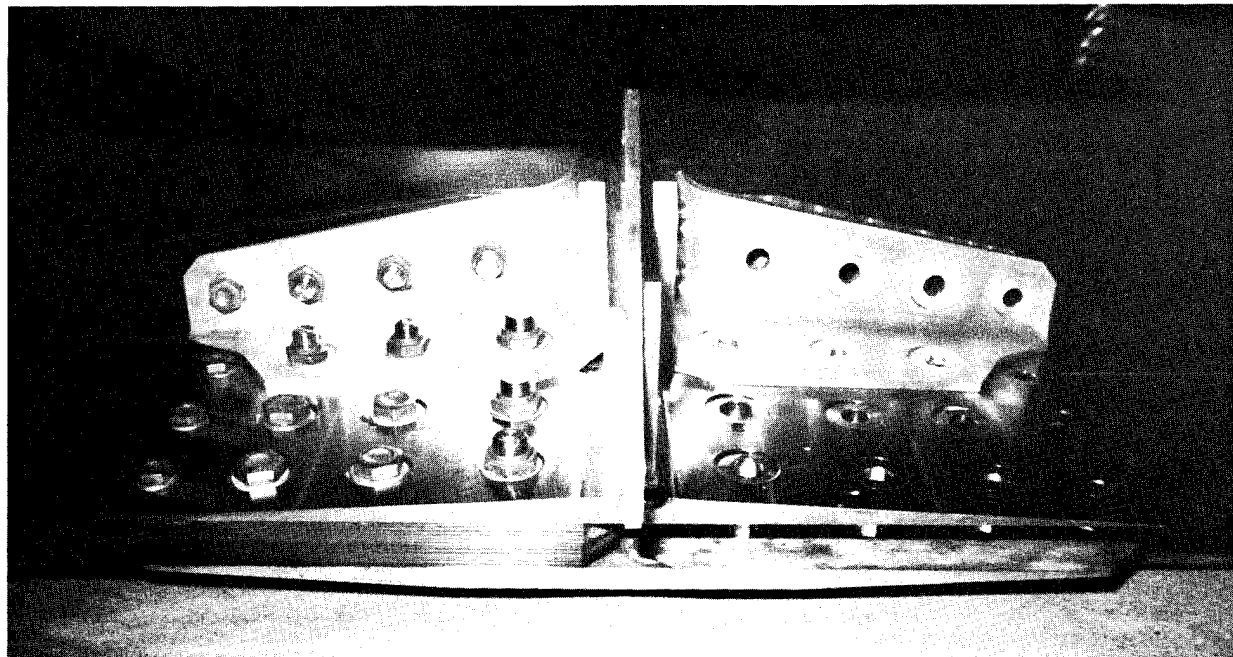


FIGURE 16.

CONCLUDING REMARKS

The Critical Joints program has been successful in meeting the original set of objectives. The feasibility of highly loaded bolted joints in composite structure was demonstrated. Useful methodology for design and analysis was developed and the accuracy of analytical strength predictions was verified by structural test. After the technology demonstration test is conducted, several minor tasks will remain to be done in the program, which is scheduled for completion by the end of 1984. It should be noted that despite the significance of these achievements, there are areas of the composite bolted joint technology which warrant further investigation. These issues as well as the detailed results of the program will be fully reported in the final reports on the NASA contract.

**RELIABLE STRENGTH PREDICTIONS FOR COMPLEX MULTI-ROW BOLTED JOINTS
IN COMPOSITE STRUCTURES WERE ACHIEVED**

**OPTIMUM MULTI-ROW JOINT PROPORTIONS HAVE BEEN IDENTIFIED AND
VERIFIED BY TEST**

**FINITE ELEMENT AND SEMI-EMPIRICAL METHODS CAN BE COMBINED FOR
COMPLEX JOINT GEOMETRIES**

**EMPIRICAL DATA ARE REQUIRED TO ESTABLISH BEARING/
BYPASS INTERACTIONS**

**USE OF METALLIC SPLICING MEMBERS AVOIDS PREMATURE FAILURES DUE TO
HIGH OUT-OF-PLANE FORCES**

**THE EFFECTS OF VARIATIONS IN MATERIAL PROPERTIES AND
MANUFACTURING TOLERANCES ON ALLOWABLE JOINT STRENGTHS WARRANT
DETAILED EXAMINATION**

**FURTHER INVESTIGATION OF COMPOSITE BOLTED JOINTS LOADED IN
COMPRESSION IS NEEDED**

REFERENCES

1. Hart-Smith, L. J.: Bolted Joints in Graphite-Epoxy Composites. NASA CR-144899, January 1976.
2. Hart-Smith, L. J.: Design Methodology for Bonded-Bolted Composite Joints. USAF Contract Report AFWAL-TR-81-3154, Vol. I, February 1982. (Available from DTIC as AD A117 342.)
3. Nelson, W. D.; Bunin, B. L.; and Hart-Smith, L. J.: Critical Joints in Large Composite Aircraft Structure. NASA CR-3710, August 1983.
4. Bunin, B. L.: Critical Composite Joint Subcomponents — Analysis and Test Results. NASA CR-3711, September 1983.

JOINTS AND CUTOPTS IN
FUSELAGE STRUCTURE
CONTRACT NAS1-17701

D. J. Watts
Douglas Aircraft Company
Long Beach, California

ACEE Composite Structures Technology Conference
Seattle, Washington
August 13-16, 1984

JOINTS AND CUTOUTS IN FUSELAGE STRUCTURE

ABSTRACT

The technical issues in the design of joints and cutouts in composite fuselage structure of large transport aircraft are being investigated in a special program conducted by Douglas Aircraft under contract to NASA. An attempt is being made to resolve issues by performing design studies and strength analyses and by manufacturing and testing representative specimens. The initial design study involves design of a 30-foot composite fuselage barrel section located forward of the wing on a large commercial transport aircraft, selected as the baseline vehicle for the program. A composite fuselage design is compared to the baseline design to show a 32-percent weight savings. The number of fasteners in the composite skin splice has been reduced, and 60 percent of the longitudinal skin splices has been eliminated so that 93,000 fewer fasteners are used than in the baseline. The longeron and shear tees are secondarily bonded to the skins to eliminate all fasteners within the skin panels. The design of a passenger entry door cutout is discussed and a method proposed for reducing harmful stress concentrations in the corners by using lower modulus glass fiber or by using low-modulus layup patterns to divert the loads away from the corners.

Out-of-plane peel forces caused by pressure pillowing action are discussed as a durability and damage tolerance concern, and are accounted for in the design and test program. The structural test plans for the technology program are presented. Ancillary tests will be conducted to provide design data, and demonstration panel tests will provide additional data and prove the design. Strain gage data will be correlated with analytical predictions. Evidence of the producibility of the design will be provided by fabrication of large composite test panels.

PROGRAM OBJECTIVES

The objectives of this contract are to develop and demonstrate the technology for joints and cutouts in composite fuselage structure which meet all design requirements of a 1990 large transport aircraft. The demonstration articles are to be representative of a section of the fuselage that contains a door cutout and joints. Manufacturing and process development will be conducted as necessary to assure the manufacture of high-quality demonstration test articles.

The design development will integrate other technologies such as durability and damage tolerance where the technology is deemed to have a significant influence on the design of the fuselage joints and cutouts.

PROGRAM OBJECTIVES

- **DEVELOP AND DEMONSTRATE THE TECHNOLOGY FOR JOINTS AND LARGE CUTOUTS IN COMPOSITE FUSELAGE STRUCTURE OF A LARGE TRANSPORT AIRCRAFT**

DEVELOPMENT PLAN

The development plan, shown in Figure 1, features the baseline vehicle for design criteria, for structural loads, and for a representative structural arrangement of doors, windows, and manufacturing joints in the shell structure. A conceptual design will be prepared of the fuselage barrel section forward of the wing featuring the basic structure, joints, and cutouts to provide a realistic basis for the development of analysis methods and development test programs. A contemporary toughened resin system has been selected for the manufacture of all test specimens including the demonstration articles.

The design of the basic structure will incorporate features for durability, damage tolerance, electromagnetic effects, repair, postbuckling, effects of defects, and other fuselage technologies where the technologies are deemed to have a significant effect on the design development of joints and cutouts.

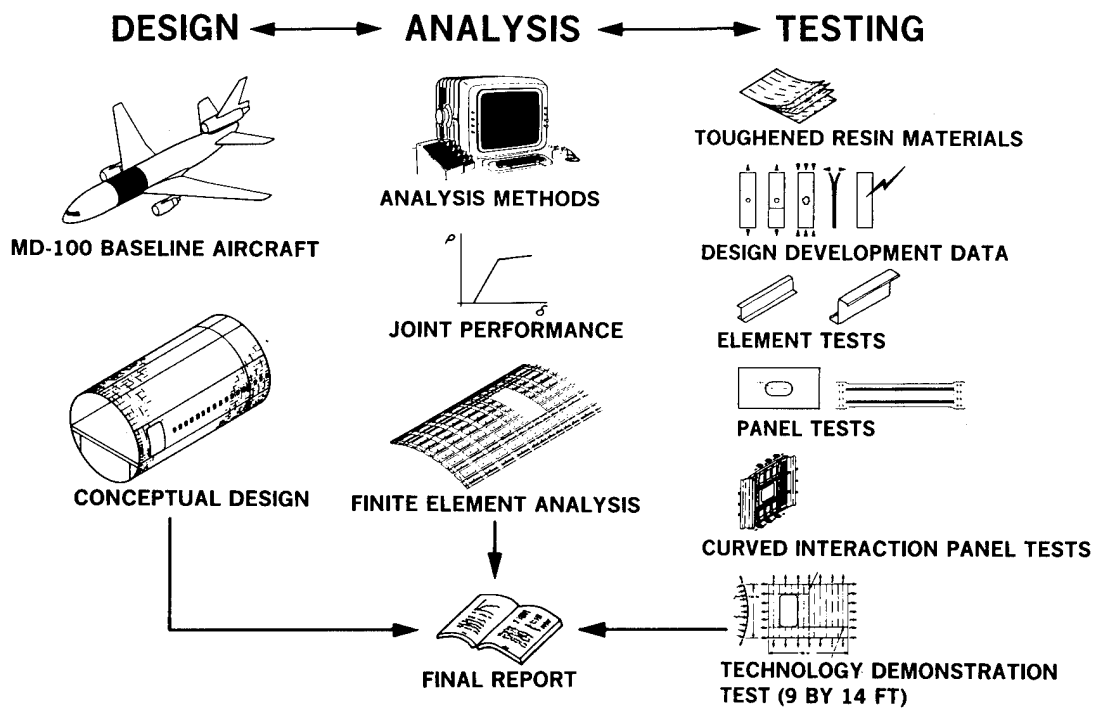


FIGURE 1.

SCHEDULE

The development of joints and cutouts composite fuselage technology program started on March 21, 1984. The draft of the final report is due 28 months after this date. The technical effort has been scheduled for 27 months to allow 1 month to complete the draft final report. The schedule is shown in Figure 2.

The critical path for the program is the design, fabrication, and test of the development and demonstration test specimens. The 24-month period for completion of all tests requires some parallel activity even though the preferred approach is to conduct the activities in series to allow more effective use of the design and process development data.

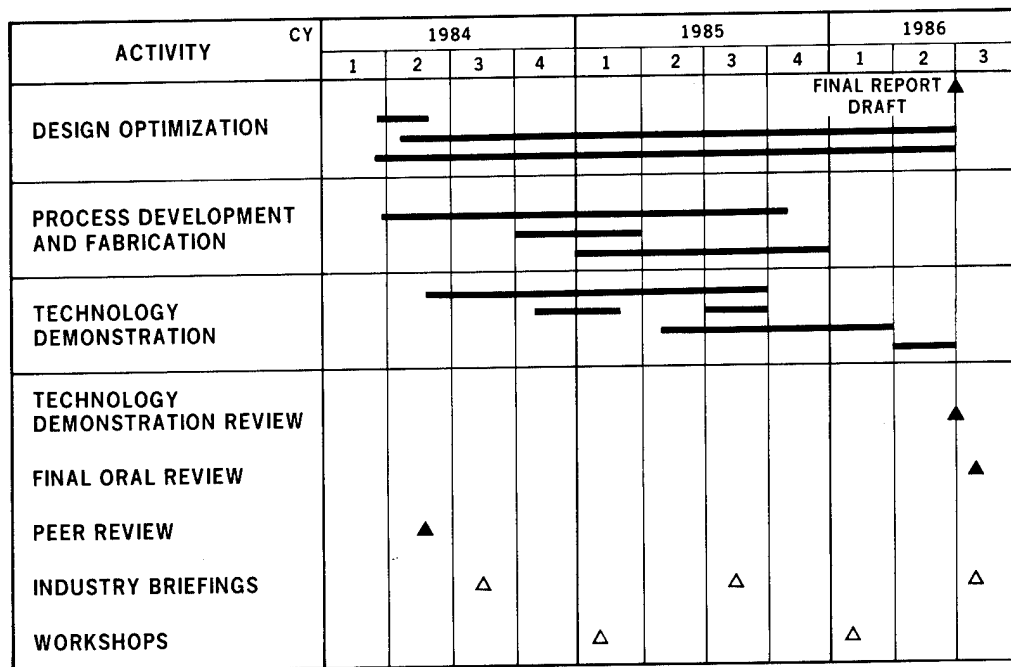


FIGURE 2.

FUSELAGE STRUCTURAL ARRANGEMENT

The baseline fuselage structural arrangement is shown in Figure 3. This arrangement has been retained for the Composite Fuselage Technology program with few exceptions. The fuselage diameter and length, and the location of major cutouts for passenger doors, windows, wheel wells, wing carry-through, and the flight compartment enclosure are established by design considerations not influenced by the substitution of composite materials. The 20-inch frame spacing assures the same shell stability characteristics. The closely spaced longerons provide shear and buckling constraint for the skin panels and give a multiple load path arrangement for good fail-safe design.

The five manufacturing breaks are the same as for the baseline as a proven size for assembly and handling. The 30-foot barrel section forward of the wing, identified by the darker shading, has been selected for design development. Conceptual design studies will be performed, supported by strength analyses, to assure that the manufacturing development and test specimens are representative of a realistic composite fuselage structure.

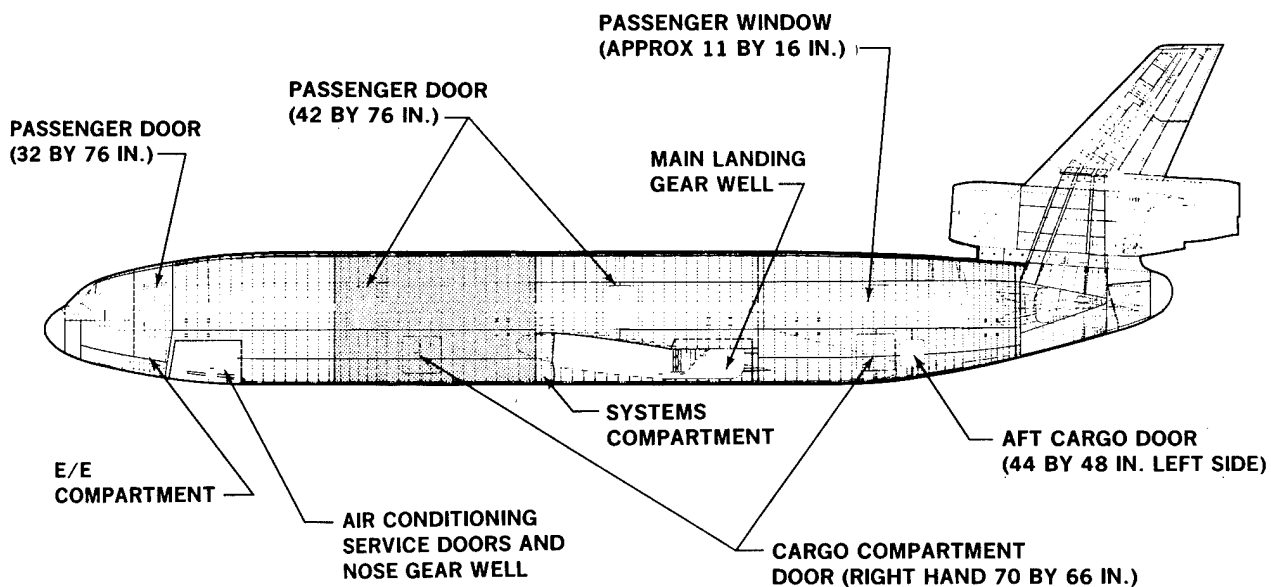


FIGURE 3.

TYPICAL FUSELAGE CROSS SECTION

A typical cross section of the fuselage is shown in Figure 4. The fuselage frame zee form provides an efficient shape for frame bending stiffness with an unobstructed side for attachment to shear tees, longerons, floor beams, struts, and interior systems. The frame depth in the passenger cabin area is locally reduced at passenger height to provide the maximum interior width. The frame depth is also reduced locally to accommodate standard cargo containers. The main function of the frames is to stabilize the fuselage shell. The composite frames are sized to have a bending stiffness (EI) equal to or greater than the baseline frame EI at the same 20-inch frame spacing. The low-density, higher modulus IM6 fiber manufactured by the Hercules Corporation will be used in woven fabric form to produce a stiff, lightweight frame design.

The 10 baseline longitudinal skin splices were reduced to 4 in the composite fuselage design. The aluminum skin panel sizes were limited by the panel size available from the mill, but it is feasible to build the larger size composite panels. This change eliminates almost 9,000 running inches of bolted splice structure.

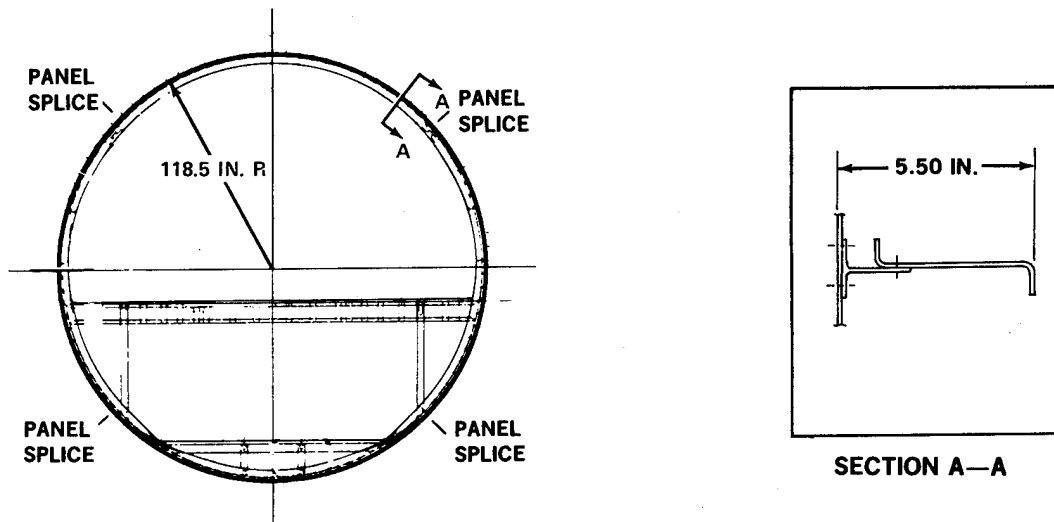


FIGURE 4.

PASSENGER DOOR CUTOUT

The size and location of the large passenger door cutouts in the fuselage shell are established as a customer requirement and are unrelated to structural considerations. The cutout shown in Figure 5 is located in the forward fuselage. Loads in the structure surrounding the cutout are a product of cabin pressure, shear, and bending. The passenger door carries only the direct pressures exerted on it and transmits those direct pressures into the jamb structure by a series of stops located on both sides of the cutout. The loads in the shell structure must be beamed around the cutout and special attention must be given to avoid stress concentrations in the corners.

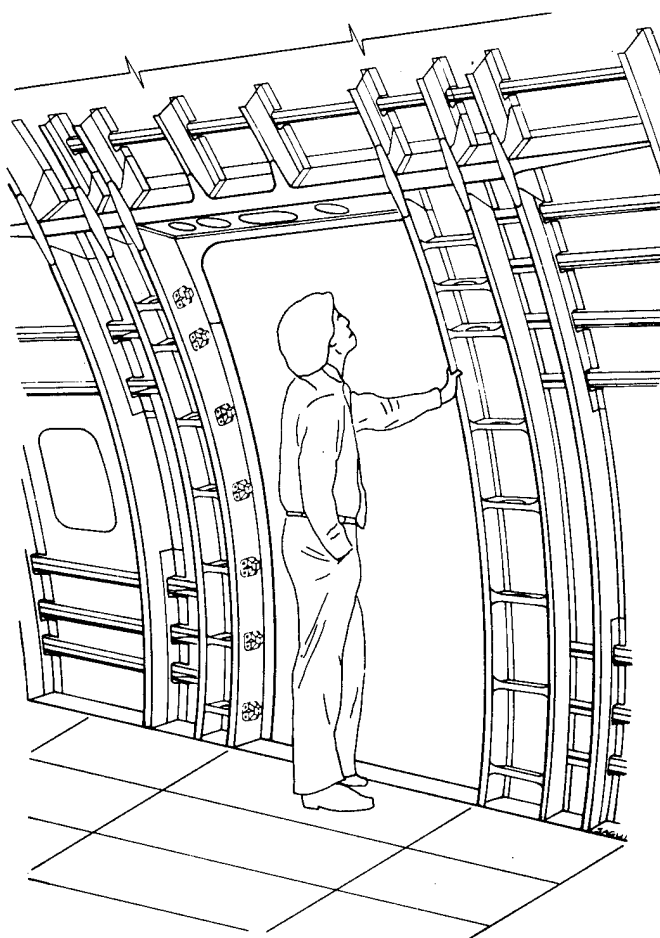


FIGURE 5.

DESIGN CRITERIA AND LOADS

The fuselage structure must be analyzed for an array of load conditions per Federal Aviation Regulations Part 25 (FAR 25). The ground conditions include taxi, landing impact, and braked roll conditions. Dynamic analyses are performed for the flexible airplane. The flight conditions include both symmetric and asymmetric cases for maneuver and continuous gust for the rigid-body and flexible airplane. A separate design ultimate condition of two times the cabin air pressure (2P) is applied independent of all other loads. A factor of safety of 1.5 is imposed on the limit design loads. The flight load conditions must be considered with and without cabin air pressure to determine which is more critical. The flight-by-flight repeated load spectrum for the baseline aircraft will be used for the composite fuselage durability and damage tolerance assessment. One lifetime is 60,000 flight hours and the average flight length is two hours.

DESIGN CRITERIA AND LOADS (FAR 25)

- **CABIN PRESSURE (P) IS 8.6 PSI + 0.5 PSI VALVE TOLERANCE**
- **FLIGHT CONDITIONS**
 - 2.5-g MANEUVER
 - CONTINUOUS GUST
 - LANDING IMPACT
- **FLIGHT-BY-FLIGHT REPEATED LOAD SPECTRUM**
 - ONE LIFETIME IS 60,000 FLIGHT HOURS
- **DESIGN ULTIMATE LOADS**
 - 2P ACTING ALONE
 - 1.5 (1P + LIMIT FLIGHT)
 - 1.5 (LIMIT FLIGHT)

FUSELAGE LOADS

The maximum symmetrical vertical bending moment and shear limit design loads for the fuselage are shown in Figure 6. These loads are combined with cabin pressure loads to produce the highest axial and shear stresses in the fuselage shell for most of the structural members. Some aft fuselage members are more critical for asymmetrical load conditions.

The low bending moment and shear forces shown in the forward fuselage illustrate why much of the fuselage skin is critical for the 2P cabin pressure condition. The theoretical stress distribution for maximum vertical bending moment will result in peak tension stresses in the crown and peak compression stresses in the lower fuselage combined with low shear stresses. The highest shear stresses occur in the side panels where the axial stresses are low.

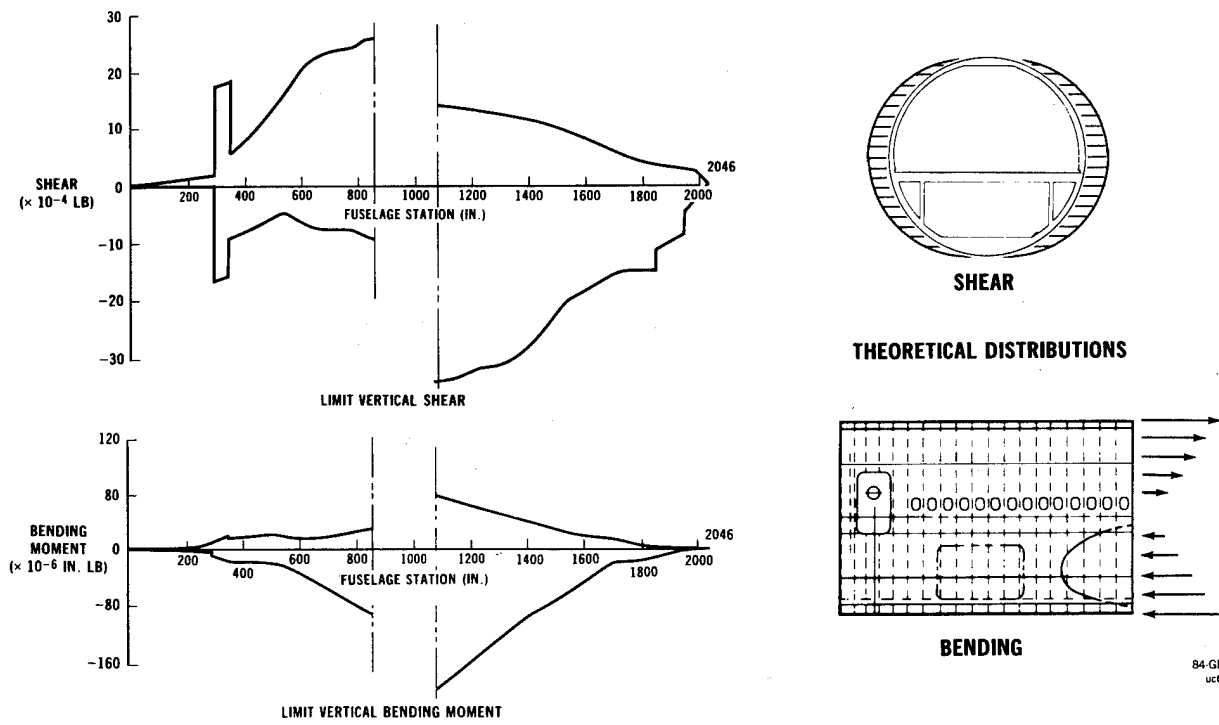


FIGURE 6.

PRESSURE PILLOWING ACTION

Pressure pillowing of the fuselage occurs when the thin skins tend to balloon outward to react the internal pressure forces by hoop tension, but are partially restrained from doing so by the frames and longeron to which they are attached.

The membrane and transverse shear forces in the skin deflect the frames and longeron outward to a point of equilibrium. The maximum skin deflection occurs at mid-bay and the maximum longeron deflection occurs midway between the frames, as shown in Figure 7.

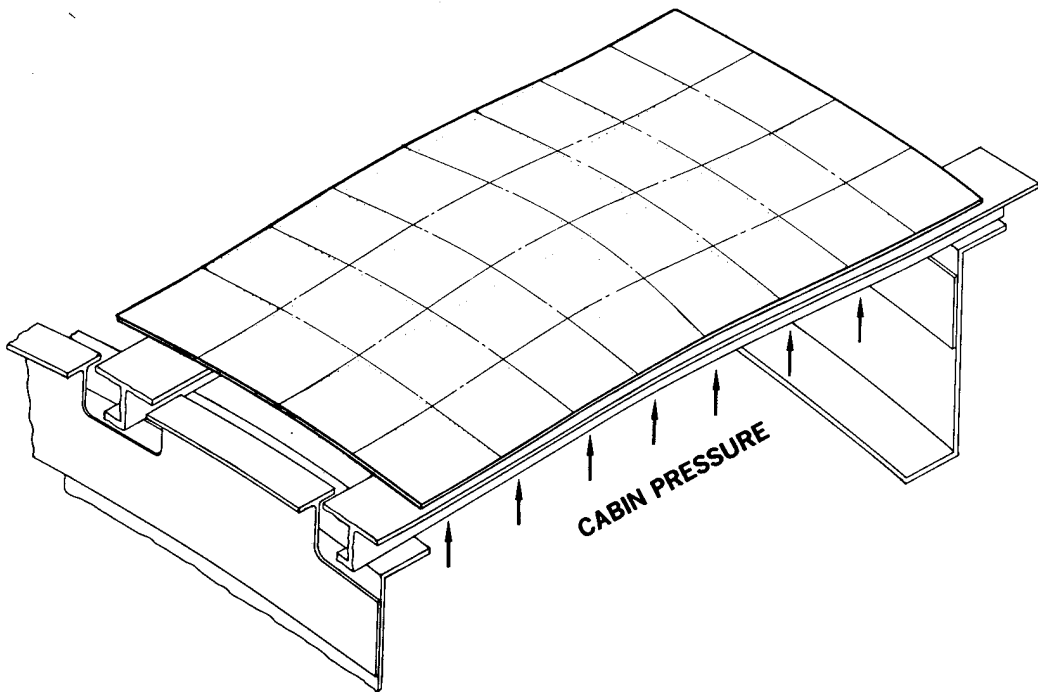


FIGURE 7.

BIAXIAL JOINT LOADS

The fuselage longitudinal and transverse skin panel splices must be analyzed for the biaxial stress fields resulting from the cabin air pressure hoop tension stresses combined with axial and shear stresses from the flight loads. A 2P cabin air pressure design ultimate load is a separate condition not combined with flight loads. The 2P case, which does not include a shear load component, will be critical in the areas where the bending moment and shear forces are low. Possibly all of the longitudinal splices will be critical for the 2P condition.

The various stress states are depicted in Figure 8.

HOOP TENSION LOADS	2,157 LB/IN.  ULTIMATE 1,078 LB/IN.  ULTIMATE	1,078 LB/IN.  LIMIT 539 LB/IN.  LIMIT
CONDITION	2P CABIN PRESSURE	1.5 (1P + LIMIT FLIGHT)
LONGITUDINAL JOINT	<p>LONGITUDINAL DIRECTION</p>	
TRANSVERSE JOINT		

FIGURE 8.

DESIGN GUIDELINES

A set of design guidelines has been compiled to provide a consistent basis for the conceptual design of the composite fuselage. The initial guidelines will be revised as design data and experience are gathered from the technology development.

An ultimate design strain level of 0.0045 in./in. was used for the conceptual design on the basis of existing test data from the NASA Critical Wing Technology program. The accrual of damage tolerance technology will influence the selection of the final design strain levels.

The baseline design included a general fail-safe criteria for the ratio of cross-sectional area. This relationship should be proven to be not valid for composite structures. Longeron size and spacing should be further optimized after composite damage tolerance technology becomes available.

An independent task is being conducted by Douglas to investigate the effects of the head size of flush fasteners, the countersink depth, and skin flexure on the strength of composite skin splices. These data will be available for the conceptual design of the splices.

THE DESIGN ULTIMATE STRAIN LEVEL IS 0.0045 IN./IN.

THE BENDING STIFFNESS (EI) OF THE COMPOSITE FRAMES AND LONGERONS IS EQUAL TO OR GREATER THAN THEIR BASELINE COUNTERPARTS

THE ALLOWABLE ONSET OF SHEAR BUCKLING IS 50 PERCENT OF LIMIT LOAD

THE MINIMUM SKIN GAGE IS 0.070 INCH

FRAME SPACING IS 20 INCHES

AVERAGE LONGERON SPACING IS 7.3 INCHES

MINIMUM THREADED FASTENER SIZE IS 3/16-INCH DIAMETER

MINIMUM FLAT AT BASE OF COUNTERSINK IN SKIN IS 0.010 INCH

MATERIAL IS HEXCEL F584/IM6 — TOUGHENED EPOXY RESIN WITH HIGH MODULUS CARBON FIBERS

BASIC PANEL CONSTRUCTION

The basic skin panel structural arrangement, shown in Figure 9, features a pseudo-isotropic solid laminate skin, J-section longerons, and shear tees to attach the zee-frames to the skin panel.

The basic cover skin is 12 plies of tape with a (25%/50%/25%) layup of a $[0^\circ, +45^\circ, 90^\circ]$ pattern for a total thickness of 0.066 inch. The addition of lightning strike protection material and surface treatment for appearance and paint adhesion will increase the total thickness. Plies are added to the skin as required for shear strength. Increased longitudinal loads from fuselage bending are accounted for by increasing the longeron area up to the thickness where splicing at the transverse barrel joints becomes a design problem. A relationship is also maintained between skin area and longeron area for skin buckling restraint and damage tolerance purposes.

The panels will be fabricated by independently curing the detail parts and adhesively bonding the longerons and shear tees to the skins. The frames will be bolted to the shear tees around the periphery and bolted shear clips will be used for the frame-to-longeron attachment.

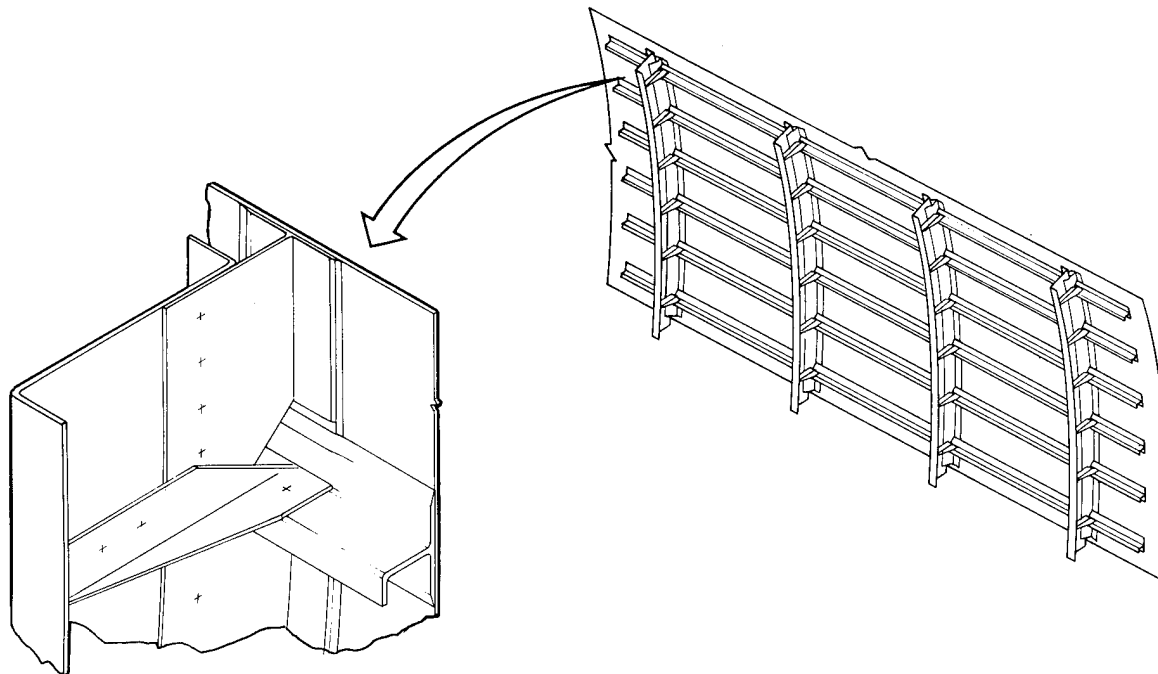


FIGURE 9.

WEIGHT SAVINGS ESTIMATES

In the course of the study, the weight savings for the total composite fuselage shell, compared to the baseline aluminum shell, were estimated to be 32 percent at a design ultimate strain level of 0.0045 in./in. The large percentage of weight savings shown in Figure 10 is attributable to the 44 percent lower density of the advanced composite and the high modulus attainable in the stiffness critical frames and longerons.

The total weight savings of 13,249 pounds includes a weight penalty of 1,230 pounds for lightning protection, for surface preparation, and for paint to protect the composite material from ultraviolet ray degradation.

The weight savings estimates were based on using an advanced composite toughened epoxy resin with AS4 carbon fibers manufactured by the Hercules Corporation. The IM6 fiber manufactured by the same company is now being used for the composite technology program. It has a higher modulus of 12 percent compared to the AS4 fiber. The higher modulus should increase the overall fuselage weight savings by 3 to 5 percent.

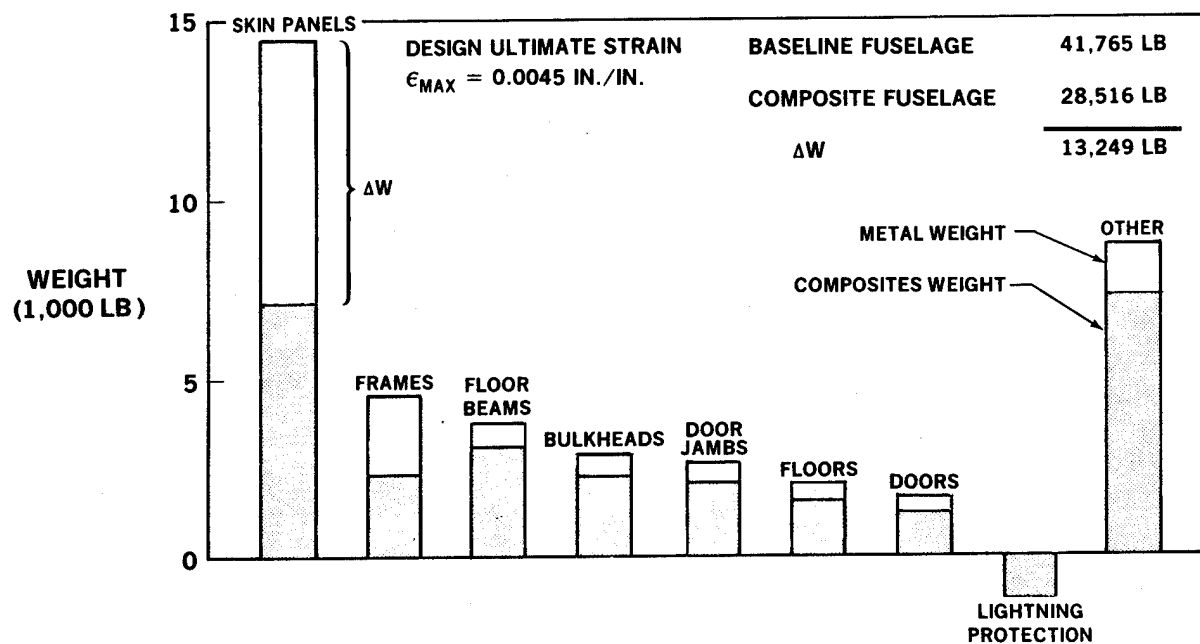


FIGURE 10.

WEIGHT SAVINGS STUDY

The weight savings for the composite fuselage longeron-stiffened skin panels, compared to the conventional baseline skin panels, were estimated as a function of the design strain level. The low rate of increase of weight saved with increasing strain, shown in Figure 11, is an indication that other design requirements are controlling the minimum member sizes. The axial stress in the crown along the length of the baseline fuselage is shown in Figure 11. A comparison can be made to illustrate the weight savings and some of the limitations. The composite cover skins and longerons together produce an equivalent extensional modulus of about 10.5 million psi, which is comparable to the modulus of the baseline aluminum material. The weight savings would be 44 percent for the same member sizes. A design ultimate strain level greater than 0.0045 in./in. would slightly increase the weight savings for only a short length of the fuselage aft of station 1500. The axial stress in the crown forward of the wing is low and the longerons will be designed to match the bending stiffness of the baseline. The skin will be designed to a minimum gage of 0.07 inch or for the 2P cabin pressure condition below a 0.0035 in./in. design ultimate strain level.

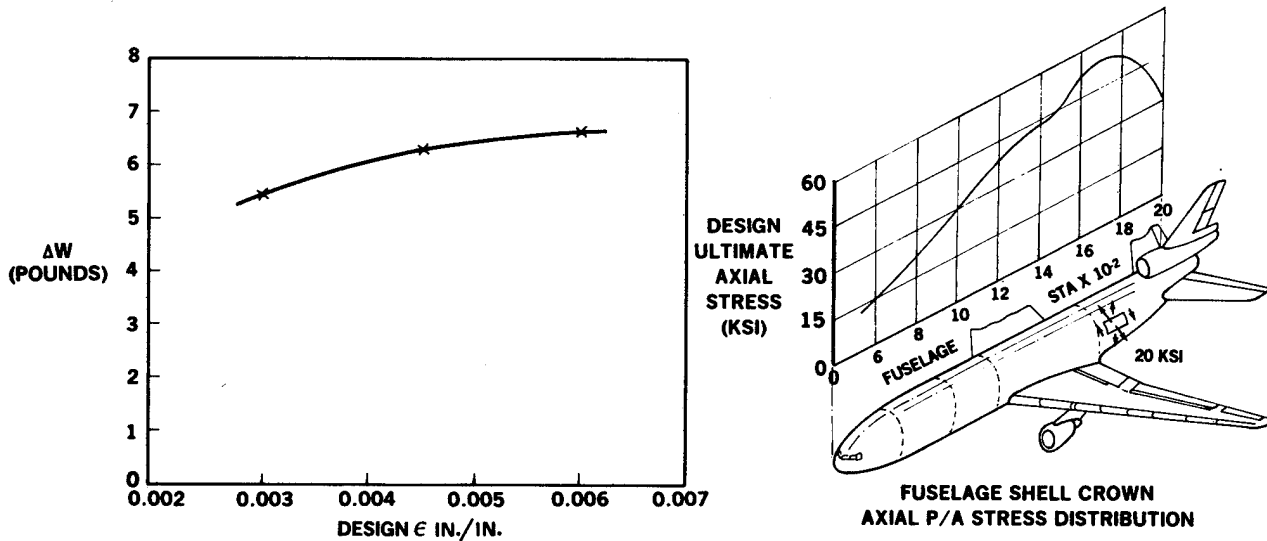


FIGURE 11.

LONGERON SELECTION

Longerons are used throughout the fuselage to carry fuselage bending loads, to stabilize the skins from shear and compression buckling, and to provide additional residual strength for damaged skin panels. The same shape and height will be generally used for all longerons but the cross-sectional area will vary, depending on load intensities and stiffness requirements.

Desirable features for the longeron configuration include a high EI for bending stiffness, a low height for minimizing the fuselage wetted area, flange and standing leg dimensions which will permit splice bolt installation, a cross-plied pattern for adequate joint strength, and a convenient method for frame-to-longeron attachment at over 5,000 intersections. Attaching to the shear webs is preferable to attaching to the cap flanges. The skin flange must also be designed to sustain peel forces from pressure pillowng action. In the study phase of this program, five different cross sections were evaluated, based on such features. The study results, shown in Figure 12, indicate that the J-section longeron is the preferred configuration.

DESIRABLE DESIGN FEATURES		OPEN HAT	CLOSED HAT	BLADE	"I"	"J"
LOW HEIGHT	— INFLUENCES USABLE CABIN SPACE FOR A GIVEN FUSELAGE OUTSIDE DIAMETER	GOOD	GOOD	POOR	BEST	GOOD
BENDING/TORSIONAL STIFFNESS	— COMPRESSION STRENGTH — PANEL INSTABILITY CONSTRAINT — RESIDUAL STRENGTH	GOOD	BEST	WORST	GOOD	GOOD
PEEL STRENGTH (FROM SKIN)	— PANEL BUCKLING — PRESSURE PILLOWING	POOR	GOOD	GOOD	GOOD	GOOD
ATTACH TO FRAME	— PREFERABLE TO ATTACH THROUGH STANDING LEG WHERE BENDING STRESSES ARE LOWER	POOR	POOR	GOOD	POOR	GOOD
SPLICING SIMPLICITY	— MANUFACTURING COST — RELIABILITY	POOR	WORST	BEST	GOOD	GOOD
RATING		4	5	3	2	1

FIGURE 12.

LONGITUDINAL SKIN SPLICES

The fuselage skin is spliced in the longitudinal direction at four locations on the fuselage, resulting in about 6,000 running inches of mechanically joined skin splice structure. Figure 13 evaluates candidate splice configurations on the basis of structural integrity and for the manufacturing costs associated with bolt installation and the adaptability of the splice members for good fitup with a minimum use of shims or other rework. The lap splice ranked the highest mostly on the basis of having three rows of fasteners through each skin panel to share the loads compared to the symmetrical configuration, which has only one row of fasteners in each skin.

SPLICE CONFIGURATION	WEIGHTED SCORES					SCORE	RANKING
	FASTENER INSTL COST	FIT UP TOLERANCE	PARTS COST	ECCENTRICITY	STRENGTH		
	48	70	50	25	40	233	3
	80	56	40	50	60	286	2
	64	70	40	40	100	314	1

FIGURE 13.

TRANSVERSE SKIN SPLICES

The fuselage shell has five transverse splices to allow the manufacture of barrel sizes with a practical size for assembly and handling. The five splices produce a total of 3,700 running inches of skin splice plus 102 longeron splices at each of the five locations.

Figure 14 quantitatively compares five different skin splice configurations on the basis of weighted scores for a set of evaluation parameters. All five configurations have undesirable joint eccentricity due to the requirement for a flush aerodynamic surface. The best-rated widely spaced configuration locates the most critical end fasteners of the splice at a point of inflection where the skin flexural stress is low. For thicker skin splices, the reverse step design is preferred to minimize the joint eccentricity.

SPLICE CONFIGURATION	WEIGHTED SCORES					SCORE	RANKING
	FASTENER INSTL COST	FIT UP TOLERANCE	PARTS COST	ECCECTRICITY	STRENGTH		
	80	70	50	30	40	270	5
	80	70	40	40	60	290	3
	80	70	40	25	60	275	4
	80	35	35	50	100	300	1**
	80	70	45	40	75	310	1*

* $t \leq 0.100$ INCH

** $t > 0.100$ INCH

FIGURE 14.

PASSENGER DOOR CUTOUT DETAIL DESIGN

High-stress concentrations have been measured at corners of large cutouts of isotropic skins even though the surrounding structure has been reinforced with header beams, frames, and doublers. Figure 15 shows a typical measured stress concentration factor for an initial design and with subsequent doubler reinforcement. The stress concentration factor results from the usual peaking of the in-plane stresses, and is intensified by out-of-plane bending induced by flexing of the curved skin at the corner of the cutout. Fatigue test results have confirmed the strain gage data. Advanced composite materials offer the opportunity to alleviate the corner stress concentration by locally softening the stiffness of the skin. This will force the load transfer around the cutout to be more uniformly distributed into the framing structure, which can be designed to accommodate a higher load transfer. The stiffness can be reduced by using glass fiber materials, a hybrid with glass and carbon fibers, or by varying the carbon fiber layup pattern.

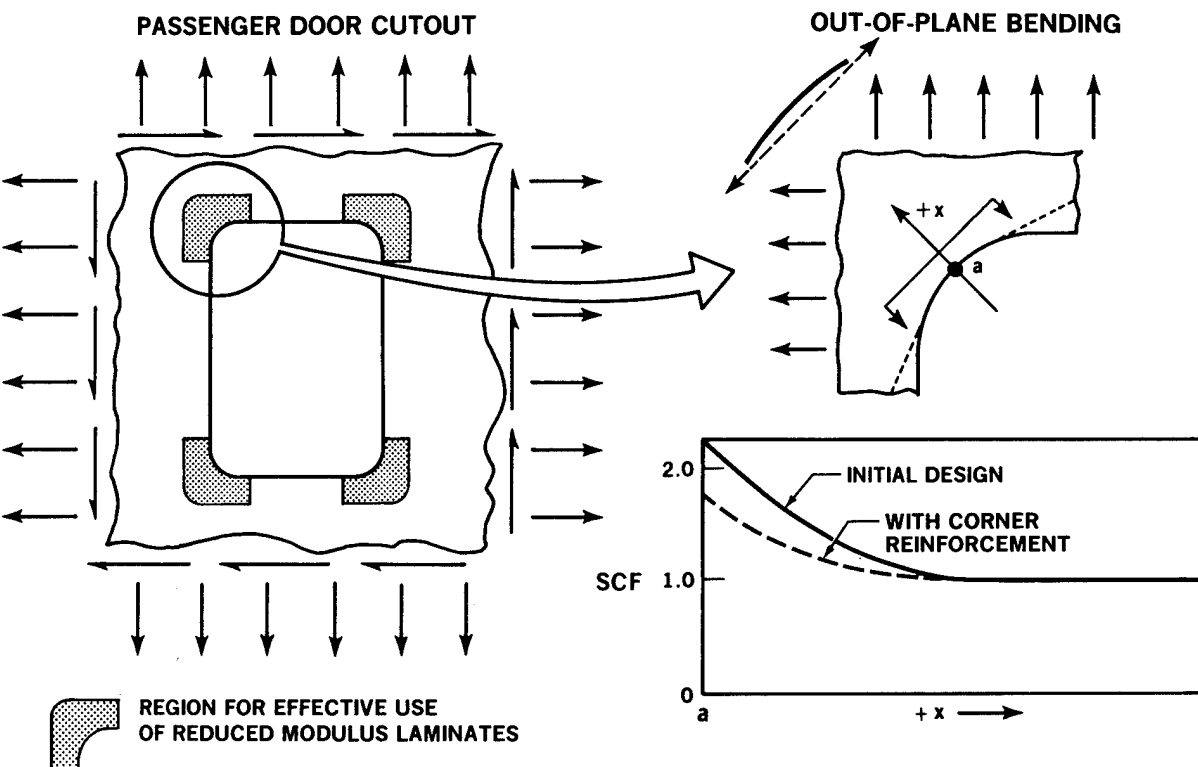


FIGURE 15.

JOINT ANALYSIS

The fuselage joint analysis approach is to determine the internal loads acting on the joint, calculate the individual bolt loads and the local stress field around each bolt, and to perform detailed strength analysis as shown in Figure 16. This effort is an extension of the Critical Wing Joint program but introduces several new technical issues:

- o Countersinking of thin skins to install flush fasteners.
- o Combined longitudinal, hoop tension, and shear force on the joint.
- o The option of adhesively bonding the thin-skin joints in lieu of or in addition to mechanical joining.

New technology is required to develop rapid methods for determining the bolt load distribution and the local stress fields for the combined loading cases. The approach will probably be to create design charts based upon finite-element analyses for a discrete number of joint configurations and load conditions. Closed-form solutions will be sought.

The Bolted Joint Stress Field Model (BJSFM) developed by McDonnell Aircraft has the capability for complex strength analysis once the bolt load and its boundary stress field are defined. The allowable strength of the countersunk thin skins must be established by test.

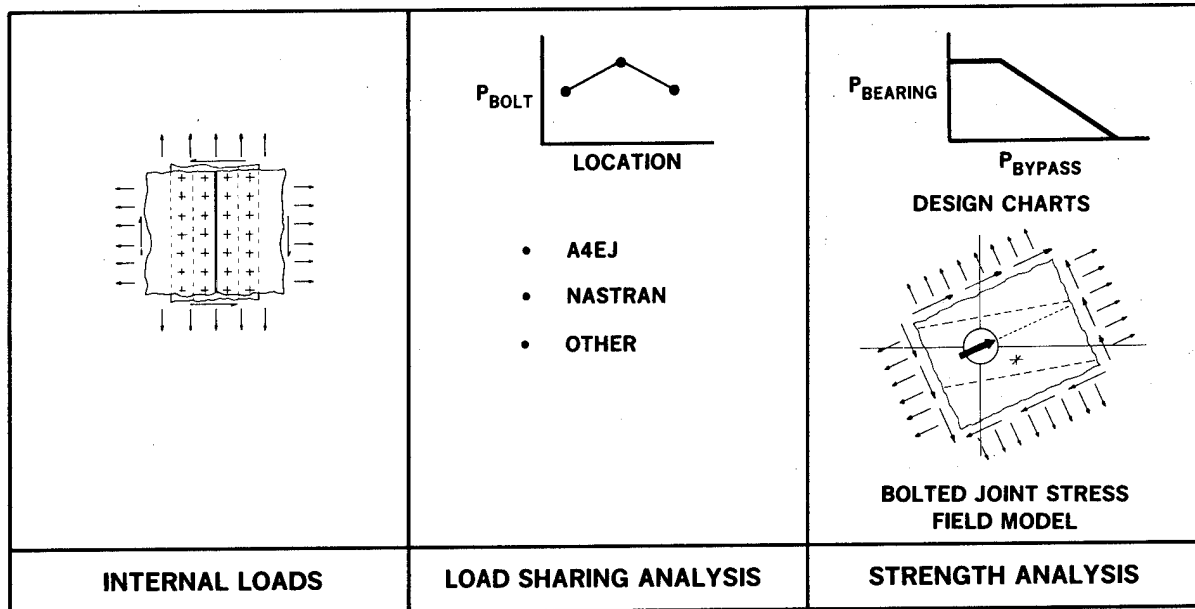


FIGURE 16.

PRESSURE PILLOWING PEEL FORCES

High-peel force occurs along the edge of the flanges of the frame shear tees and longerons where they attach to the cover skin, as shown in Figure 17. A high width-to-thickness ratio (b/t) for the flange is desirable to reduce the peel stresses, but is a counter requirement to the low b/t ratio needed for local longeron compression stability and for restraint of panel buckling. Tapering at the edge will reduce the peel stresses.

The effects of pressure pillowing have been investigated extensively on adhesively bonded metal fuselage structures. Two differences are encountered with composite fuselages: the composite skins have a much lower transverse shear strength, and the epoxy matrix material is less ductile than the adhesive so that peel failure can occur in the matrix at lower stress levels. Durability and damage tolerance must be investigated since the epoxy resin can fail in fatigue and drastically reduce the panel buckling and compression strength.

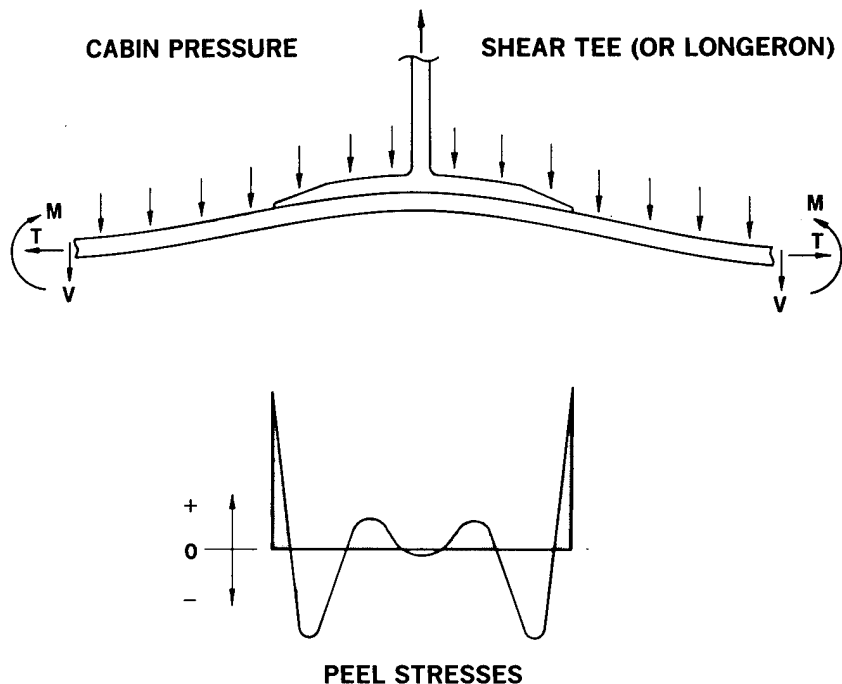


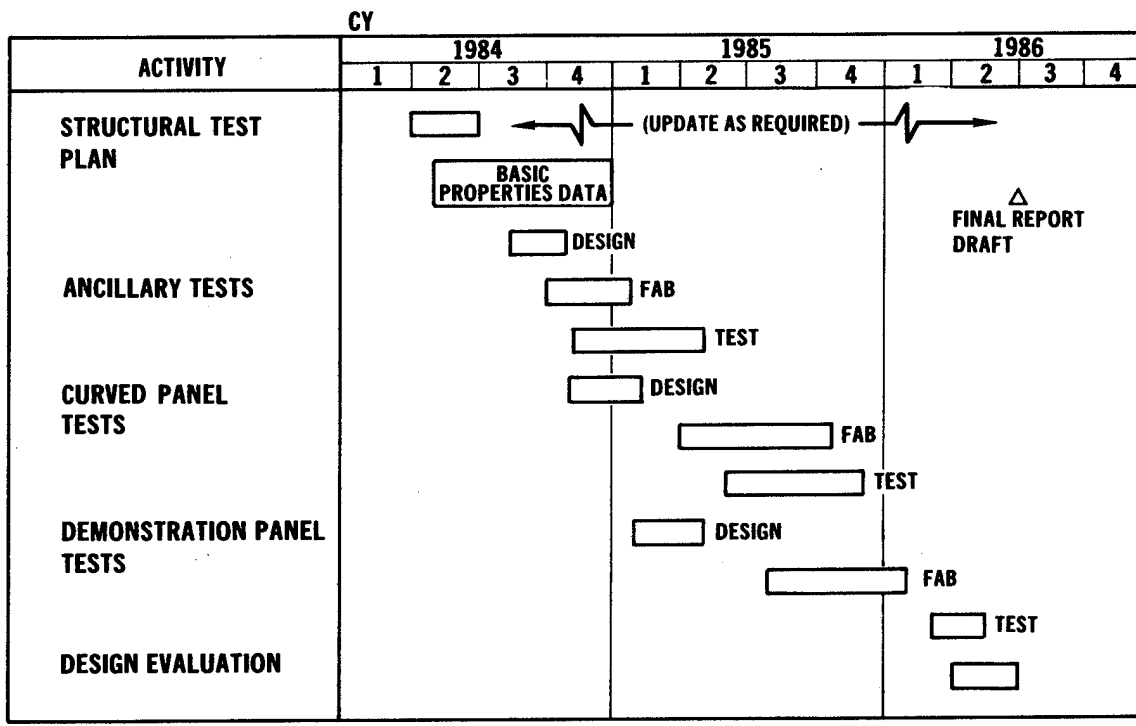
FIGURE 17.

STRUCTURAL TEST SCHEDULE

A preliminary structural test plan has been prepared for the test program. The plan will be updated throughout the program to incorporate changes prompted by design development data acquired subsequent to the initial issue of the test plans.

Basic material properties which are needed for design and analysis purposes are being compiled from existing Hexcel and industry sources. Coupon tests for basic monolayer properties, NAS RP 1092 toughened resin tests, and tests for the effects of lightning protection coatings and temperature and moisture effects will be conducted as required to supplement the existing data base.

The test program schedule (Figure 18) has been established so that the specimen design is preceded by design development and the specimen fabrication by manufacturing and process development. The design of the curved panels and the large demonstration panel will be deferred to allow data input from the preceding test program to be used provided the data are available in time to permit all testing to be completed by 15 May 1986.



84-GEN-22530
u632 i2570a

FIGURE 18.

ANCILLARY TEST PROGRAM

An ancillary test program has been established to support the development of new technology for joints and large cutouts in the fuselage shell. Five types of tests are planned:

- o Basic material property tests such as those defined by NAS RP 1092, "Toughened Resin Tests."
- o Basic loaded hole data similar to that generated by the Critical Wing Joint Technology/Program with layup patterns, thicknesses, and bolt sizes representative of fuselage constructions.
- o Structural element tests of the longitudinal and transverse skin splices and the longeron splices.
- o Stiffened and unstiffened cutout specimens to investigate the stress distribution around the cutout for several configurations which reduce the modulus of the material in the corners of the cutout by varying the layup pattern or by replacing carbon fiber plies with lower modulus glass fiber plies.
- o Stiffener/skin pull-off tension tests to establish a data base for designing for pressure pillowing action.

Examples of the latter three test types are shown in Figure 19.

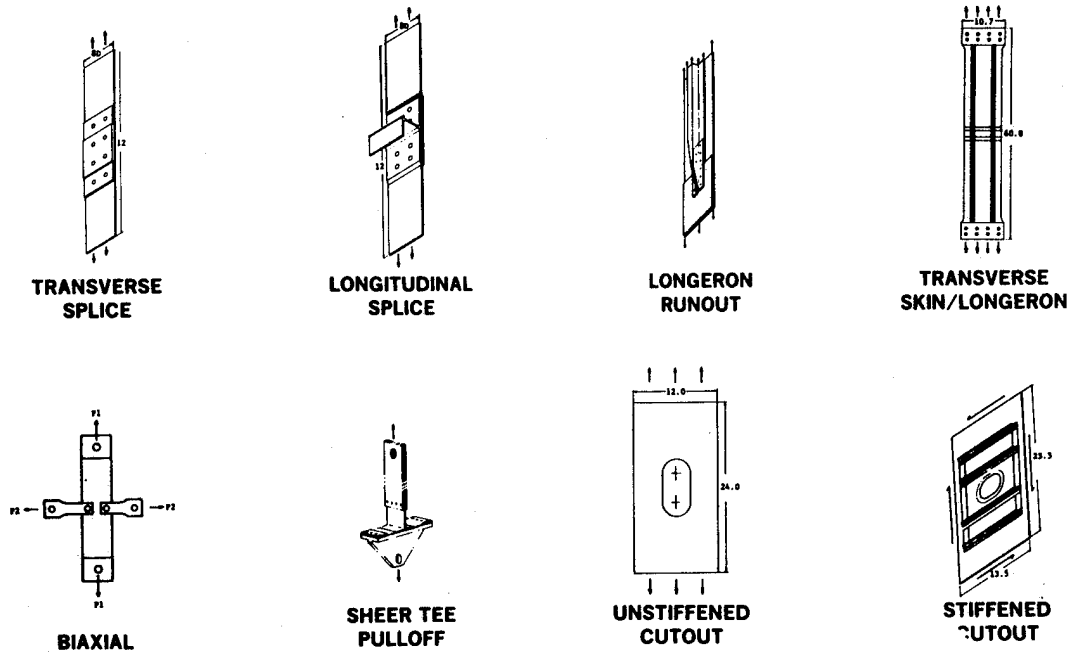


FIGURE 19.

CURVED PANEL TESTS

The curved fuselage panel test specimens are shown in Figure 20. One panel will represent typical panel construction, one will feature a transverse skin/longeron splice, and the third will contain a large reinforced cutout with softened corners. The test machine used for this series of tests has the capability of applying shear longitudinal tension or compression, and normal air pressure to a curved fuselage panel up to 48 by 60 inches in size. Loads can be applied separately or in combination through computer load control. The panels will be instrumented to measure the interaction effects and the stress distributions around the modified cutout. Cyclic load tests will interrogate the panel durability in the presence of peel forces induced by panel buckling and pressure pillowing action.

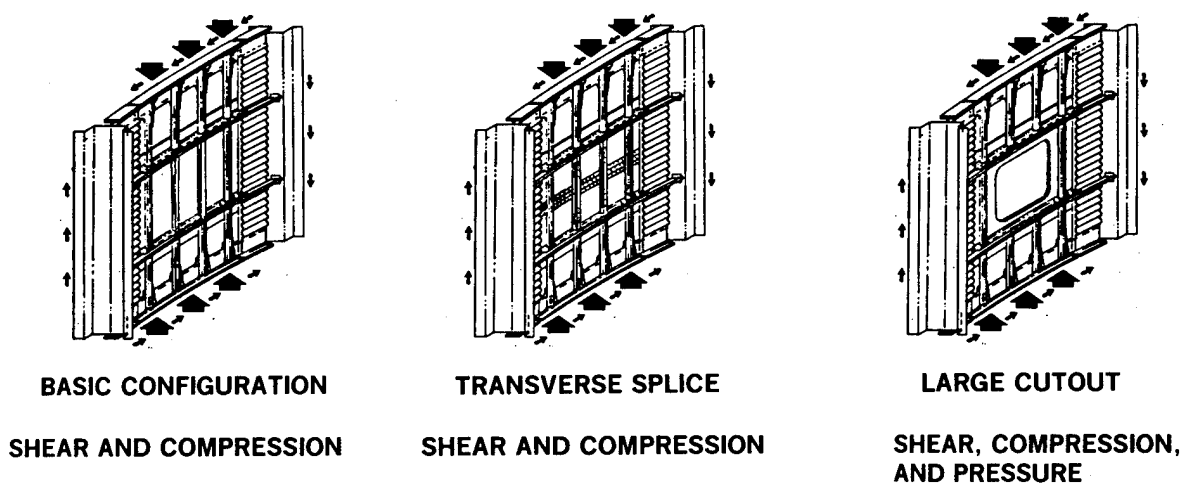
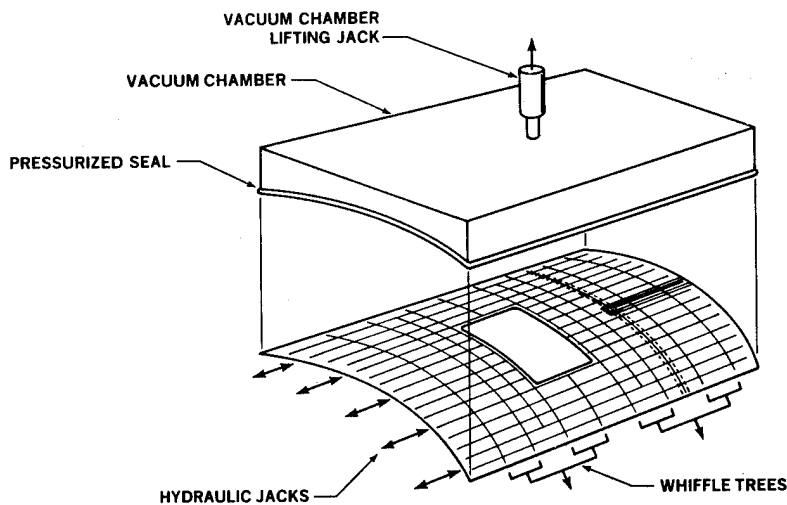


FIGURE 20.

DEMONSTRATION TEST PANEL

A large panel test is planned to demonstrate the composite fuselage technology developed and to investigate those issues which could not be resolved on a lesser scale. The test setup is shown in Figure 21. The test machine can accommodate a curved panel size of 110 by 160 inches. The cabin air pressure is actually applied through a vacuum chamber on the outside surface of the panel. This permits cyclic load tests of damaged structure to be conducted in order to establish damage growth and residual strength data without the danger of explosive decompression. Longitudinal loads are applied by hydraulic actuators mounted around the periphery at one end of the panel. Internal load distribution in the panel will be measured and correlated with analytical prediction to prove the analysis methodology. Static load strain surveys will be conducted to at least limit loads, and two lifetimes of flight-by-flight spectrum loads will be applied. Delaminations will be introduced to simulate service abuse at the start of the second lifetime. Damage growth will be monitored and the residual strength will be verified after two lifetimes. The final failing test will be longitudinal compression without cabin pressure.



- STRAIN GAGES TO MEASURE RESPONSE
- DESIGN LIMIT LOAD CONDITIONS
- ONE-LIFETIME CYCLIC LOADS
- RESIDUAL STRENGTH TEST
- INFILCT DAMAGE TO PANEL
- SECOND-LIFETIME CYCLIC LOADS
- RESIDUAL STRENGTH TEST
- REPAIR IF NECESSARY
- FAILING LOAD TEST

FIGURE 21.

COMPOSITE FUSELAGE TECHNOLOGY

CONCLUDING REMARKS

- 30-MONTH PROGRAM STARTED 21 MARCH 1984
- HEXCEL F584/IM6 CARBON/EPOXY WAS SELECTED FOR THE MATERIAL SYSTEM
- ESTIMATED WEIGHT SAVINGS IS 32 PERCENT
- MINIMUM SKIN GAGE IS 0.070 INCH
- COMPOSITE PROGRAM RETAINS THE BASELINE FRAME AND LONGERON LOCATIONS
- 9,000 RUNNING INCHES OF BOLTED LONGITUDINAL SKIN-SPlice STRUCTURE HAS BEEN ELIMINATED
- 83,000 FEWER FASTENERS ARE REQUIRED FOR SKIN SPLICES
- SHEAR TEES AND J-SECTION LONGERONS ARE SECONDARILY BONDED TO SKINS
- PASSENGER DOOR CUTOUT STRESS CONCENTRATIONS WILL BE ALLEVIATED BY REDUCING THE MODULUS IN THE CORNERS
- PEEL STRESSES PRODUCED BY THE PRESSURE PILLOWING ACTION MUST BE ACCOUNTED FOR IN THE DURABILITY AND DAMAGE TOLERANCE ASSESSMENT
- FABRICATION OF 9 FEET BY 14 FEET DEMONSTRATION TEST ARTICLE WILL PROVIDE MANUFACTURING DEVELOPMENT EXPERIENCE
- LABOR INTENSITY LOWER THAN BASELINE BECAUSE OF REDUCTION IN NUMBER OF FASTENERS PLUS AUTOMATED FABRICATION AND ASSEMBLY OPERATIONS